



**SYNTHESIS AND EVALUATION OF MUCOADHESIVE NANOPARTICLES
FOR ANTICANCER DRUG DELIVERY**



**A Thesis Submitted in Partial Fulfillment of the Requirements
for Doctor of Philosophy (PHARMACEUTICAL TECHNOLOGY)**

INTERNATIONAL PROGRAM

Department of PHARMACEUTICAL TECHNOLOGY

Graduate School, Silpakorn University

Academic Year 2021

Copyright of Silpakorn University

การสังเคราะห์และประเมินอนุภาคนาโนยัดติดเยื่อเมือกสำหรับการนำส่งยาต้านมะเร็ง



โดย
นางสาวนิจวรรณ สหัสพันธ์

วิทยานิพนธ์นี้เป็นส่วนหนึ่งของการศึกษาตามหลักสูตรปรัชญาดุษฎีบัณฑิต
สาขาวิชาเทคโนโลยีสารสนเทศ (หลักสูตรนานาชาติ) แบบ 1.2 ปรัชญาดุษฎีบัณฑิต
ภาควิชาเทคโนโลยีสารสนเทศ
บัณฑิตวิทยาลัย มหาวิทยาลัยศิลปากร
ปีการศึกษา 2564
ลิขสิทธิ์ของมหาวิทยาลัยศิลปากร

**SYNTHESIS AND EVALUATION OF MUCOADHESIVE
NANOPARTICLES FOR ANTICANCER DRUG DELIVERY**



A Thesis Submitted in Partial Fulfillment of the Requirements
for Doctor of Philosophy (PHARMACEUTICAL TECHNOLOGY)
INTERNATIONAL PROGRAM
Department of PHARMACEUTICAL TECHNOLOGY
Graduate School, Silpakorn University
Academic Year 2021
Copyright of Silpakorn University

Title SYNTHESIS AND EVALUATION OF MUCOADHESIVE
 NANOPARTICLES FOR ANTICANCER DRUG DELIVERY
By Nitjawan SAHATSAPAN
Field of Study (PHARMACEUTICAL TECHNOLOGY) INTERNATIONAL
 PROGRAM
Advisor Associate Professor Prasopchai Patrojanasophon , Ph.D.

Graduate School Silpakorn University in Partial Fulfillment of the
Requirements for the Doctor of Philosophy

..... Dean of graduate school
(Associate Professor Jurairat Nunthanid, Ph.D.)

Approved by

..... Chair person
(Assistant Professor Sureewan Duangjit , Ph.D.)

..... Advisor
(Associate Professor Prasopchai Patrojanasophon , Ph.D.)

..... Co advisor
(Professor Praneet Opanasopit , Ph.D.)

..... Committee
(Associate Professor SUWANNEE PANOMSUK , Ph.D.)

..... Committee
(Boonnada Pamornpathomkul , Ph.D.)

59353803 : Major (PHARMACEUTICAL TECHNOLOGY) INTERNATIONAL PROGRAM

Keyword : MUCOADHESIVE POLYMER / POLYMERIC NANOPARTICLES / CHITOSAN / ALGINATE / MALEIMIDE / CATECHOL / THIOL / DOXORUBICIN / GM EXTRACT

MISS NITJAWAN SAHATSAPAN : SYNTHESIS AND EVALUATION OF MUCOADHESIVE NANOPARTICLES FOR ANTICANCER DRUG DELIVERY THESIS ADVISOR : ASSOCIATE PROFESSOR PRASOPCHAI PATROJANASOPHON, Ph.D.

The purpose of this study was to synthesize and characterize new mucoadhesive polymers and fabricate mucoadhesive polymeric nanoparticles (NPs) for anticancer drug delivery. 6-maleimidohexanoic acid (MHA)-conjugated chitosan (CS) (MHA-CS), L-cysteine-conjugated CS (Cys-CS) and catechol-conjugated alginate (Cat-Alg) were synthesized by a coupling reaction using 1-ethyl-3-(3-dimethylamino propyl) carbodiimide (EDAC) and N-hydroxysulfosuccinimide (NHS) as catalysts. Structure elucidation of the synthesized polymers was then carried out using Nuclear magnetic resonance (NMR) and Fourier transform-infrared (FT-IR) spectrometers. The molecular weight was determined by gel permeation chromatography (GPC). The maleimide and catechol contents bearing on the polymer, the mucoadhesive capability and biocompatibility of the obtained polymers were also evaluated. Polymeric NPs were fabricated from the synthesized polymers using the ionic gelation technique by mixing the polymers with thiamine pyrophosphate (TPP) or calcium chloride (CaCl_2). Either GM extract or doxorubicin (DOX) was selected to be incorporated into each NPs. The physicochemical properties, mucoadhesive properties, drug incorporation and release were evaluated. In addition, anticancer activity and cellular uptake of the NPs on cancer cells were determined. The findings conveyed that MHA-CS exhibited superior mucoadhesive capability compared with Cat-Alg and Cys-CS. The maleimide and thiol contents on the MHA-CS and Cys-CS, respectively, were 466 and 253 $\mu\text{mol/g}$. The degree of substitution of catechol groups on the Cat-Alg was 0.564. Minimal toxicity of the synthesized polymers on normal human cells (HGF) was confirmed by the cytotoxicity test. *Garcinia mangostana* (GM) extracts were successfully incorporated into MHA-CS, Cys-CS and Cat-Alg NPs with particles sizes in the nanometer range. The extract was sustainably released from the NPs and was able to be accumulated inside the colon cancer cells and kill the cancer cells. Moreover, the DOX-loaded NPs also exhibited a sustained release from the NPs, and were able to kill MB49 bladder cancer cells with low IC_{50} . In vitro cellular internalization study revealed that DOX-loaded NPs could be highly uptaken by MB49 cells. In conclusion, the polymer conjugated with MHA and catechol provided excellent mucoadhesive properties with low toxicity. NPs developed from the synthesized polymers can adhere to mucosal membranes providing a sustained release of anticancer drugs. These NPs may be promising mucoadhesive carriers for local delivery of an anticancer drug.

ACKNOWLEDGEMENTS

I would like to convey my deepest appreciation to my supervisors, Associate Professor Dr. Prasopchai Patrojanasophon and Professor Dr. Praneet Opanasopit for their helpful guidance and marvelous advice that carried me through all stages of my research project. I am so pleased with all my time studying Ph.D. under the supervision of my supervisors. My supervisors offered me many opportunities to have memorable experiences which improve my skills and competence.

I would also like to acknowledge Professor Dr. Mont Kumpugdee Vollrath for accepting me to join the Fachbereich II: Labor Pharmazeutische Technologie and Chemical Engineering and offering me a marvelous opportunity to broaden my knowledge and experience at Berliner Hochschule für Technik (BHT), Germany. I have gathered many ideas, skills, and support from Professor Dr. Mont Kumpugdee Vollrath.

The Faculty of Pharmacy, Silpakorn University and staff members are also acknowledged for all the support. In addition, I would like to express thanks to all members of the Pharmaceutical Development of Green Innovation Group (PDGIG) for providing me with a lot of support.

Most importantly, a debt of gratitude is also owed to my dear family for their love and continuous support.

MISS Nitjawan SAHATSAPAN

TABLE OF CONTENTS

	Page
ABSTRACT.....	D
ACKNOWLEDGEMENTS.....	E
TABLE OF CONTENTS.....	F
LIST OF TABLES.....	K
LIST OF FIGURES.....	N
LIST OF ABBREVIATIONS.....	1
CHAPTER 1.....	4
INTRODUCTION.....	4
1.1 Statement and significance of the research problem.....	4
1.2 Objective of this research.....	8
1.3 The research of hypothesis.....	8
CHAPTER 2.....	9
LITERATURE REVIEWS.....	9
2.1 Bladder cancer.....	11
2.1.1 Anatomical aspects of bladder.....	12
2.1.2 Treatment options.....	13
2.1.3 DDS for targeted bladder cancer treatment.....	14
2.1.3.1 Systemic chemotherapy.....	14
2.1.3.2 Intravesical chemotherapy.....	15
2.1.4 Polymeric NPs for intravesical drug delivery.....	16
2.2 Colon cancer.....	17
2.2.1 Anatomic characteristics of colon.....	17
2.2.2 Stages of colon cancer.....	17
2.2.3 Treatment options.....	18
2.3 NPs for treatment of cancer.....	20

2.3.1 Types of NPs	20
2.3.1.1 Solid lipid NPs (SLNs).....	20
2.3.1.2 Nanostructured lipid carriers (NLCs).....	21
2.3.1.3 Liposomes.....	22
2.3.1.4 Polymeric NPs (PNPs)	23
2.3.1.5 Dendrimers	23
2.3.2 Therapeutics NPs.....	24
2.4 Doxorubicin (DOX).....	25
2.4.1 Chemical structure.....	25
2.4.2 Mechanisms of action of DOX.....	25
2.4.3 Side effects	26
2.5 Garcinia mangostana (GM)	26
2.5.1 The medicinal properties of GM extracts.....	29
2.6 Mucoadhesive DDS	30
2.6.1 Mucoadhesive polymer	31
2.6.1.1 First-generation mucoadhesive polymer	32
2.6.1.2 Second generation mucoadhesive polymer	36
2.6.1.3 Synthesis of mucoadhesive polymer	39
2.6.1.4 Mucoadhesive mechanism.....	40
CHAPTER 3	41
MATERIALS AND METHODS.....	41
3.1 Material.....	43
3.2 Equipment.....	44
3.3 Methods	46
3.3.1 Synthesis of mucoadhesive polymers.....	46
3.3.1.1 Synthesis of Cys-CS	46
3.3.1.2 Synthesis of MHA-CS	46
3.3.1.3 Synthesis of Cat-Alg.....	46
3.3.2 Characterization of the synthesized polymers.....	47

3.3.2.1 NMR.....	47
3.3.2.2 FT-IR.....	47
3.3.3 Determination of mucoadhesive functional group.....	47
3.3.3.1 Thiol content of Cys-CS.....	47
3.3.3.2 Maleimide group content of MHA-CS.....	47
3.3.3.3 Catechol group content of Cat-Alg.....	48
3.3.4 Mucoadhesive properties of the synthesized polymer.....	48
3.3.4.1 Rheology method.....	48
3.3.4.2 Ex-vivo mucoadhesion assay (Tensile testing method).....	48
3.3.5 Cytotoxicity of the synthesized polymers on normal cells.....	49
3.3.6 Preparation of the mucoadhesive NPs.....	50
3.3.6.1 Cat-Alg NPs.....	50
3.3.6.2 MHA-CS and Cys-CS NPs.....	50
3.3.6.3 MHA-CS-Alg-Cat NPs.....	50
3.3.7 Evaluation of NPs.....	50
3.3.7.1 DLS measurements.....	50
3.3.7.2 Morphology of the NPs.....	51
3.3.7.3 Mucoadhesive properties of the NPs.....	51
3.3.7.3.1 Porcine bowel mucosa.....	51
3.3.7.3.2 Porcine bladder mucosa.....	51
3.3.8 GM extract-loaded NPs.....	52
3.3.8.1 Standardization and assay of GM extract.....	52
3.3.8.2 Preparation of GM extract-loaded NPs.....	52
3.3.8.3 Determination of percentage loading efficiency (LE) and loading capacity (LC).....	52
3.3.8.4 Release of GM-extract loaded NPs.....	53
3.3.9 DOX-loaded NPs.....	53
3.3.9.1 Preparation of DOX-loaded NPs.....	53
3.3.9.2 DOX assay.....	53

3.3.9.3 Release of DOX-loaded NPs	54
3.3.10 Anticancer activity on cancer cells.....	54
3.3.11 Cellular uptake analysis.....	54
3.3.12 Confocal laser scanning microscopy (CLSM) analysis	55
3.3.13 Statistical analysis	55
CHAPTER 4	56
RESULTS AND DISCUSSION	56
4.1 Chemical characterization of the synthesized polymers.....	57
4.1.1 Synthesis of Cys-CS.....	57
4.1.2 Synthesis of MHA-CS.....	59
4.1.3 Synthesis of Cat-Alg	60
4.1.4 Molecular weight (MW) of the obtained polymers.....	62
4.2 Mucoadhesive properties.....	63
4.2.1 Polymer-mucin interaction.....	63
4.2.2 <i>Ex-vivo</i> mucoadhesion assay (Tensile testing method).....	64
4.3 Biocompatibility of the synthesized polymers.....	66
4.4 Development of the mucoadhesive NPs	68
4.4.1 Particle size, size distribution and zeta potential measurements.....	68
4.4.2 Morphology of the NPs	68
4.4.3 Mucoadhesive properties of the NPs on <i>ex vivo</i> porcine bowel mucosa..	69
4.4.4 Mucoadhesive properties of the NPs on <i>ex vivo</i> porcine bladder mucosa	72
4.5 Development of GM extract loaded NPs	74
4.5.1 Extraction and standardization of GM extract	74
4.5.2 Particle size, size distribution and zeta potential measurements.....	74
4.5.3 Determination of drug loading and drug content	75
4.5.4 Release studies	76
4.5.5 Cytotoxicity on cancer cells	77
4.6 Development of DOX loaded NPs.....	79
4.6.1 DLS measurements.....	79

4.6.2 Determination of drug loading and drug content	80
4.6.3 Release of DOX-loaded NPs	81
4.6.4 <i>In vitro</i> cytotoxicity using MTT assay	82
4.6.5 Cellular Uptake of the NPs.....	83
4.6.6 Confocal laser scanning microscopy (CLSM) analysis of the NPs.....	84
CHAPTER 5	86
CONCLUSIONS.....	86
5.1 Development of Mucoadhesive polymer	86
5.2 Development of GM extracts loaded mucoadhesive NPs for colon cancer	86
5.3 Development of DOX loaded mucoadhesive NPs for bladder cancer.....	86
REFERENCES	88
APPENDIX.....	105
APPENDIX A.....	106
APPENDIX B	126
APPENDIX C	131
APPENDIX D.....	139
VITA.....	143

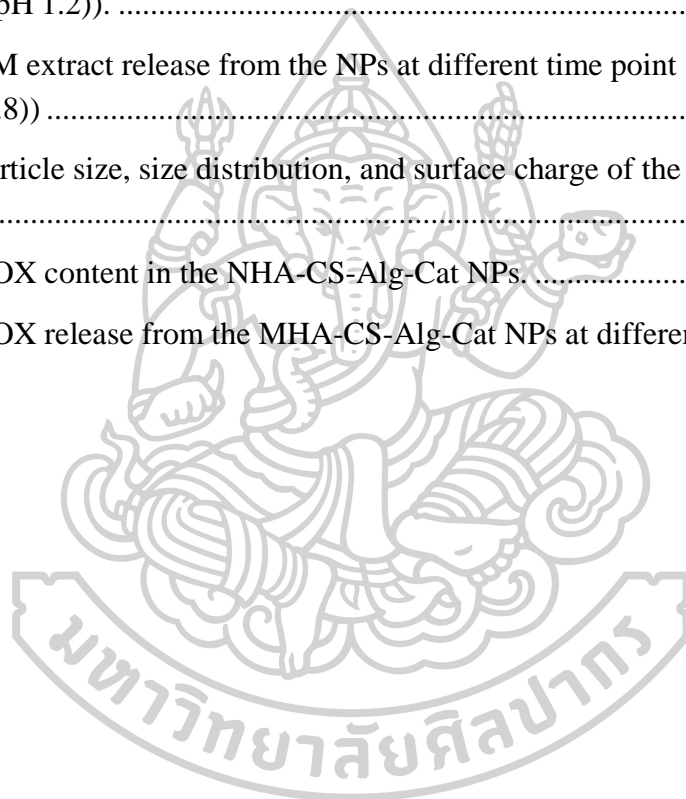


LIST OF TABLES

	Page
Table 1 The MW and polydispersity of the CS, Alg, Cys-CS, MHA-CS and Cat-Alg	63
Table 2 Shear viscosity of the polymer-mucin mixture (at the polymer and mucin concentrations of 5%), and the <i>ex-vivo</i> mucoadhesive strength of the compressed polymer tablets on a porcine buccal mucosal tissue. *Statistically significant difference from CS (negative control), ** Statistically significant difference from Cys-CS (positive control).	65
Table 3 Shear viscosity of the polymer-mucin mixture (at the polymer and mucin concentrations of 5%), and the <i>ex-vivo</i> mucoadhesive strength of the compressed polymer tablets on a porcine buccal mucosa. * Statistically significant difference from Alg (negative control).	66
Table 4 The mean particle size, size distribution and zeta potential of the NPs. Each value is shown as the mean \pm SD of triplicate experiments.....	68
Table 5 Fluorescence images of sodium fluorescein-loaded NPs remained on the porcine bowel mucosa after washing for different intervals. Data are presented as mean \pm SD (n = 3)	70
Table 6 Fluorescence images of sodium fluorescein-loaded NPs remained on the porcine bowel mucosa after washing for different periods. Data are expressed as mean \pm SD (n = 3).	71
Table 7 Fluorescence images of sodium fluorescein-loaded NPs remained on the porcine bladder mucosa after washing for different periods. Data are expressed as mean \pm SD (n = 3).....	73
Table 8 Particle size, size distribution and zeta potential measurements of GM extract-loaded NPs.	75
Table 9 %Loading efficiency and loading capacity of the drug loading NPs.	76
Table 10 The mean particle size, PDI and zeta potential of the NPs. Each number is displayed as the mean \pm SD from three separated experiments.	80

Table 11 The mean particle size, size distribution, zeta potential, loading efficiency and loading capacity of the DOX loaded mucoadhesive NPs. Data are expressed as mean \pm SD (n = 3).	81
Table 12 The amount of thiol groups on the Cys-CS	107
Table 13 The amount of maleimide groups on the MHA-CS	107
Table 14 The <i>ex vivo</i> mucoadhesive strength of the compressed tablets made of the polymers after being contacted with a porcine buccal mucosa	108
Table 15 Viscosity of 5% mucin solution	109
Table 16 Viscosity of 5% CS solution	110
Table 17 Viscosity of 1% CS solution/5% mucin mixtures	111
Table 18 Viscosity of 3% CS solution/5% mucin mixtures	112
Table 19 Viscosity of 5% CS solution/5% mucin mixtures	113
Table 20 Viscosity of 5% Cys-CS	114
Table 21 Viscosity of 1% Cys-CS/5% mucin mixtures	115
Table 22 Viscosity of 3% Cys-CS/5% mucin mixtures	116
Table 23 Viscosity of 5% Cys-CS/5% mucin mixtures	117
Table 24 Viscosity of 5% MHA-CS	118
Table 25 Viscosity of 1% MHA-CS/5% mucin mixtures	119
Table 26 Viscosity of 3% MHA-CS/5% mucin mixtures	120
Table 27 Viscosity of 5% MHA-CS/5% mucin mixtures	121
Table 28 Viscosity of 5% Cat-Alg	122
Table 29 Viscosity of 1% Cat-Alg/5% mucin mixtures	123
Table 30 Viscosity of 3% Cat-Alg/5% mucin mixtures	124
Table 31 Viscosity of 5% Cat-Alg/5% mucin mixtures	125
Table 32 Particle size, size distribution, and surface charge of the NPs.	127
Table 33 Percentage remaining of CS, Cys-CS NPs and MHA-CS NPs on porcine bowel mucosa	128
Table 34 Percentage remaining of Alg and Cat-Alg NPs on porcine bowel mucosa.	129

Table 35 Percentage remaining of dextran, CS-Alg NPs and MHA-CS-Alg-Cat NPs on bladder mucosa.	130
Table 36 Particle size, size distribution, and surface charge of the GM extract loaded NPs.....	132
Table 37 Volume ratios of acetonitrile and 0.1% orthophosphoric acid use as a mobile phase for HPLC.....	133
Table 38 GM extract content in the NPs.....	136
Table 39 GM extract release from the NPs at different time point (Simulated Gastric (0.1M HCl pH 1.2)).	137
Table 40 GM extract release from the NPs at different time point (Simulated Intestinal Fluid (pH 6.8))	138
Table 41 Particle size, size distribution, and surface charge of the DOX loaded NPs.	140
Table 42 DOX content in the NHA-CS-Alg-Cat NPs.	141
Table 43 DOX release from the MHA-CS-Alg-Cat NPs at different time point.....	142



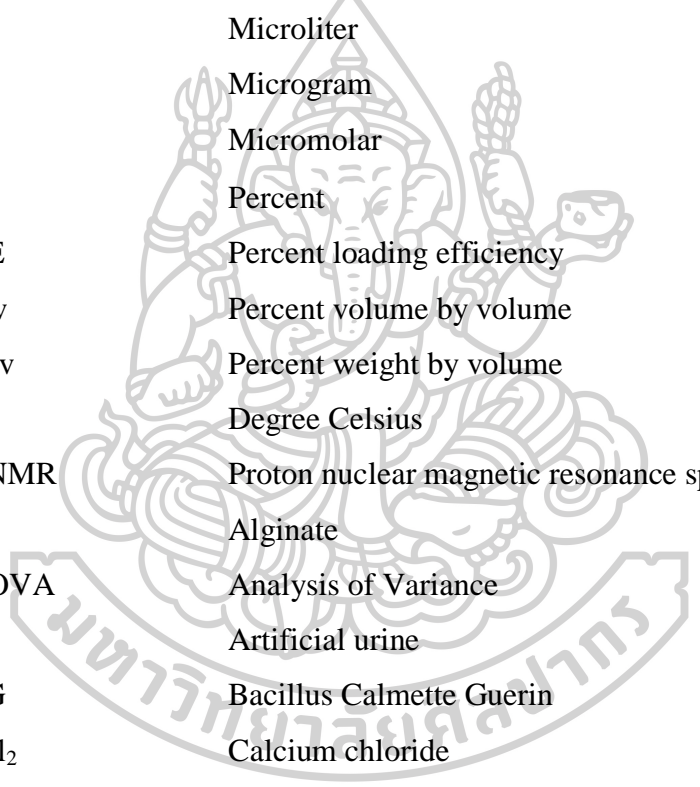
LIST OF FIGURES

	Page
Figure 1 Illustration of the bladder cancer	12
Figure 2 Structure of the bladder	13
Figure 3 Stages of colon cancer	18
Figure 4 Structure of solid lipid NPs (SLNs).....	21
Figure 5 Structure of nanostructured lipid carriers (NLCs).....	22
Figure 6 Structure of liposome	23
Figure 7 Schematic picture of sub-classes in the dendritic family.	24
Figure 8 Structure of DOX	25
Figure 9 Chemical structure of the most common xanthenes found in GM.....	28
Figure 10 The chemical structure of CS	33
Figure 11 The chemical structures of carbopol.....	34
Figure 12 The chemical structures of G-block, M-block and alternating block in Alg.	35
Figure 13 The chemical structures of hydroxypropyl methylcellulose	35
Figure 14 Schematic of thiolated polymers covalently binding mucin glycoproteins.	36
Figure 15 Schematic of acrylate polymers covalently binding mucin glycoproteins..	37
Figure 16 Adhesion in the marine mussel <i>Mytilus californianus</i> . (A) Adult mussel exhibiting extensive byssus attached to a mica surface. (B) Schematic mussel on a half-shell.	38
Figure 17 Examples of catechol-containing molecules used to modify polymer backbones.....	38
Figure 18 Schematic of maleimide material covalently binding mucin glycoproteins	39
Figure 19 Mucoadhesive mechanism.....	40
Figure 20 Mucoadhesion test using a texture analyzer with a tissue holder.....	49
Figure 21 Synthetic route of Cys-CS.	57
Figure 22 ¹ H NMR spectra of a) CS b) Cys-CS and c) MHA-CS in 2% CD ₃ COOD/D ₂ O	58

Figure 23 FT-IR spectra of CS, Cys-CS and MHA-CS.....	59
Figure 24 Synthetic route of MHA-CS.....	59
Figure 25 Synthetic route of Cat-Alg.....	61
Figure 26 ¹ H NMR spectra of Alg and Cat-Alg in D ₂ O.....	61
Figure 27 FT-IR spectra of Alg and Cat-Alg.....	62
Figure 28 Viscosity of a mixture of a) CS and mucin b) Cys-CS and mucin c) MHA-CS and mucin and d) Cat-Alg and mucin compared with the polymer solution or mucin solution alone.....	64
Figure 29 Cytotoxic effect of a) CS, Cys-CS and MHA-CS and b) Alg and Cat-Alg on HGF cells. Data are presented as the mean ± SD (n = 5) *Statistically significant difference from control and **statistically significant difference from Alg (p < 0.05).....	68
Figure 30 Morphology observed under TEM of a) Cys-CS, b) Cat-Alg, c) MHA-CS and d) MHA-CS-Alg-Cat NPs.....	69
Figure 31 Percentage retention of CS, Cys-CS NPs and MHA-CS NPs on porcine bowel mucosa. Data are shown as mean ± SD (n = 3). *Statistically significant difference from CS (p < 0.05), **Statistically significant difference from Cys-CS NPs.....	70
Figure 32 Percentage remaining of Alg and Cat-Alg NPs. Data are expressed as mean ± SD (n = 3) *statistically significant (p < 0.05).....	72
Figure 33 Percentage retention of dextran, CS-Alg NPs and MHA-CS-Alg-Cat NPs on porcine bladder mucosa after washing with AU pH 6.2. Data are expressed as mean ± SD (n = 3). *Statistically significant difference from dextran (p < 0.05), **Statistically significant difference from CS-Alg NPs.....	74
Figure 34 The <i>in vitro</i> release of α-mangostin from the GM extract-loaded NPs was studied in two different release media including a) simulated gastric fluid (0.1M HCl pH 1.2) containing 2% tween 20 and b) simulated intestinal fluid (pH 6.8) containing 2% tween 20.....	77
Figure 35 Percentage cell viability of HT29 cells after being treated with the blank MHA-CS NPs, Cys-CS NPs and Cat-Alg NPs.....	78

Figure 36 Cytotoxicity of a) free GM extract and b) GM extract-loaded NPs on HT29 cells.	79
Figure 37 Cumulative release profiles of free DOX and DOX-loaded MHA-CS-Alg-Cat NPs. Data are expressed as mean \pm SD (n = 3) * statistically significant (p < 0.05).	82
Figure 38 Percentage cell viability of MB49 cells after being treated with the blank NPs.	83
Figure 39 Mean fluorescence intensity (MFI) of free DOX and DOX-loaded MHA-CS-Alg-Cat NPs by flow cytometry. Data are expressed as mean \pm SD (n = 3). *statistically significant (p < 0.05).	84
Figure 40 CLSM images of MB49 cells incubated with free DOX, DOX-loaded MHA-CS-Alg-Cat NPs for 24 h. The cells were stained by Hoechst (blue) and DOX (red).	85
Figure 41 Chromatogram of standard α -mangostin.	134
Figure 42 Chromatogram of GM extract.	134
Figure 43 Standard curve of α -mangostin.	135
Figure 44 Standard curve of GM extract.	135
Figure 45 Standard curve for DOX content quantification.	140
Figure 46 Standard curve of DOX.	141

LIST OF ABBREVIATIONS



®	Registered trademark
™	Trademark
α	Alpha
β	Beta
γ	Gamma
λ	Lambda (wavelength)
μL	Microliter
μg	Microgram
μM	Micromolar
%	Percent
%LE	Percent loading efficiency
%v/v	Percent volume by volume
%w/v	Percent weight by volume
°C	Degree Celsius
¹ H-NMR	Proton nuclear magnetic resonance spectroscopy
Alg	Alginate
ANOVA	Analysis of Variance
AU	Artificial urine
BCG	Bacillus Calmette Guerin
CaCl ₂	Calcium chloride
Cat	Catechol
Cat-Alg	Catechol-functionalized alginate
CLSM	Confocal laser scanning microscopy
Cm	Centimeter
CO ₂	Carbon dioxide
COOH	Carboxylic acid
CS	Chitosan
Cys	L-Cysteine
Cys-CS	Cysteine-functionalized chitosan

Da	Dalton
DD	Degree of deacetylation
DMEM	Dulbecco's modified Eagle's medium
DMF	Dimethyl formamide
DMSO	Dimethyl sulfoxide
D ₂ O	Deuterium oxide
DOX	Doxorubicin
DS	Degree of substitution
DTNB	5,5-dithio-bis-(2-nitrobenzoic acid)
EDAC	1-ethyl-3-(3-dimethylamino propyl) carbodiimide
Eq	Equation
e.g.	exempli gratia (Latin); for example,
EPR	Enhanced permeability and retention
et. al	And others
etc.	et cetera (Latin); and other things/ and so forth
FT-IR	Fourier-transformed infrared spectroscopy
g	Gram
GM	<i>Garcinia mangostana</i>
HGF	Human gingival fibroblast cells
HT29	Human Colorectal Adenocarcinoma Cell Line
FBS	Fetal bovine serum
FTIR	Fourier-transformed infrared spectroscopy
h	Hour
HCl	Hydrochloric acid
IC ₅₀	The half maximal inhibitory concentration
kg	Kilogram
L	Liter
LC	Loading capacity
M	Molar
MB49	Mouse urothelial carcinoma cell line
mg	Milligram
MHA	6-maleimidohexanoic acid

MHA-CS	Maleimide-functionalized chitosan
MIBC	Muscle invasive bladder cancer
min	Minute
mL	Milliliter
mM	Millimolar
mm	Millimeter
mmol	Millimole
MTT	3-(4,5-dimethylthiazole-2-yl) -2,5-diphenyl tetrazolium bromide
mV	Millivolt
MW	Molecular weight
N	Normality
N ₂	Nitrogen
NHS	N-hydroxysulfosuccinimide
nm	Nanometer
NPs	Nanoparticles
PBS	Phosphate buffer saline
pH	Potentia hydrogenii
ppm	Part per million
rpm	Round per minute
s	Second
TEM	Transmission Electron Microscope
TPP	Thiamine pyrophosphate
wt%	Percent weight by weight

CHAPTER 1

INTRODUCTION

1.1 Statement and significance of the research problem

Cancer can occur in any organ or tissue of the body. It is caused by uncontrollable abnormal cell growth, in which the cell growth goes beyond its usual boundaries and invades the neighboring parts of the body or spreads to other organs. The spread of cancer cells to other organs is termed metastasis, which is the primary cause of death from cancers. Nowadays, cancer has become the second most prevalent cause of death around the globe (Fitzmaurice et al., 2017) although many therapeutic options (such as chemotherapy, surgery, radiotherapy, immunotherapy, combination treatment, and lifestyle change) are available (Arruebo et al., 2011; Kaidar-Person et al., 2018). Chemotherapy is one of the cancer management approaches which use anticancer agents to treat cancer (Pornpitchanarong et al., 2020a). Chemotherapeutic drugs, for instance, docetaxel, cisplatin, epirubicin, camptothecin, and doxorubicin, are widely employed for cancer therapy; nevertheless, the use of these drugs is limited by adverse reactions and drug resistance (Din et al., 2017). Conventional chemotherapeutic drugs for anticancer treatment usually target cells that multiply rapidly and do not discriminate between tumor cells and healthy cells. This results in the side effects of chemotherapy; chemotherapy can induce myelosuppression (resulting in a reduction of blood cells and platelets) (Maxwell and Maher, 1992), mucositis (inflammation of the lining of the digestive tract) (Chaveli-López and Bagán-Sebastián, 2016), and alopecia (hair loss). Therefore, current research focuses on the development of drug carriers for cancer treatment with the aim to improve the efficacy and reduce the toxicity of chemotherapeutic drugs. Clinical studies conveyed that patients had a positive response to new treatment options, and the goal of these new chemotherapeutics is to extend the survival time and the quality of life for cancer patients (Brannon-Peppas and Blanchette, 2004).

Various anticancer drugs are used in the treatment of cancers. Doxorubicin (DOX) is one of the most commonly used chemotherapeutic agent, functioning by inhibition of nucleic acid synthesis in cancer cells (Yoo et al., 2000). DOX is a well-known anthracycline antibiotic that is effective against many types of cancers; for

example, leukemias, malignant lymphomas, bone sarcomas, as well as bladder, gastric, prostate, ovarian, breast and bronchogenic carcinomas (Zeng et al., 2013). DOX has adverse effects such as high myelosuppression and cardiotoxicity, which is an important problem (Brannon-Peppas and Blanchette, 2004). Therefore, new delivery systems is needed to optimize efficacy and minimize toxicity of DOX. In addition, intravesical instillation of DOX is used as adjuvant or neoadjuvant chemotherapy for invasive bladder cancer to treat micrometastases and to improve the surgical of large tumors (Takata et al., 2005). The usefulness of intravesical instillation of DOX is the reduction of systemic side effects and the risk of recurrence, especially in patients with superficial bladder cancer (Fukuokaya et al., 2020).

Due to the numerous adverse effects of chemotherapeutic drugs, scientists have attempted to study and apply natural compounds for cancer prevention and treatment. Mangosteen (*Garcinia mangostana* L.) was effective against various types of cancer. Mangosteen is a tropical fruit found in Southeast Asia. It has been used as a traditional medicine for treating diseases. The mangosteen peel consists of xanthone, α -, β - and γ -mangostin, 8-deoxygartanin, gartanin, and garcinone E (Ovalle-Magallanes et al., 2017a). Many studies found that xanthenes isolated from mangosteen peels exhibit antibacterial, anti-cancer, antioxidant, anti-inflammatory, antifungal, and antiviral effects (Cui et al., 2010). α -Mangostin is a yellowish compound that is isolated from the bark, dried sap, and pericarp of mangosteen (Pedraza-Chaverri et al., 2008). Recently, it has been reported to cause cell-cycle arrest and apoptosis in different types of cancer cells. α -Mangostin also inhibits cell invasion and migration of breast, colon, and prostate cancer cells (Shibata et al., 2011), and it may be a candidate compound for cancer treatment.

Nanoparticle systems have been developed to enhance the efficacy and decrease the toxicity of a chemotherapeutic agent. Nanoparticulate systems have the advantage of targeting cancer by simply being accumulated and entrapped in tumors (Vyas et al., 2016). This is known as the enhanced permeability and retention (EPR) effect. This effect facilitates the extravasation of nanoparticles (NPs) circulating within the interstitial tumor and also increases the concentration of the anticancer drug within the tumor tissue (Parveen and Sahoo, 2008). NPs are one of the most widely used delivery systems for chemotherapeutic drugs. They are colloidal drug carriers

with a particle size ranging from 10 to 1000 nm (Mudshinge et al., 2011). Polymeric NPs (PNPs) are particles prepared from polymers. PNPs attract great attention as a multifunctional nano-drug delivery system (DDS). Drugs may be incorporated to the NPs by entrapment, encapsulation, or conjugation to a nanoparticle. Moreover, their tiny size facilitate efficient permeability through cell membranes and increased stability in the bloodstream. The pros of PNPs such as protection of drug molecules, controlled release, and reduced toxicity (Prabhu and Jasmine, 2014).

Various types of polymers have been used for developing PNPs. The most widely used ones are chitosan (CS) and alginate (Alg). CS is copolymer of N-acetyl-D-glucosamine and D-glucosamine which is made by alkaline deacetylation of chitin. CS is insoluble at neutral and alkaline pH but is soluble in acidic media (Rinaudo, 2006), and this has limited the straightforward application of CS as biomaterials. CS has been widely studied for drug delivery, biomedical, and other pharmaceutical applications because of its biocompatibility, biodegradability, and non-toxicity (Zhong et al., 2010). CS can interact with the anionic mucin leading to an excellent mucoadhesive property (Lehr et al., 1992). Some functionalization can enhance the mucoadhesion of CS. Alg, an anionic mucoadhesive polymer, is a linear polysaccharide linked by 1,4-glycosidic linkages. This anionic biopolymer is commonly used in the biotechnological and pharmaceutical fields. Alg is biodegradable and non-toxic, and it is mucoadhesive (Davidovich-Pinhas and Bianco-Peled, 2011; Paques et al., 2014). Usually, Ca^{2+} is one of the divalent cations commonly used to crosslink Alg (Sun and Tan, 2013). Currently, CS and Alg NPs are commonly used in anticancer DDS. Janes et al. developed DOX-loaded CS NPs by ionotropic gelation of CS with tripolyphosphate (TPP) (Janes et al., 2001). Wang et al. developed paclitaxel (PTX)-loaded CS/Alg NPs and folate-CS/Alg NPs by double emulsion cross-linking technique (Wang et al., 2016). The NPs could provide improved stability and cancer targeting effect.

The concept of mucoadhesion has received a great deal of interest in the pharmaceutical field as an approach to improving the resident times of DDS at a specific delivery site (Shaikh et al., 2011; Sosnik et al., 2014). Nowadays, various polymers have been shown to possess mucoadhesive competency owing to the ability to form interaction with mucin. However, most of the polymers generate interaction

with mucin through physical or non-covalent interaction such as Van der Waals forces, ionic or hydrogen bonds, etc. which are not able to provide sufficient resident time (Bernkop-Schnürch et al., 2003). Thus, researchers are trying to enhance the mucoadhesive properties of the polymers and/or drug carriers by transforming the polymers or the drug carriers to express certain functional moieties that can form covalent interaction with mucins such as thiols (Bernkop-Schnürch et al., 2003), catechols (Lee et al., 2013), acrylates (Shitrit and Bianco-Peled, 2017) and maleimides (Tonglairoum et al., 2016), thus augments the therapeutic effect of the drug. Recently, new mucoadhesive polymers have been synthesized such as thiolated CS and CS-poly(ethylene glycol) diacrylate (CS-PEGDA), which can form interaction with the mucin glycoprotein via disulfide bond formation and Michael-type reaction, respectively. These functionalized polymers have better mucoadhesive properties compared to intact CS (Shitrit and Bianco-Peled, 2017; Werle et al., 2009).

Herein, 6-maleimidohexanoic acid (MHA)-conjugated chitosan (CS) (MHA-CS), L-cysteine-conjugated CS (Cys-CS) and catechol-conjugated alginate (Cat-Alg) were synthesized to improve the mucoadhesive properties of the polymers. The polymers were modified to present functional groups that form specific covalent bonds, including thiols, maleimides, and catechols. The synthetic polymers were verified and characterized using nuclear magnetic resonance (NMR) and Fourier transform-infrared (FT-IR) spectrometers. The thiol content of Cys-CS and the maleimide group content of MHA-CS were quantified using Ellman's assay and modified Ellman's assay, respectively. Besides, the mucosal adhesion of the polymers was investigated by rheological measurements and tensile testing using a rheometer and a texture analyzer, respectively. Moreover, the cytotoxicity of the polymers on HGF cells was evaluated. To assess the feasibility of the polymers to be employed in a DDS, different types of PNPs were prepared from the synthesized polymers through the ionotropic gelation method. DOX and GM extract were selected as the model compounds representing a widely used chemotherapeutic drug and a natural anticancer compound, respectively. The physicochemical properties, morphology, drug content, *in vitro* release, *ex vivo* mucoadhesive properties, and anticancer activities of the prepared NPs were investigated.

1.2 Objective of this research

1.2.1 To synthesize new mucoadhesive polymers for the preparation of mucoadhesive DDS.

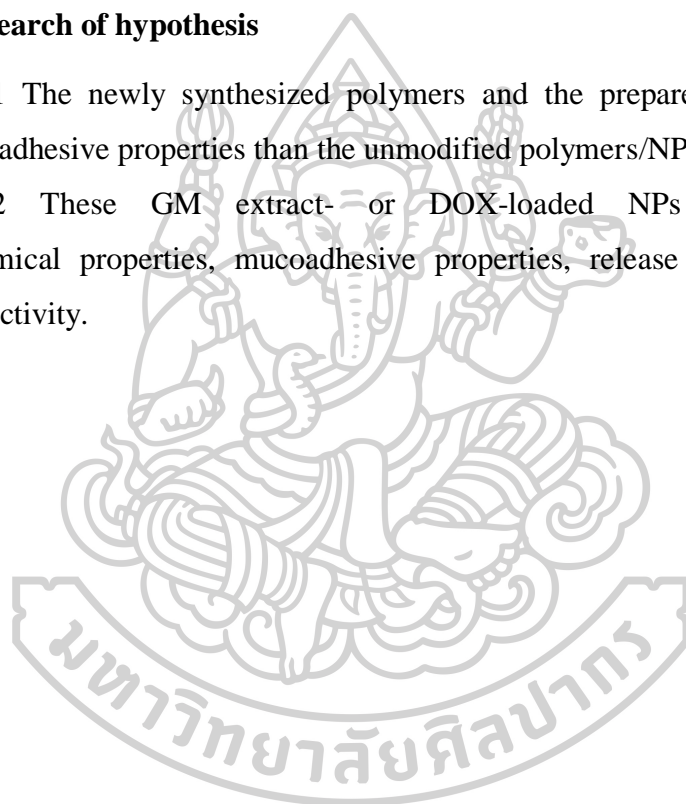
1.2.2 To develop mucoadhesive NPs containing GM extract and DOX for colon cancer and bladder cancer treatment.

1.2.3 To investigate the physicochemical and mucoadhesive properties, release characteristics, and anticancer activity of the developed NPs.

1.3 The research of hypothesis

1.3.1 The newly synthesized polymers and the prepared NPs demonstrate better mucoadhesive properties than the unmodified polymers/NPs.

1.3.2 These GM extract- or DOX-loaded NPs exhibit desirable physicochemical properties, mucoadhesive properties, release characteristics, and anticancer activity.



CHAPTER 2

LITERATURE REVIEWS

2.1 Bladder cancer

- 2.1.1 Anatomical aspects of bladder
- 2.1.2 Treatment options
- 2.1.3 DDS for targeted bladder cancer treatment
- 2.1.4 Polymeric NPs for intravesical drug delivery

2.2 Colon cancer

- 2.2.1 Anatomic characteristics of colon
- 2.2.2 Stages of colon cancer
- 2.2.3 Treatment options

2.3 NPs for cancer treatment

- 2.3.1 Types of NPs
 - 2.3.1.1 Solid lipid NPs (SLNs)
 - 2.3.1.2 Nanostructured lipid carriers (NLCs)
 - 2.3.1.3 Liposomes
 - 2.3.1.4 Polymeric NPs (PNPs)
 - 2.3.1.5 Dendrimers

- 2.3.2 Therapeutics NPs

2.4 Doxorubicin (DOX)

- 2.4.1 Chemical structure
- 2.4.2 Mechanisms of action of DOX
- 2.4.3 Side effects

2.5 Garcinia mangostana (GM)

- 2.5.1 The medicinal properties of GM extracts

2.6 Mucoadhesive DDS

- 2.6.1 Mucoadhesive polymer
 - 2.6.1.1 First-generation mucoadhesive polymer
 - Chitosan
 - Carbopol
 - Alginate

Hydroxypropyl methylcellulose (HPMC)

2.6.1.2 Second generation mucoadhesive polymer

Thiolate polymers

Acrylates

Catechols

Maleimide

2.6.1.3 Synthesis of mucoadhesive polymer

2.6.1.4 Mucoadhesive mechanism



2.1 Bladder cancer

Bladder cancer is initiated by the incessant proliferation of the cells lining the bladder wall. It is the ninth most common cancer in the world (Colombel et al., 2008). There are many risk factors associated with bladder cancer such as increasing age, smoking habits and regular exposure to carcinogens (Wirth et al., 2009). As divided by the type of the cancer cells, almost all types of bladder cancer are transitional cell carcinomas, whereas a minor proportion can be squamous cell or adenocarcinomas (Kaufman et al., 2009). The phase of bladder cancer counts on the degree of dissemination or invasive characteristic of cancer. The tumors which initiate and stay limited within the urothelial boundary are characterized as noninvasive or superficial tumors (Grasso, 2008). Generally, transitional cell carcinomas are treated primarily by transurethral resection (Kaufman, 2006), accompanied by continuation treatment using intravesical chemotherapy to reduce the risk of recurrence (Kaufman, 2006; Kaufman et al., 2009). Besides the goal to eliminate remaining tumors, the main principle of intravesical therapy is to facilitate the contact of the tumors situated in the bladder cavity with a chemotherapeutic drug and decrease the systemic side effect (Shen et al., 2008). Intravesical therapy is an essential component of bladder cancer treatment. However, the specialized asymmetric unit membrane of the bladder urothelium is the main barrier to drug diffusion (Chai et al., 1994). Moreover, frequent catheterizations can cause irritation during voiding and the drug can be rapidly washed out during bladder emptying resulting in the undesired therapeutic effect. The effectiveness of the intravesical therapy hinges on the retention time and the concentration of the drug in the bladder cavity (GuhaSarkar and Banerjee, 2010). Thus, the development of sustained intravesical DDS that are able to provide persistent contact between the drug and the cancer cells is required.

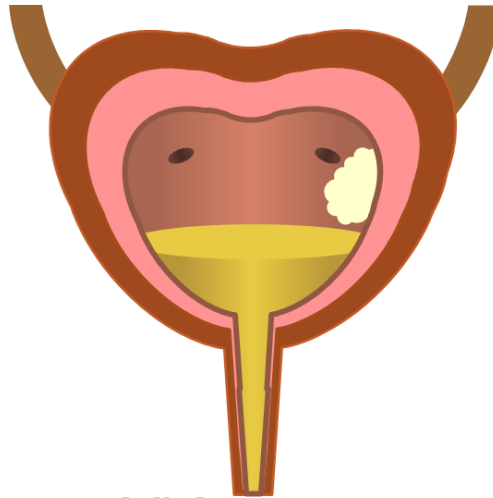


Figure 1 Illustration of the bladder cancer

2.1.1 Anatomical aspects of bladder

The bladder is a hollow, distensible organ with the function to store urine. It consists of the mucosal layer, submucosal tissue, detrusor muscle, and perivesical fat. (Chen et al., 2015; Korossis et al., 2006). The size of the bladder depends upon the amount of urine filled in the bladder. Normally, the capacity of the bladder is 400–600 mL, but loading of around 150–300 mL can stimulate the urge to urinate (GuhaSarkar and Banerjee, 2010). The bladder consists of the bladder permeability barrier which is comparatively impermeable to avoid the reabsorption of waste products. The bladder permeability barrier is composed of the basal germinal cell layer, an intermediate layer and umbrella cells. The umbrella cells are made of an asymmetrical unit membrane covering 70–90% of the luminal surface and are enclosed by hinge membranes. In addition, the cells are joined together by tight junctions. These distinctive attributes produce a wall between urine and plasma (Douglass and Schoenberg, 2016). Furthermore, a layer of mucin adhered to the luminal side on top of the umbrella cells can also hinder liquids and foreign compounds from passing through and reaching the underlying tight junctions or cell membranes as shown in Figure 2 (Douglass and Schoenberg, 2016; Soler et al., 2008). However, this layer of mucin can be a target for mucoadhesive DDS.

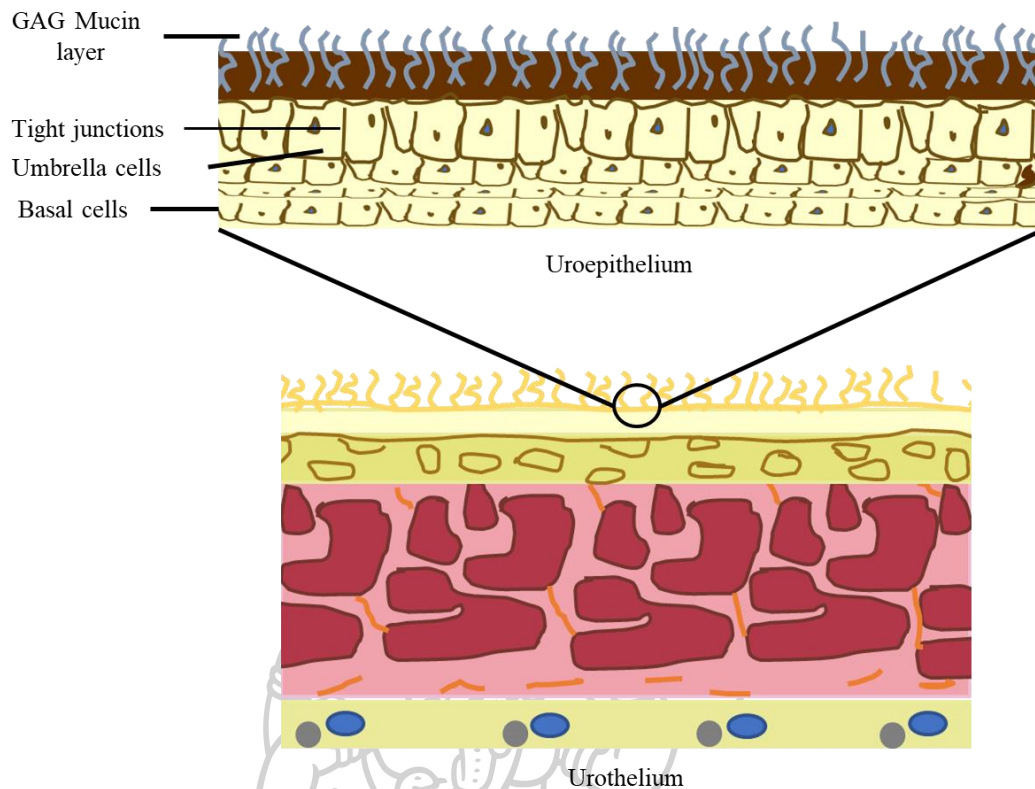


Figure 2 Structure of the bladder

2.1.2 Treatment options

Therapeutic alternatives for bladder cancer are governed largely by the progression of the tumor (early stages, non-muscle-invasive cancer, and advanced muscle-invasive cancer). Bladder cancer treatment options may include:

Surgery

Surgery (transurethral resection of the bladder) is used to remove the tumor. The surgical instrument is put into the bladder through the urethra to remove the tumor tissue. It is the most common option for the treatment of bladder cancer in the early stages. As part of the surgical procedure, chemotherapy drugs may be administered into the bladder to eradicate any residual cancer cells and to prevent tumor recurrence (Lenis et al., 2020).

Immunotherapy

Treatment with Immunotherapy intravesically may be considered to eliminate initial staged bladder cancers (non-muscle invasive cancer) or it may be

used in adjunct with surgery to remove the residual cancer cells. In this therapeutic option, bacillus Calmette Guerin (BCG) is employed to cause stimulate human's immune reaction to fight the cancer from being growth and invasive (Donin et al., 2017; Siefker-Radtke et al., 2018).

Radiation Therapy

Radiation therapy is associated with the use of radiation with high energy to destroy tumor cells. The patients need to be continuous treated by radiation many days a week for several weeks. Radiation can only be used in an early-stage bladder cancer or used after the surgery to eradicate the residual cancer.

Chemotherapy

Chemotherapy is used to instill in the bladder (intravesical chemotherapy) to treat the cancer that are confined to the lining of the bladder but have a high potential to recur or progress to a higher stage. Chemotherapy is used before radiotherapy and surgery to reduce the size of the tumor before the treatment or use together with radiotherapy prior to surgery (chemoradiation). DOX is one of the most effective chemotherapeutic agents employed to treat bladder cancer. Soares et al. have studied the combination of chemotherapy drugs (DOX and resveratrol) which was found to be more effective than DOX or resveratrol alone (Alhusaini et al., 2022; Soares et al., 2022). For muscle-invasive bladder cancer, cisplatin chemotherapy is more common for the treatment (Taber et al., 2020).

2.1.3 DDS for targeted bladder cancer treatment

2.1.3.1 Systemic chemotherapy

Systemic chemotherapy is commonly used for locally advanced and metastatic bladder cancer. It is used as a neoadjuvant therapy to reduce the size of the cancer and destroy the metastasized cancer cells. It can also be used as adjuvant therapy following cystectomy in patient with high risk of relapse to destroy remaining cancer cells. Because of the severe adverse effects caused by the conventional systemic chemotherapy, various DDS have been developed with a great potential for eliminating bladder cancer. Moreover, the DDS can also overcome common problems related to the use of systemic chemotherapy such as collateral toxicity to healthy surrounding cells and poor accumulation in the tumor (Yoo et al.,

2019). Advances in nanotechnology have offered great potential to improve the therapeutic efficacy for bladder cancer therapies by passive and active targeting.

2.1.3.2 Intravesical chemotherapy

In the intravesical chemotherapy the drug is given directly into the bladder by instillation using a urinary catheter. It is used to treat superficial or non-muscle invasive bladder cancers which are accounted for about 70% of the patients with bladder cancer. Treatment of bladder cancer by intravesical chemotherapy is aimed to decrease the recurrent of the cancer. Intravesical therapy is an important alternative to systemic bladder cancer chemotherapy because the drug is instilled directly into the bladder resulting in decreased systemic side effect and increased concentration of the drug at the cancer site. However, there are some major challenges of intravesical chemotherapy that still need to be solved (Tyagi et al., 2016). Intravesical therapy is commonly limited by the relatively short retention time of the drug in the bladder as well as the drug concentration which is continuously diluted by the urine accumulated in the bladder. In addition, the permeation ability of the drug through the the bladder mucosa and the environment of the bladder also the difficulties for the therapy (Zargar et al., 2014). Insufficient drug accumulation in the cancer cells and dilution of drug concentration by urine in the bladder can lead to an unsuccessful treatment. New DDS with an ability to retain in the bladder for a prolonged period are necessary in intravesical therapy. Researchers have attempted to develop mucoadhesive DDS using mucoadhesive macromolecular polymers to increase retention of the DDS in the bladder. Lu et al. developed paclitaxel-loaded gelatin NPs for bladder drug delivery (Lu et al., 2011). In addition, CS or poloxamer and glyceryl monooleate could also be used as delivery systems for intravesical therapy owing to their mucoadhesive capability (Karavana et al., 2018; Lee et al., 2005). Literature has reported that bladder urothelium expresses many receptors that can be a target for therapeutic DDS in the bladder through intravesical drug delivery (Tyagi et al., 2016). The conjugation of specific ligand- or receptor-based compounds on the DDS may improve the targeting specificity and selectivity of the DDS, and thereby increasing the deposition of drug at the cancer site and reducing the drug at the normal tissue. Plattner et al. conveyed that lectins can specifically target and bind

to human bladder cancer cells. Such localized cell adhesion can greatly enhance urothelial uptake efficiency (Plattner et al., 2008). Therefore, it is believed that lectin-modified DDS could be a hopeful tool for intravesical chemotherapy for bladder cancer (Neutsch et al., 2011; Zupančič et al., 2014). Moreover, some specific antigens expressed over the surrounding bladder cancer cells can also be targets. Folate receptors are also expressed in most bladder cancer cells (Dhawan et al., 2013).

2.1.4 Polymeric NPs for intravesical drug delivery

NPs are submicron-sized colloidal particles. The diameters of the NPs are in the range of 10 to 1000 nm, in which a drug compound of interest can be incorporated, adsorbed or conjugated within/on their polymeric scaffold. NPs are the progression of nanotechnology that is believed to be a forthcoming platform to deliver an active compound into a targeted area, specific cell, or tissue (Brannon-Peppas and Blanchette, 2004; Parveen and Sahoo, 2008). NPs can heighten the therapeutic effects due to more specific targeting of affected tissues through superior pharmacokinetics and pharmacodynamics. These attributes count on the characteristics of the particles such as size and surface properties (Davis et al., 2008). Moreover, compared with other DDS, polymeric NPs are easy to synthesize, cost-effective and exhibit better biocompatibility and biodegradability. They are also reported to be non-immunogenic and non-toxic (Chen et al., 2015). NPs with desirable particle size and morphology can offer great capability for intravesical delivery. This is because they can improve the penetration and transportation of the drug across the urothelium. Furthermore, NPs exhibit a massive surface to volume ratio, which could augment the transvesical absorption of the encapsulated drugs (Lu et al., 2004; Tyagi et al., 2016). Previous researches revealed a great potential of the bladder cancer treatment using drug-loaded polymeric NPs (Huang et al., 2012; Yan et al., 2013). In addition, Lu et al. developed rapid-releasing gelatin NPs containing paclitaxel with the particle sizes in the range of 600-1,000 nm. The results revealed that the developed NPs provided a higher drug concentrations in the tissue compared with a commercial product, paclitaxel-loaded cremophor emulsion and demonstrated substantial inhibition effects against human bladder cancer cells (Lu et al., 2004).

2.2 Colon cancer

The colon or large intestine is a tube-like organ that joins the small intestine and the rectum. Colon cancer is initiated by the abnormal and uncontrolled growth of cells that line the colon or the rectum. It occurs due to the changes of DNA within cells. Colorectal cancer is the third most common type of cancers in men and the second most widespread cancer in women. Over 1.9 million new cases of colorectal cancers have been reported in 2020 (Arnold et al., 2017; Rositch, 2020). At the early stage of colon cancer, an abnormal growth of tissues is occurred, which is known as polyps. However, if they abandoned or untreated, they can further grow into cancer. There are many risk factors for colorectal cancer such as a family history of colorectal cancer, food, alcohol consumption, smoking and bowel diseases (Labianca et al., 2010). In patients with colon cancer, the clinical manifestation depends on size, location and the stage. The clinical symptoms such as involuntary weight loss, vomit, nausea, anorexia, malaise, abdominal distension, abdominal pain, changes in bowel movements and alteration of chronic bowel habits (Mármol et al., 2017).

2.2.1 Anatomic characteristics of colon

The right colon consists of the cecum, the ascending colon, the bending of the liver, and the right half of the transverse colon. The left colon consists of the left half of the transverse colon, the spleen, the descending colon, and the sigmoid.

The surgical accessibility of colon cancer plays an important role in clear clinical management. The organ's colon begins in the lower right quadrant of the peritoneum through which the ileocecal valve moves to the bending forces of the liver in the upper right quadrant converge. In front from right to left to the spleen bend and go below the bottom. At the bottom left the quadratic colon swings towards the middle and exits the abdomen cavity into the pelvis (Hong et al., 2012).

2.2.2 Stages of colon cancer

Colon cancer is clinically defined according to the stages that the cancer is detected. The stages of colon cancer can be indicated by the invasion depth of the cancer through the intestinal wall and also the invasion into the lymph nodes and

other organs (metastases). Figure 3 shows the stages of colon cancer; each stage can be described as follows (Granados-Romero et al., 2017).

Stage 0: The cancer is still in the inner layer of the colon which can be treated by eliminating the cancer cells by local excision.

Stage I: The cancer has grown through the inner layer of the bowel, or into the muscle layer but have not spread beyond the wall.

Stage II: The cancer has spread into the outer wall of the bowel or into tissue or organs next to the bowel.

Stage III: The cancer has reached one to three lymph nodes but it has not spread to distant organs.

Stage IV: The cancer has spread to one distant site.

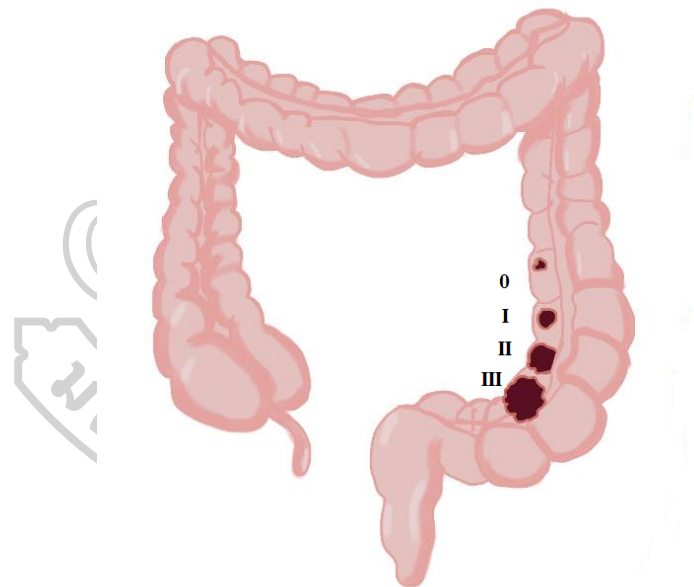


Figure 3 Stages of colon cancer

2.2.3 Treatment options

The treatment of colon cancer largely depends on the stage of the disease. Mostly, surgery is recommended for the management of colon cancer. In the late-stage cancer, the treatment may include surgery, chemotherapy, and possibly radiation therapy.

Surgery

Surgery is the key option for the management of early-stage colon cancer. If the cancer is only present in a polyp, people can require a polypectomy to remove the cancerous polyp. Surgical procedures can be performed either plain (open) or laparoscopic. Surgical continuation of the gastrointestinal tract with proximal anastomosis and colon distal (Bullard Dunn and Rothenberger, 2015). Laparoscopic colon surgery has many advantages, more than a typical open operation. The benefit in terms of short-term results is very good such as shorter hospital stays, faster return to work, better well-being, less pain after surgery, less risk of bleeding and bloating (Fleshman et al., 2007; Guillou et al., 2005).

Radiotherapy

Radiotherapy is not commonly used for the treatment of colon cancer but it is more common for the treatment of rectal cancer. The use of radiation to treat cancer depends on the stage of the disease, the type of cancer, and the health of the patient. In colon cancer, radiotherapy may be used in some specific cases; for example, it is used to shrink the tumor before surgery to facilitate cancer removal or it may be used to kill the residual cancer cells during or after the surgery. High-energy radiation is employed to destroy the cancer cells. Radiotherapy may be used for stage II or III colon cancer. The locations of colon cancer that can be targeted with radiation are the lower abdomen (Folkesson et al., 2005).

Chemotherapy

Chemotherapy is associated with the use of chemotherapeutic drugs to destroy the cancer cells. Chemotherapy can be used before the surgery in combination with radiotherapy to shrink the tumor cells. It can also be used after surgery to decrease the risk of cancer recurrence. In addition, it may slow the spread of late-stage bowel cancer and control the symptoms. However, chemotherapy can cause mild or severe side effects due to the low specificity to the cancer cells. The side effects that may occur such as nausea, vomiting, diarrhea, mouth sores, loss of appetite, and hair loss (Cascinu et al., 2003; Moertel et al., 1990).

2.3 NPs for treatment of cancer

NPs are a type of colloidal DDS with a size in the range of 10-1000 nm. NPs may provide marvelous attributes that are different from those of conventional formulation. Owing to the exceptional properties of NPs; for instance, high surface-to-mass ratio as well as their capability to carry and deliver drug compounds (De Jong and Borm, 2008). The use of NPs as drug delivery carrier can offer various advantages including:

1) They can enhance the bioavailability of the delivered drug by increasing the aqueous solubility.

2) Retention of the delivered drug in the body can be extended.

3) They can deliver a drug to the target area or a specific location in the body.

This results in the decrease in the required amount of the drug for the treatment and may lead to the decreased toxicity and side effects (Mudshinge et al., 2011).

2.3.1 Types of NPs

2.3.1.1 Solid lipid NPs (SLNs)

SLNs primarily consist of solid lipids and surfactants (Figure 4). The mean diameters size range of SLN for colloid drug delivery applications is in the range of 50 to 1,000 nm. The lipid used to formulate SLN should be non-irritant and non-toxic (Wissing and Müller, 2003). SLNs offer remarkable characteristics; for example, tiny size, high specific surface area, high drug loading ability. These properties make SLNs attractive for pharmaceutical field. In addition to the above-mentioned information, SLNs use biocompatible lipids and can be produced by organic solvent-free preparation method. Moreover, They offer improved bioavailability, improved physical stability, protection of the loaded drug from the environment, controlled and targeted drug release and low cost compared to liposomes (Mehnert and Mäder, 2001; Mudshinge et al., 2011).

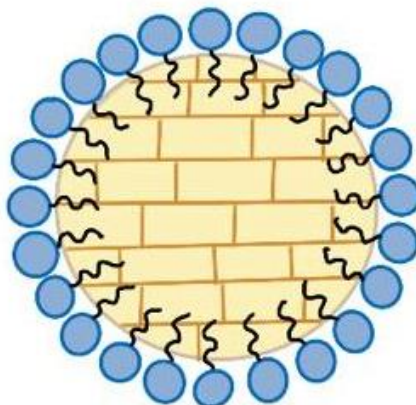


Figure 4 Structure of solid lipid NPs (SLNs)

2.3.1.2 Nanostructured lipid carriers (NLCs)

NLCs are the second-generation solid lipid nanocarriers composed of physiological and biocompatible lipids, surfactants and co-surfactants (Figure 5). They are produced by mixing solid with liquid lipids with the aim to overcome the shortcomings of SLNs in term of the drug loading and stability. NLCs are a lipid nanocarriers with a less ordered crystalline nanostructure which help to improve the payload encapsulation and prevent drug leakage. Nanoparticulate NLCs can be generated using various techniques but the most preferable one is microemulsion method. There are three types of NLCs, based on the distribution of the liquid lipid within the solid lipid matrix: Imperfect type NLCs, amorphous type NLC and multiple types NLC (Uner and Yener, 2007). They have become a promising carrier system for the delivery of drugs via various routes of application. NLCs are also being employed in cancer and gene therapy.

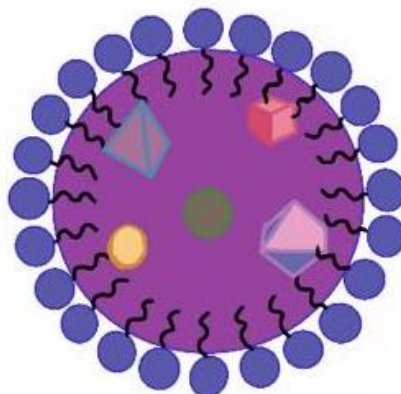


Figure 5 Structure of nanostructured lipid carriers (NLCs)

2.3.1.3 Liposomes

Liposomes are nanosized spherical vesicles consisted of phospholipids and cholesterol. They have vesicular structures with an aqueous core encircled by a hydrophobic lipid bilayer (Figure 6). Phospholipids can generate bilayers structure of liposomes due to their amphiphilic nature, having a hydrophilic polar head, and the lipophilic tail. Based on the amphiphilic properties, liposomes can be loaded with both hydrophilic and hydrophobic substances. Hydrophilic compounds are stored in the aqueous core and hydrophobic compounds are incorporated into the lipid bilayer (Pierre and dos Santos Miranda Costa, 2011). The vesicles size of liposome is an important factor affecting the circulation half-life of liposomes. On the other hand, the drug entrapment efficiency relies on both the size and the number of bilayers of liposomes. Unilamellar lipid vesicle is a single bilayer enclosing an aqueous compartment, which can be categorized into two types based on their size including small unilamellar vesicles (size between 25-100 nm) and large unilamellar vesicles (size between 100-400 nm). In case there is more than one bilayer presented in the vesicle, this type of liposomes is multilamellar vesicles (size between 0.2-10 μm) (Akbarzadeh et al., 2013; Vemuri and Rhodes, 1995). Liposomes have been exploited as potent carriers for a number of drugs; for example, antibacterials, antivirals, insulin, anticancers, and plasmid DNA.

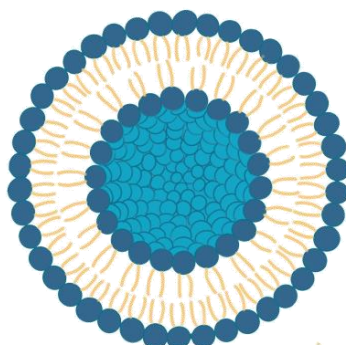


Figure 6 Structure of liposome

2.3.1.4 Polymeric NPs (PNPs)

PNPs are particulate structures with a size in the range of 10-100 nm. The PNPs are prepared from a natural polymer (albumin, CS, gelatin etc.) or synthetic polymers (polyacrylamide, polyacrylate, etc.). PNPs for drug delivery should be biodegradable and biocompatible (Parveen et al., 2012). Researchers have been interested in developing biodegradable PNPs as DDS. Drugs can be immobilized on the surface of PNPs after a polymerization reaction or encapsulated in the PNPs structure during the particle formation. Biodegradable nanosystems comprised biodegradable polymers can undergo hydrolysis in the body, producing biodegradable monomers. Kumari et al. conveyed negligible systemic toxicity related to the use of PLGA NPs as drug delivery carriers (Kumari et al., 2010; Parveen et al., 2012; Wilczewska et al., 2012).

2.3.1.5 Dendrimers

Dendritic polymers can be divided into several subclasses such as dendrimers, hyperbranched polymers, dendrigraft polymers, and dendronized polymers as presented in Figure 7. Dendrimers are polymeric materials constituted of multiple branched monomers that allocate outwardly from an innermost core. Many polymers can be utilized to generate dendrimers; for example, polyesters, polyamidoamines (PAMAMs), poly (aryl ethers), polyamines, polyamides (polypeptides), etc. Generally, PAMAM dendrimers are exploited for drug delivery

(Parveen et al., 2012). Due to their specific features, dendrimers are promising materials for drug delivery. Although dendrimers have a tiny size, their dendritic features and branching permit drug loading to the exterior surfaces of the dendritic structure. Conjugation of specific antibodies on the surface of dendritic structure may also increase the targeting ability (De Jong and Borm, 2008).

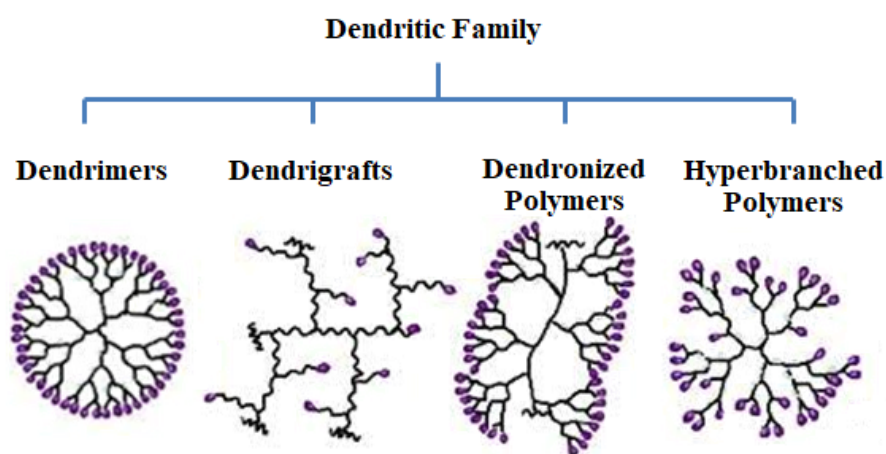


Figure 7 Schematic picture of sub-classes in the dendritic family.

2.3.2 Therapeutics NPs

NPs have been widely used as drug delivery platforms. NPs can be applied to deliver a number of therapeutic agents including anticancer therapeutics, genetic materials, antimicrobial agents, vaccine, etc. They can also offer site-specific targeting to a target area to avert the adverse effects of the drugs being delivered. Various anticancer agents; for example, paclitaxel, DOX, carboplatin, etoposide, etc., have been successfully loaded onto NPs, and these nanocarriers demonstrate potent activity against many types of tumors. Moreover, biomolecule can be conjugated onto the surface of NPs to obtain potential therapeutic agents with improved targeting ability. Biomolecule-functionalized NPs are being exploited for targeted gene silencing. Numerous NPs are developed as potential therapeutic systems (Parveen et al., 2012).

2.4 Doxorubicin (DOX)

DOX is an anthracycline antitumor derived from the *Streptomyces peucetius*. It is commonly used in the treatment of several cancers including gastric cancer, thyroid cancer, breast cancer, lung cancer, ovarian cancer, pediatric cancers, multiple myeloma, lymphoma, and sarcoma (Arcamone et al., 1969; Cortés-Funes, 2007; Keizer et al., 1990; Thorn et al., 2011). DOX inhibits cell growth by directly hindering DNA synthesis and transcription (Yu et al., 2020). DOX has the widest range of clinical application compared to other anticancer medications. Although it has well-defined toxicity profile including cardiac toxicity and myelosuppression, DOX are generally used in combination chemotherapy treatment (Cortés-Funes, 2007)

2.4.1 Chemical structure

The chemical structure of DOX is presented in Figure 8. DOX contains insoluble tetracycline aglycone and soluble reduced sugar daunosamine sugar many parts of the molecule can participate in the metabolism of DOX.

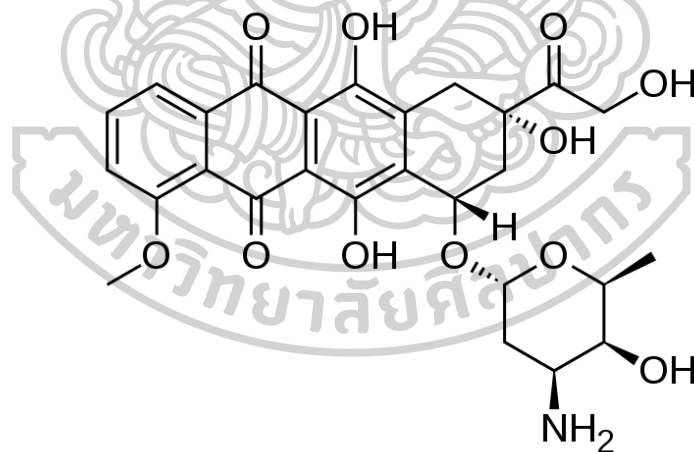


Figure 8 Structure of DOX

2.4.2 Mechanisms of action of DOX

DOX inhibits tumor growth by intercalating between base pairs in the DNA helix which results in constraint of DNA replication and eventual protein synthesis hindrance. In addition, DOX inhibits topoisomerase II which leads to an increased and

stabilized cleavable enzyme-DNA linked complex during DNA replication and subsequently prevents the ligation of the nucleotide strand after double-strand breakage. DOX also forms oxygen free radicals which cause cytotoxicity by lipid peroxidation of cell membrane lipids; the formation of oxygen free radicals also related to the cardiotoxicity of DOX (Zunino and Capranico, 1990).

2.4.3 Side effects

Besides the efficacy, DOX can cause undesirable effects. The common side effects of DOX include:

- Cough together with fever or chills
- Darkening skin or skin redness
- Shortness of breath
- heart arrhythmia
- Stomach pain
- Joint pain
- Lower back pain along with fever or chills
- Painful or difficult urination along with fever or chills
- Red streaks along the injected vein
- Pain at the injection site
- Swollen feet and lower legs

Rare side effects of DOX include:

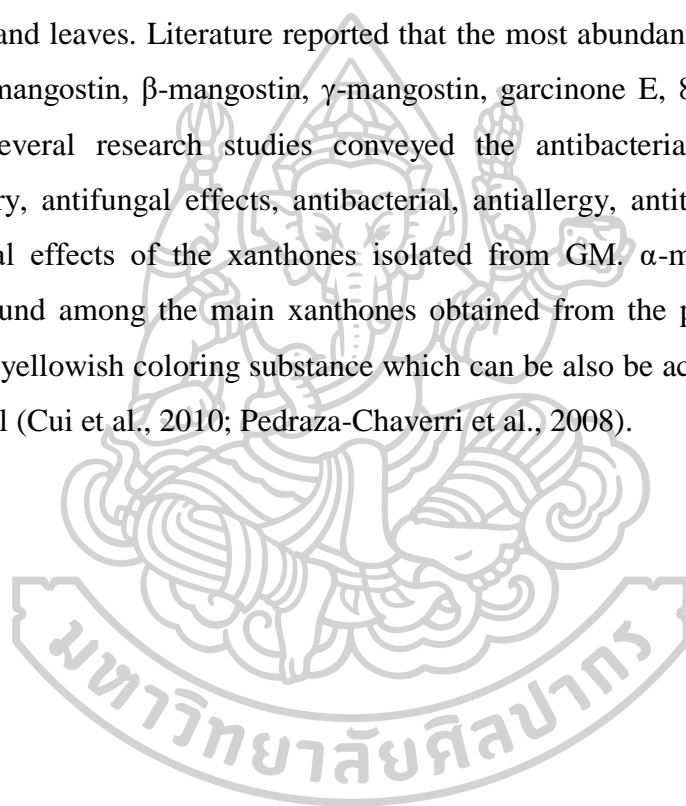
- Hematuria
- Unusual bleeding
- Isolate red spots on the skin
- Black, tarry stools

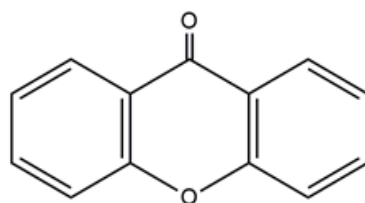
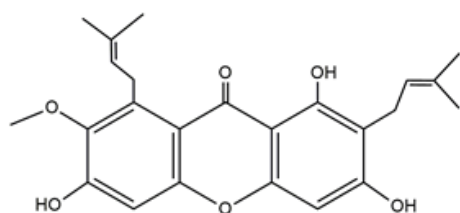
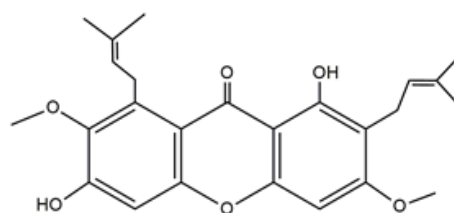
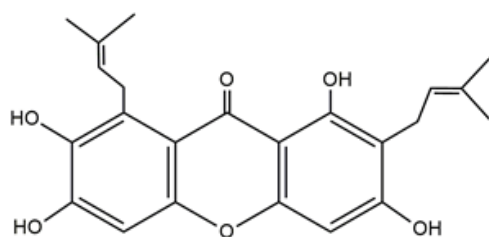
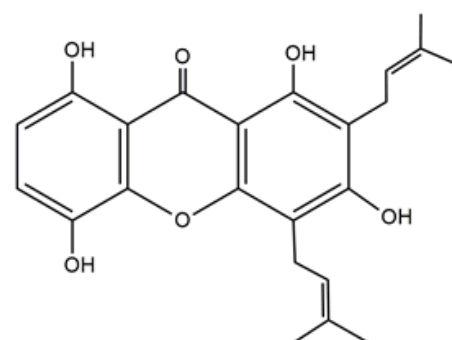
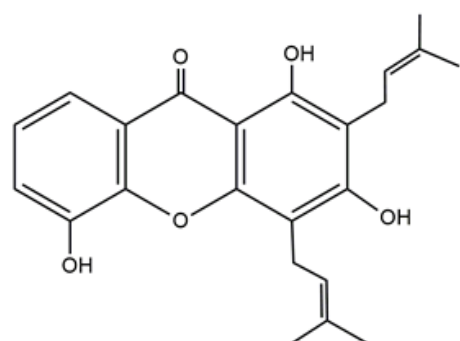
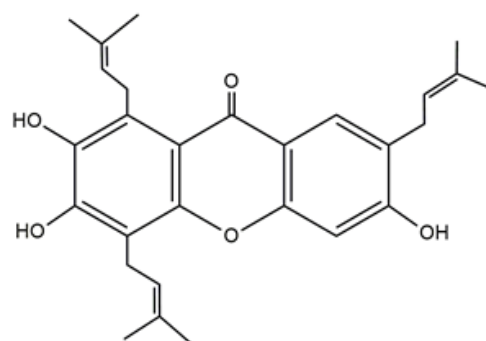
2.5 *Garcinia mangostana* (GM)

Mangosteen (*Garcinia mangostana* L.) is a kind of fruit in the Clusiaceae family that cultivates in the Asian countries such as Sri Lanka, Malaysia, Myanmar, Philippines, India and Thailand (Pedraza-Chaverri et al., 2008). The fruit is dark purple or reddish and comprises soft and juicy eatable white pulps inside. GM is also defined as the “queen of fruits” owing to its exceptional flavor. The taste is

somewhat acidic and sweet and it has a pleasant smell. GM has been exploited as traditional medicine for a long time in treatment of various illnesses; for instance, wounds, skin infections, and amoebic dysentery. In Ayurvedic medicine, the pericarp of GM fruit can be used for inflammation, trauma, diarrhea chronic ulcer, abdominal pain, cholera, and dysentery (Ovalle-Magallanes et al., 2017b; Pedraza-Chaverri et al., 2008).

Mangosteen contains many active phytochemical compounds. Prenylated xanthenes have been discovered in many parts of GM such as the pericarp, whole fruit, bark, and leaves. Literature reported that the most abundant xanthenes found in GM are α -mangostin, β -mangostin, γ -mangostin, garcinone E, 8-deoxygartanin, and gartanin. Several research studies conveyed the antibacterial, anti-cancer, anti-inflammatory, antifungal effects, antibacterial, antiallergy, antitumoral, antioxidant, and antiviral effects of the xanthenes isolated from GM. α -mangostin (Figure 9) which is found among the main xanthenes obtained from the pericarps of the GM fruit. It is a yellowish coloring substance which can be also be acquired from the GM plant as well (Cui et al., 2010; Pedraza-Chaverri et al., 2008).



**Xanthone nucleus** **α -mangostin** **β -mangostin** **γ -mangostin****Gartanine****8-deoxygartanine****Garcinone E****Figure 9** Chemical structure of the most common xanthones found in GM.

2.5.1 The medicinal properties of GM extracts

Antioxidant properties

The antioxidant activity of GM extracts and xanthenes isolated from GM has been extensively reported. Antioxidant assay of GM extract and their xanthone derivatives using 2,2-diphenyl-1-picrylhydrazyl (DPPH) and the 2,20-azino-bis-(3-ethylbenzthiazoline-6-sulfonic acid (ABTS) were conveyed (Haruenkit et al., 2007). Chomnawang et al. (2007) revealed that ethanolic extracts of GM exhibited a high antioxidant activity as determined by DPPH assay ($IC_{50}= 6.13 \mu\text{g/mL}$) (Chomnawang et al., 2007). Haruenkit et al. (2007) also reported the potent antioxidant activity of GM extracts determined by DPPH and ABTS assays (Haruenkit et al., 2007).

Antitumor activity

Matsumoto et al. (2003) investigated the anticancer activity of the xanthenes obtained from GM fruit pericarp, including α -, β - and γ -mangostins, mangostinone, garcinone E, and 2-isoprenyl-1,7-dihydroxy-3-methoxy xanthone on human leukemia cell line (HL60). After 72-h treatment with the xanthenes at 5 or 40 μM , all xanthenes demonstrated a significant inhibition effect. The most abundant xanthone found in the GM extract is α -mangostin, and it exhibited the highest inhibitory effect compared to other xanthenes. The anticancer activity of α -mangostin is also demonstrated in other leukemia cell lines such as K562, NB4 and U937 cells, and the finding revealed a potent inhibition effect of α -mangostin against these leukemia cell lines (Matsumoto et al., 2004). Moongkarndi et al. (2004) also assessed the antiproliferative activity of 9 Thai medicinal plants against the SKBR3 human breast adenocarcinoma cell line, and they found that GM extract provided the most potent effect with an IC_{50} value of $15.45 \pm 0.5 \mu\text{g/mL}$ (Moongkarndi et al., 2004). The anticancer effects of xanthenes extract, α -mangostin and γ -mangostin on human colorectal cancer cells line (HCT 116) were also investigated by Aisha et al. In addition, the *in vivo* anticancer activity was also conducted on subcutaneous tumors formed in colon of nude mice. The xanthenes extract, α -mangostin and γ -mangostin exhibited inhibition effect against colon cancer cells in dose-dependent manner, with IC_{50} value of $6.5 \pm 1.0 \mu\text{g/mL}$, $5.1 \pm 0.2 \mu\text{g/mL}$ and $7.2 \pm 0.4 \mu\text{g/mL}$ respectively. In addition, the xanthenes extract was able to significantly inhibit the growth of

subcutaneous tumor of HCT 116 cells in nude mice. Therefore, α -mangostin may be a potential candidate compound for cancer treatment (Aisha et al., 2012).

Antibacterial and antifungal properties

The antibacterial and antifungal properties of xanthenes and GM extracts have been conveyed in many publications. Sundaram et al. (1983) investigated the antibacterial and antifungal activities of α -mangostin and its derivatives. Their findings revealed that α -mangostin was able to completely inhibit various bacteria including *S. aureus*, *P. aeruginosa*, *S. typhimurium*, and *B. subtilis*, whereas *Proteus spp.*, *Klebsiella spp.* and *E. coli* showed partial susceptibility to the xanthenes. The antimicrobial effect on various fungi was also reported. *E. floccosum*, *A. solani*, *Mucor spp.*, *Rhizopus spp.*, and *C. echinulata* were shown to be susceptible to xanthenes, whereas *T. mentagrophytes*, *M. canis*, *A. niger*, *A. flavus*, *Penicillium spp.*, *F. roseum*, and *C. lunata* showed only partial susceptibility to the compounds. The antibacterial and antifungal efficiency of the xanthenes was as in the order: α -mangostin > isomangostin > 3-O-methyl mangostin > 3,6-di-O-methyl mangostin. Mangostin triacetate exhibited no activity against the tested microorganisms (Pedraza-Chaverri et al., 2008; Sundaram et al., 1983).

2.6 Mucoadhesive DDS

In 1980, the concept of mucosal adhesion was first introduced by a researcher. Since then, the concept of mucosal adhesion has received more attention from researchers around the world (Ahuja et al., 1997). The mucosal adhesion of polymers can be enhanced by various techniques; for instance, the use of polyethylene glycol (PEG) or polymer adhesion conjugate etc. The benefit of the mucosal attachment system was initially found to be a promising system for increasing the retention time to release the drug at the absorption site and develop a DDS that can overcome the barriers that result from human anatomy.

Mucosal DDS can extend the retention of the dosage form at the application area or absorption site. The DDS facilitate a close contact of the formulation with the underlying absorption membrane and thus augment the therapeutic efficacy of the drug (Ahuja et al., 1997). Generally, drugs often have to pass through a mucosal surface in the body to be effectively absorbed into the body. Mucous membranes are

located in several parts of the body such as the eyes, GI tract, reproductive organs and respiratory tract. Mucoadhesive materials may take a variety of forms such as patches, tapes, semisolids, films, powders, tablets, *in situ* gelling systems, microgels, and NPs (Shitrit and Bianco-Peled, 2017). Advanced micro- and nano-carriers with new strategies including mucoadhesive and mucopenetration are developed to improve transmucosal drug delivery (Bernkop-Schnürch, 2005).

Xu et al. developed catechol-CS hydrogel by crosslinking catechol-CS with genipin for buccal drug delivery with improved mucoadhesion. The functionalized catechol moieties considerably increased the adhesive properties of the materials as investigated on a porcine buccal mucosal membrane. In addition, the hydrogel was able to successfully deliver lidocaine through rabbit buccal mucosal membrane *in vivo* (Xu et al., 2017). Shitrit and Bianco-Peled developed a novel mucoadhesive polymer by conjugating CS with poly(ethylene glycol)diacrylate (PEGDA) using the Michael-type addition reaction. The synthesized polymer demonstrated improved mucoadhesive properties compared to non-modified CS and thiolated CS as investigated by tensile study and rotating systems. The rheology study showed a synergistic rise in the viscosity of the CS-PEGAc/mucin mixtures representing the strong interaction between the synthesized CS and mucin (Shitrit and Bianco-Peled, 2017).

2.6.1 Mucoadhesive polymer

Mucoadhesive polymers generally contain various hydrophilic moieties; for example, hydroxyl, amide, carboxyl, and sulfate in their polymer chains. These groups are able to attach to mucosal membrane by several forces including hydrogen bonding and hydrophobic or electrostatic interactions. These hydrophilic polymers can also swell once contact with water and become sticky. The potential polymer for a mucoadhesive DDS should demonstrate the following features; nontoxic, non-absorbable, nonirritant, Strong bond formation and quick adherence to the mucus membrane, allowance of drug incorporation and release, good stability, and low cost (Shaikh et al., 2011).

The polymer with mucoadhesive properties can be divided into first-generation and second-generation polymers.

2.6.1.1 First-generation mucoadhesive polymer

The first-generation mucoadhesive polymers are natural or synthetic hydrophilic polymers consisting of many chemical groups that can form hydrogen bonds with mucous membrane such as carboxyl, hydroxyl, and amino groups. First-generation mucoadhesive polymers adhere nonspecifically to mucosal surfaces and cannot provide sufficient retention time, and may not have the potential for specific drugs delivery (Boddupalli et al., 2010).. The polymers in this group can be divided into 3 types: cationic polymers (CS), anionic polymers (carbopol and Alg) and nonionic polymer (hydroxypropyl methylcellulose, carboxymethylcellulose or carboxymethylcellulose sodium salt, etc.).

Chitosan

CS is a natural cationic polysaccharide which is the copolymer of N-acetyl-D-glucosamine and D-glucosamine generated by alkaline deacetylation of chitin (Figure 10). Chitin is the second most abundant biopolymer retrieved from the shell of crustaceans, the cuticles of insects, and the cell walls of fungi. Structurally, chitin is a straight-chain polymer composed of β -1,4-N-acetylglucosamine and chitin is in nature in three different polymorphic forms, with varying properties, and the different polymorphic forms are classified into α -, β - and γ -chitin (Anitha et al., 2014). CS is a derivative of chitin with a pKa of around 6.5-7.0. Based on the pKa value, CS is insoluble at neutral and alkaline media but is soluble in acidic pH (Rinaudo, 2006). CS is promising polymer for drug deliver due to its biocompatibility, biodegradability, and low toxicity. In addition, it exhibited excellent antimicrobial activity against a broad range of bacteria, fungi, and yeast (Badawy and Rabea, 2013). CS also displays other specific properties such as hemostatic activity, osteo-compatibility, osteoconductivity, and mucoadhesive properties. CS has been applied in various fields such as in food and nutrition, material science, biotechnology, environmental protection, agriculture, and pharmaceutical fields.

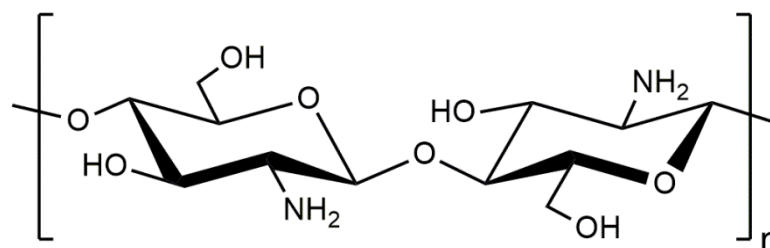


Figure 10 The chemical structure of CS

Mucoadhesive properties of CS are associated with the generation of secondary chemical bonds such as hydrogen bonds or ionic interactions between the positively charged amino groups of CS and negatively charged sialic acid groups of mucin glycoproteins (Rossi et al., 2001; Singla and Chawla, 2001).

Carbopol

Carbopol is an anionic synthetic hydrophilic polymer. The chemical structure of carbopol is presented in Figure 11. Carbopol can form gels at pH above 7.3 and therefore provide a pH-dependent release. There are many grades of Carbopol including carbopol 910, carbopol 934, carbopol 940, carbopol 941, and carbopol 1342. Different grades of Carbopol have different properties; carbopol 934 is not resistant to light, heat, and electrolytes, resulting in the reduction of the viscosity after long-time exposure. It is well known that cationic drugs form complexes with either anionic polymer. Carbopol has been reported to have good mucoadhesive properties, biodegradable, and environmentally responsive. The polymer can protect a drug from its physiological environment by improving its stability *in vivo* (Putz and Burghelea, 2009; Sahoo et al., 2011).

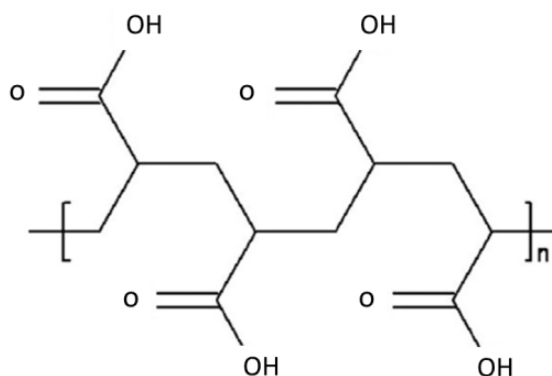


Figure 11 The chemical structures of carbopol

Alginate (Alg)

Alg is a natural anionic polymer, obtained from brown algae and bacteria. Alg is a polysaccharide with heteropolymers of 1→4 linked α -L-galuronic acid (G) and β -D-mannuronic acid (M), linearly linked by 1,4-glycosidic linkages (Figure 12) (Paques et al., 2014). Due to its unique property, Alg can form complex with calcium to form calcium-Alg gel through interaction between Ca^{2+} ions and carboxylate residues of G-blocks of Alg. This property of Alg has been employed to develop Alg beads for drug delivery of various compounds such as indomethacin, acetaminophen, and ketoconazole (Mallikarjuna Setty et al., 2005). Ca^{2+} has been reported to be used a crosslinking agent for the acid groups of Alg, it selectively binds to the guluronic acid units to form an ‘egg-box’ model (Patil and Sawant, 2009). Preparation of Alg hydrogels is reported by conventional crosslinking with calcium salts (Lee et al., 2013). Alg polymers have been broadly applied in pharmaceutical and biotechnological fields, including DDS, as they are biodegradable, biocompatible, and mucoadhesive.

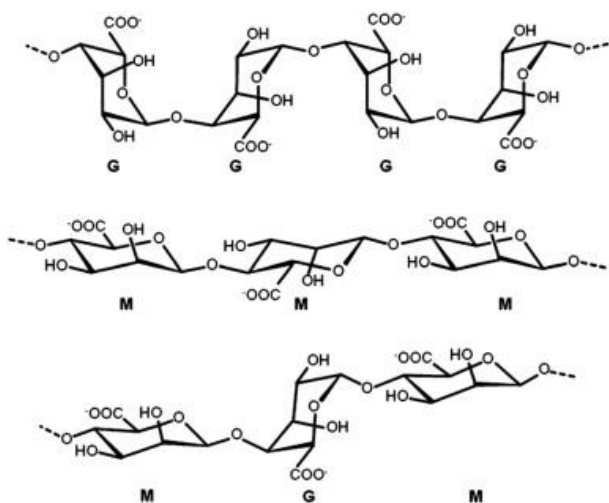


Figure 12 The chemical structures of G-block, M-block and alternating block in Alg. Source: Paques, J. P. et al. "Preparation methods of Alg NPs." *Advances in Colloid and Interface Science* 209, (2014): 163-171.

Hydroxypropyl methylcellulose (HPMC)

HPMC is a non-ionic cellulose ether derivative (Figure 13) for use in controlled-release preparations. It can be dissolved as well in water and organic solvents but is insoluble in hot water and alcohol (Ishikawa et al., 2000). The polymers are non-toxic, easy to handle, and do not require any special manufacturing technology. HPMC provides release, which is dependent on the pKa of the drug (Tahara et al., 1995).

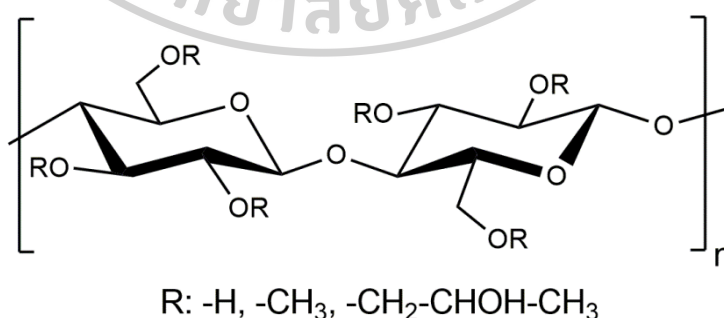


Figure 13 The chemical structures of hydroxypropyl methylcellulose

2.6.1.2 Second generation mucoadhesive polymer

The polymers in this group contain specific chemical structures that could strongly bind or adhere to the cell or mucus surface. Some species have some inhibitory properties and some are specific to certain epithelial tissues, some can form specific covalent bonds that form functional groups. Examples of second-generation mucoadhesive polymers are thiolated polymer or thiomers, acrylates, catechols, and maleimides.

Thiolate polymers

Thiolated polymers or thiomers are a molecular design of polymers that contain free thiol groups (-SH) on the polymer backbone. The thiol groups are supposed to interact with cysteine-rich subdomains of mucus glycoproteins, prolonging the adhesion of the polymer to the mucus layer (Duggan et al., 2017). Due to these beneficial features for mucoadhesive drug delivery, several groups worldwide work on the modification of CS to further improve its properties. Besides derivatives such as CS iminothiolane, PAA homocysteine, PAA cysteine, and Alg cysteine (Figure 14) (Madhav and Tangri, 2011).

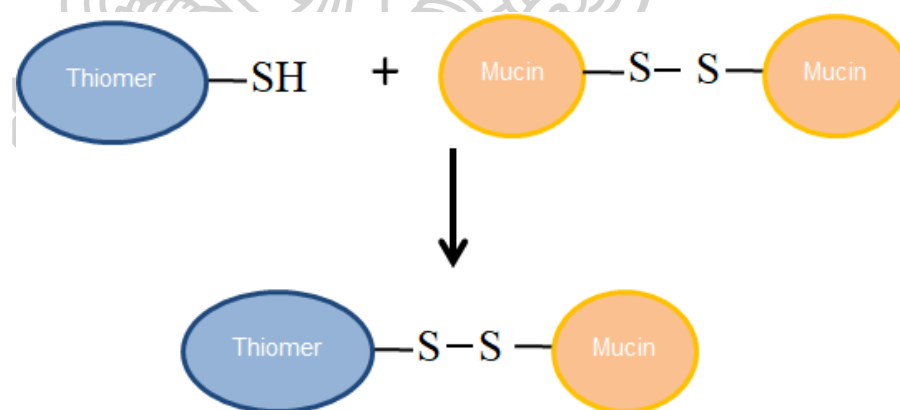


Figure 14 Schematic of thiolated polymers covalently binding mucin glycoproteins

Acrylates

Acrylate polymers are conveyed as a new class of mucoadhesive materials due to an acrylate end group that can form interaction with the mucin-type glycoprotein by the Michael-type addition reaction (Figure 15) (Davidovich-Pinhas and Bianco-Peled, 2010). There are many reports conveyed about the development of acrylate mucoadhesive materials. For example, CS grafted poly(ethylene

glycol)diacrylate (PEGDA) was synthesized to improve the mucoadhesive properties of the DDS. It was found that the new polymer could increase the mucoadhesive properties of CS and provided promising potential to be used as delivery vehicle for mucosal drug delivery (Shitrit and Bianco-Peled, 2017).

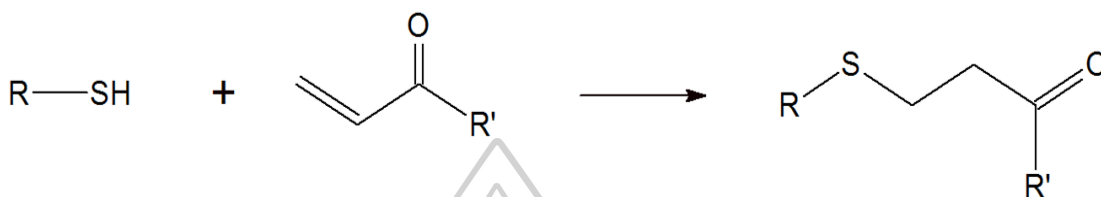


Figure 15 Schematic of acrylate polymers covalently binding mucin glycoproteins

Catechols

1,2-Dihydroxybenzene (Catechol) is found in a marine mussel called *Mytilus californianus*. Their adhesion potential was first studied by Waite (Waite, 1985). It secretes catechol-containing compound which takes part in the underwater adhesion of marine mussels. Attachment is mediated by the byssus, a bundle of silky threads that is proximally connected to the animal by a rootlike process and distally connected to a foreign surface by adhesive pads (Figure 16). Which can physically adhere to biotic and abiotic objects for essential activities such as movement and self-defense (Ninan et al., 2003). Although there have been significant advances in the introduction of catechols such as pyrocatechol, hydrocaffeic acid and dopamine, etc. (Figure 17) as enhance adhesion through chemical modifications of natural and synthetic polymers. The application of these materials as mucoadhesive has been somewhat limited to the enhancement of the mucoadhesive properties. One advantage of using catechol is that catechol derivatives are commercially available for bioconjugation to amine or carboxylic acid groups. Furthermore, it has the ability to form irreversible covalent bonds with thiols and amines via the formation of o-quinone by catechol oxidation.

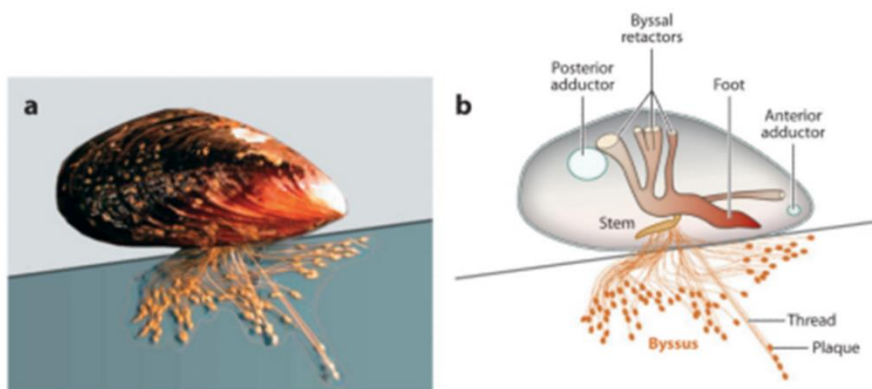


Figure 16 Adhesion in the marine mussel *Mytilus californianus*. (A) Adult mussel exhibiting extensive byssus attached to a mica surface. (B) Schematic mussel on a half-shell.

Source: Lee, B. P. et al. "Mussel-Inspired Adhesives and Coatings" **Annual Review of Materials Research** 41, (2011): 99-132.

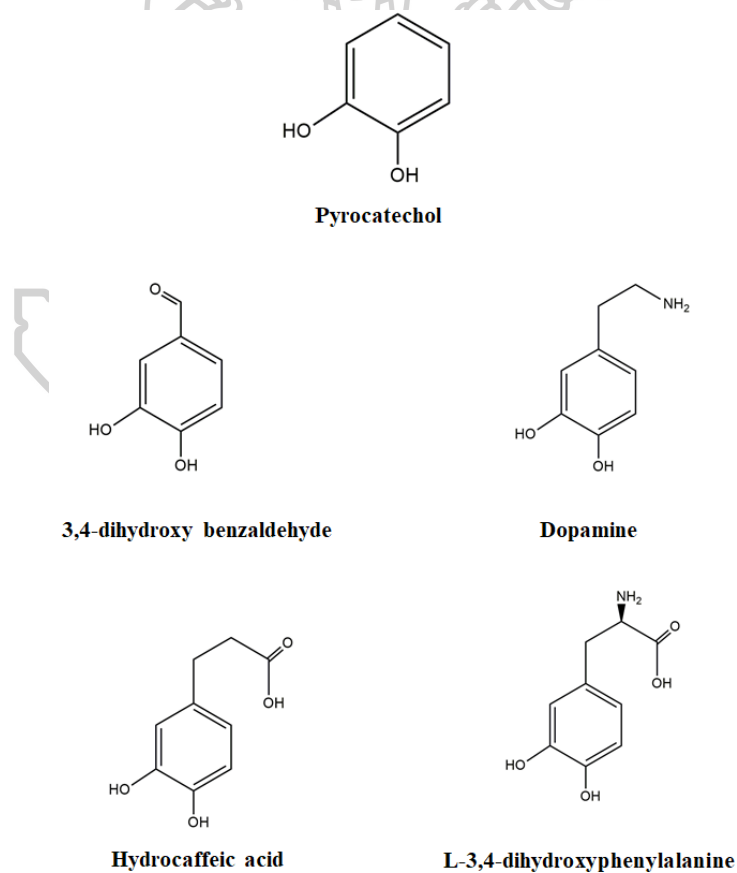


Figure 17 Examples of catechol-containing molecules used to modify polymer backbones.

Maleimides

One of the latest advances in the synthesis of mucoadhesive material is the exploitation of the well-known maleimide. Some studies reported that maleimide, vinyl sulfone, iodoacetamide, and orthopyridyl disulfide units can interact with a free cysteine residue in the protein, and they have been used in bioconjugation with protein. A recent study indicated that maleimide has high activity and selectivity toward the cysteine residues present at the mucin surface (Figure 18).

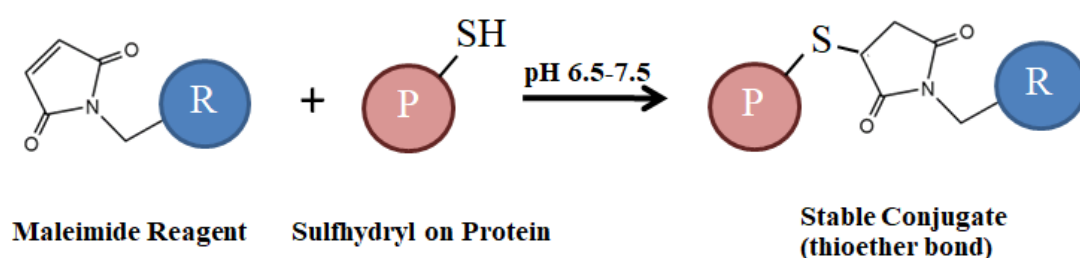


Figure 18 Schematic of maleimide material covalently binding mucin glycoproteins

2.6.1.3 Synthesis of mucoadhesive polymer

Recently, researchers have discovered that polymers with catechol functional groups offer excellent mucoadhesive properties. The catechol-containing compound from *Mytilus edulis* mussel is used by the mussels to stick to many surfaces under the sea. This compound is protein-rich in 3,4-dihydroxyphenylalanine (DOPA). DOPA contains catechol functional groups, which are responsible for the strong adhesion bond such as hydrogen bonds and covalent bonds with a surface. DOPA-quinone can further react with other functional groups by three main pathways: self-crosslinking, involving coupling of two DOPA molecules, Michael addition with $-SH$ or $-NH_2$ group and Schiff-base reaction with $-NH_2$ (Xu et al., 2015). The catechol polymers (such as CS-catechol, poly(acrylic acid-g-dopamine), etc.) have been developed to increase the mucoadhesive properties (Kim et al., 2015; Lee et al., 2018).

In 2016, Tonglairoum et al. firstly introduced the use of polymeric nanogels containing maleimide on the surface of nanogels to assist in mucoadhesion. The maleimide functional group has high reactivity and selectivity toward the

sulfhydryl group (-SH) at the mucin surface *via* a Michael-type addition reaction between the maleimide group and sulfhydryl group (-SH) of mucin. This group is normally used in the delivery of protein. Adhesion between polymeric materials and the mucosal layer has been investigated as a means for prolonging residence times of delivery vehicles at the site of application or absorption, therefore, providing an improvement in drug bioavailability and therapeutic effects (Tonglairoum et al., 2016).

2.6.1.4 Mucoadhesive mechanism

The basic process of mucosal adhesion consists of two steps including contact stage and consolidation stage, as illustrated in Figure 19. In the contact phase, the polymer comes close to the moist surface of the mucosal layer, then it becomes wet or swollen. In the consolidation stage, the polymers interpenetrate into the surface of the mucin and form physical or chemical bonds with the mucosal membrane through various interaction such as Van der Waals forces, electrostatic interactions, a hydrogen bond or strong covalent bonds (Boddupalli et al., 2010).

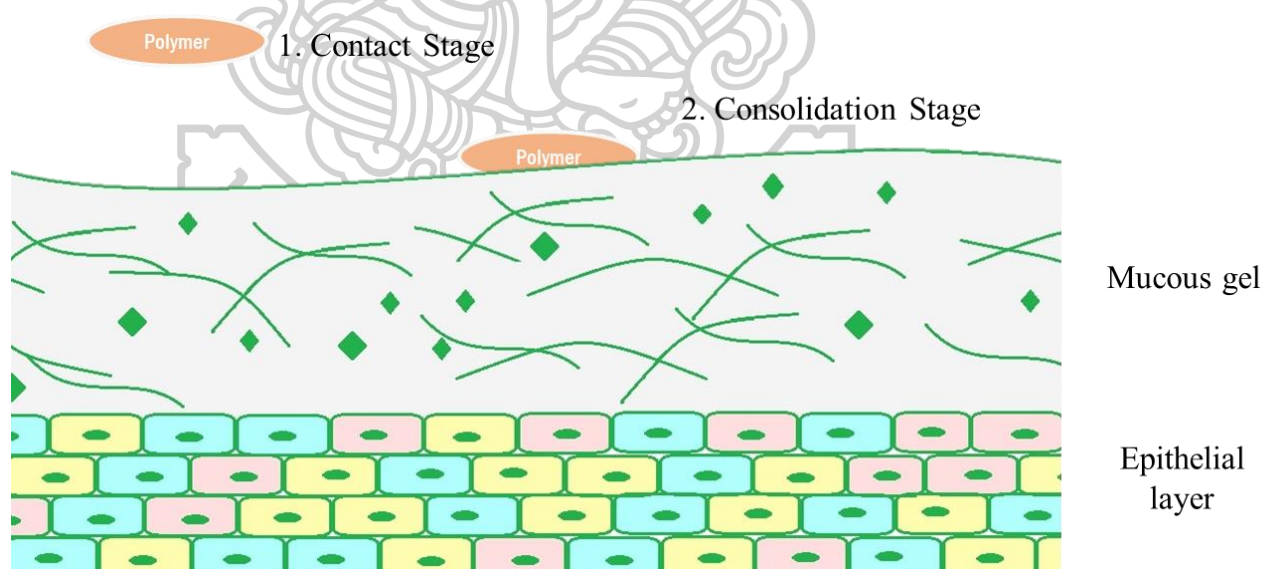


Figure 19 Mucoadhesive mechanism

CHAPTER 3

MATERIALS AND METHODS

3.1 Materials

3.2 Equipment

3.3 Methods

3.3.1 Synthesis of mucoadhesive polymers

3.3.1.1 Synthesis of Cys-CS

3.3.1.2 Synthesis of MHA-CS

3.3.1.3 Synthesis of Cat-Alg

3.3.2 Characterization of the synthesized polymers

3.3.2.1 NMR

3.3.2.2 FT-IR

3.3.3 Determination of mucoadhesive functional groups

3.3.3.1 Thiol content of Cys-CS

3.3.3.2 Maleimide group content of MHA-CS

3.3.3.3 Catechol group content of Cat-Alg

3.3.4 Mucoadhesive properties of the synthesized polymer

3.3.4.1 Rheology method

3.3.4.2 *Ex-vivo* mucoadhesion assay (Tensile testing method)

3.3.5 Cytotoxicity of the synthesized polymers on normal cells

3.3.6 Preparation of the mucoadhesive NPs

3.3.6.1 Cat-Alg NPs

3.3.6.2 MHA-CS and Cys-CS NPs

3.3.6.3 MHA-CS-Alg-Cat NPs

3.3.7 Evaluation of NPs

3.3.7.1 DLS measurements

3.3.7.2 Morphology of the NPs

3.3.7.3 Mucoadhesive properties of the NPs

3.3.7.3.1 Porcine bowel mucosa

3.3.7.3.2 Porcine bladder mucosa

3.3.8 GM extract-loaded NPs

3.3.8.1 Standardization and assay of GM extract

3.3.8.2 Preparation of GM extract-loaded NPs

3.3.8.3 Determination of percentage loading efficiency and loading capacity

3.3.8.3 Standardization and assay of GM extract

3.3.8.4 Release of GM extract-loaded NPs

3.3.9 DOX-loaded NPs

3.3.9.1 Preparation of DOX-loaded NPs

3.3.9.2 DOX assay

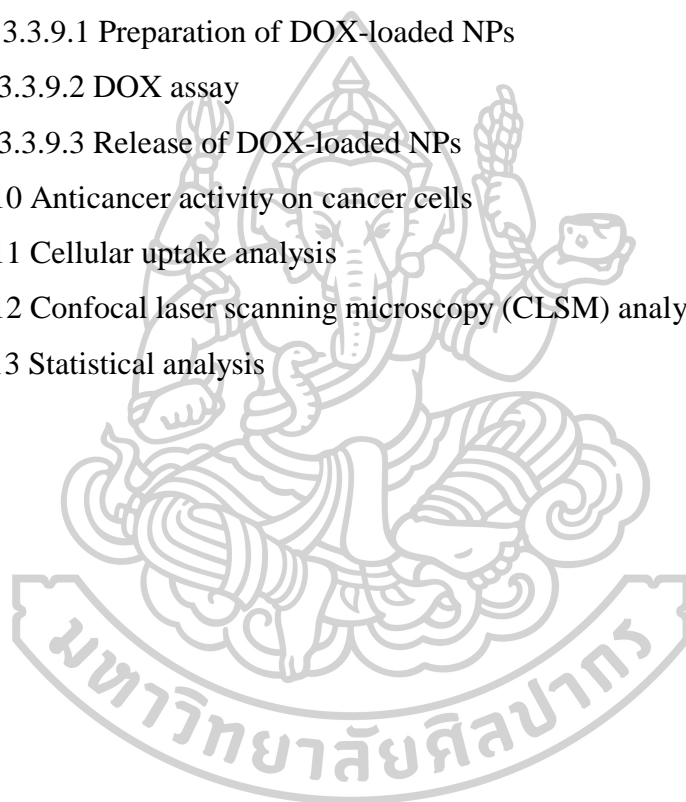
3.3.9.3 Release of DOX-loaded NPs

3.3.10 Anticancer activity on cancer cells

3.3.11 Cellular uptake analysis

3.3.12 Confocal laser scanning microscopy (CLSM) analysis

3.3.13 Statistical analysis



3.1 Material

Chitosan (degree of deacetylation = 0.95, molecular weight = 11 KDa)

(OliZac Technologies Co., Ltd., Pathumthani, Thailand)

Alginic acid sodium salt (Sigma Aldrich[®], St. Louis, MO, USA)

6-maleimidohexanoic acid (MHA)(Sigma Aldrich[®], St. Louis, MO, USA)

1-ethyl-3-(3-dimethylamino propyl) carbodiimide (EDAC) (Sigma Aldrich[®], St. Louis, MO, USA)

N-hydroxysulfosuccinimide (NHS) (Sigma Aldrich[®], St. Louis, MO, USA)

Dopamine hydrochloride(Sigma Aldrich[®], St. Louis, MO, USA)

L-Cysteine hydrochloride monohydrate (Sigma Aldrich[®], St. Louis, MO, USA)

5,5-dithio-bis-(2-nitrobenzoic acid) (DTNB)(Sigma Aldrich[®], St. Louis, MO, USA)

α -Mangostin (Sigma Aldrich[®], St. Louis, MO, USA)

Doxorubicin hydrochloride (Sigma Aldrich[®], St. Louis, MO, USA)

Mucin from the porcine stomach (Type II) (Sigma Aldrich[®], St. Louis, MO, USA)

Calcium chloride anhydrous (QR \ddot{e} C, New Zealand)

All other chemicals

Acetic acid (Fisher Scientific, UK Limited, UK)

Acetronite HPLC grade (RCI Labscan Limited, Bangkok, Thailand)

Dimethyl sulphoxide (DMSO) (Fisher Scientific, UK Limited, UK)

Ethanol (RCI Labscan Limited, Bangkok, Thailand)

Hydrochloric acid (37%) (Scharlau Chemie S.A., Spain)

Methanol (RCI Labscan Limited, Bangkok, Thailand)

Orthophosphoric acid (Fluka, Buchs, Switzerland)

Potassium chloride (Ajax Finechem Australia, New Zealand)

Potassium dihydrogen phosphate (Ajax Finechem Australia, New Zealand)

Potassium phosphate (Ajax Finechem Australia, New Zealand)

Sodium chloride (Ajax Finechem Australia, New Zealand)

Sodium dihydrogen phosphate (Ajax Finechem Australia, New Zealand)

Sodium phosphate (Ajax Finechem Australia, New Zealand)

Sodium tripolyphosphate (Sigma Aldrich[®], St. Louis, MO, USA)

3.2 Equipment

Aluminium foil

Beakers (50, 100, 250, 500, 1000 mL)

Centrifuge (HERMLE Z300K: Labnet; Lab Force Co., Ltd., Bangkok, Thailand)

Cylinders (10, 25, 50, 100, 1000 mL)

Dialysis bag (SnakeSkin[®] 3.5K, 3.5 mm, USA)

Filter papers

Fourier transform infrared spectrophotometer (FT-IR, Nicolet 4700, USA)

Freeze-dryer (Model: Freezone 2.5, LABCONCO, USA)

Freeze/Refrigerator -20 °C, -80 °C

Hand hydraulic press machine (Specac P/N 15011/25011, UK)

High-performance liquid chromatography (HPLC) instrument (Agilent Technology, USA)

Hot air oven (WTB Binder, Germany)

Magnetic stirrer and magnetic bar (Framo, Germany)

Micropipette (2-20 µL, 20-200 µL, 100-1000 µL)

Micropipette tips

Microplate (96 Well plate)

Nuclear magnetic resonance (NMR) (NMR 300 MHz, AVANCE III HD, Bruker)

pH meter (Horiba compact pH meter B-212, Japan)

Rheometer (DSR Malvern–Kinexus Pro, USA)

Shaking incubator (SHEL LAB, Model: SI4, Gibtahi Co., Ltd., Bangkok, Thailand)

Syringe 5, 10 mL

A syringe pump (Model: NE-300, New Era Pump Systems Inc.)

Texture analyzer (TA.XT plus, stable MicroSystems, UK)

Vacuum rotary evaporator

VertiSep[®] AQS C18 column (250 mm × 4.6 mm, 5 µm particle size)

Vortex mixer (VX100, Labnet, NJ, USA)

Water bath (Hetofrig CB60, Heto High Technology of Scandinavia, Birkerod, Denmark)

Well-plate (96 Well plate) (Corning Incorporated, NY, USA)

Zetasizer Nano ZS (Malvern Instruments, Malvern, UK)



3.3 Methods

3.3.1 Synthesis of mucoadhesive polymers

3.3.1.1 Synthesis of Cys-CS

Cys-CS conjugate was created by a chemical reaction between chitosan and L-cysteine employing EDAC as a catalyst. CS and L-cysteine were separately dispersed and liquified in 1% v/v HCl and deionized (DI) water, respectively. The carboxylic acid moieties of L-cysteine were activated with 150 mM EDAC for 20 min. The solutions are mixed for 6 h using a magnetic stirrer before being purified via dialysis and lyophilization. The obtained polymer was characterized using FT-IR and NMR.

3.3.1.2 Synthesis of MHA-CS

MHA-CS was produced from MHA and CS using EDAC as a catalyst. MHA was liquified in DI water. The carboxylic acid groups of MHA were activated with 150 mM EDAC for 20 min. Then, the mixture solution was contained in the CS solution dissolved in 1% v/v HCl in a reaction flask and continuously mixed for 18 h at 25 °C before being dialyzed against DI water followed by lyophilization. The synthesized product was confirmed using FT-IR and NMR.

3.3.1.3 Synthesis of Cat-Alg

The Cat-Alg conjugate was synthesized by a chemical reaction using EDAC and NHS as catalysts. To perform the synthesis, Alg was dispersed in distilled water at a concentration of 1% (w/v). EDAC and NHS were then included in the Alg solution at a molar ratio equivalent to the Alg. Afterward, dopamine HCl was contained in the mixture at a 1:1 molar ratio of dopamine to Alg at pH 4–5. The reaction was continued at 25 °C overnight. The obtained solution was then dialyzed against Dulbecco's phosphate-buffered saline (DPBS, pH = 4) and acidic distilled water (pH 5–6) for 12 h and subsequently freeze-dried. The successful synthesis of the Cat-Alg conjugate was determined by NMR and FT-IR.

3.3.2 Characterization of the synthesized polymers

3.3.2.1 NMR

^1H NMR spectra were collected on an NMR 300 MHz (AVANCE III HD, Bruker) spectrometer at 298 K. All chemical shifts are reported as δ in parts per million (ppm), using the chemical shift of the solvent resonances as references (DMSO: $\delta = 2.50$ ppm, D_2O : $\delta = 4.80$ ppm).

3.3.2.2 FT-IR

The FT-IR was carried out in a wavenumber range of $600\text{--}4000\text{ cm}^{-1}$ using a PerkinElmer spectrum 100 infrared spectrophotometers and Spectrum software for the analysis.

3.3.3 Determination of mucoadhesive functional group

3.3.3.1 Thiol content of Cys-CS

The thiol content was determined using Ellman's reagent. Briefly, the Cys-CS samples (10 mg) are hydrated with PBS (pH 8) 500 μL in Eppendorf tubes. Then 500 μL of Ellman's reagent (5,5-dithio-bis-(2-nitrobenzoic acid) (DTNB); 3 mg/10 mL) was added to the sample. All tubes were kept in dark for 90 min. Cysteine standard was used for quantification of the thiol groups immobilized on the Cys-CS.

3.3.3.2 Maleimide group content of MHA-CS

The maleimide content on the MHA-CS was quantified using a reverse Ellman's assay. The synthesized polymer was first reacted with an exact quantity of excess thiol, and then the residual unreacted thiol was measured by Ellman's assay. Briefly, the polymer samples (10 mg) are contained Eppendorf tubes containing 1,000 μL of L-cysteine HCl solution (3 mg/mL) prepared in PBS (pH 8). The polymer sample was allowed to swell and react with cysteine for 1 h. Then, the polymer sample was separated from the aqueous solutions by centrifugation at 13,000 rpm for 10 min. The supernatant sample was used for the determination of the remaining thiol using Ellman's reagent. DTNB (3 mg, 7.6 mmol) was dissolved in 10 mL of PBS. Then 500 mL of DTNB stock solution was added to 500 mL of the sample and stored in the dark for 90 min. The absorbance at 420 nm was measured using a microplate

reader (Fusion Universal Microplate Analyzer Model: A153601). The unreacted thiol was then determined. The free cysteine solution without being mixed with the polymer sample was used as a control. The quantity of free maleimide presented on the MHA-CS was computed by subtracting the initial thiol content and the quantity of unreacted thiol after reacting with the polymer.

3.3.3.3 Catechol group content of Cat-Alg

The DS of catechol on the Alg was analyzed based on the procedure specified in a previous study (Woraphatphadung et al., 2015). ^1H NMR was exploited in the determination of substitution levels.

$$\text{DS} = \frac{(\text{I}_{\text{aromatic protons. H}})/3}{(\text{I}_{\text{H2-H5}})/4} \quad (1)$$

3.3.4 Mucoadhesive properties of the synthesized polymer

3.3.4.1 Rheology method

Rheological analysis was performed using a rheometer (DSR Malvern–Kinexus Pro, USA). Cone plate (Cp4/40) systems were employed as the measuring equipment. All the measurements were performed at a constant temperature of 37 °C. The polymer concentrations of 1%, 3%, and 5% (w/v) in 0.1M HCl were used for the test. Mucin solution at the concentration of 5% (w/v) in PBS pH 7.4 was made freshly on the day of experiment. The mucin and polymer solutions were combined at a polymer: mucin weight ratio of 1:1, and well mixed for 1 h prior to the analysis.

3.3.4.2 *Ex-vivo* mucoadhesion assay (Tensile testing method)

The *ex-vivo* mucoadhesion test was conducted using a texture analyzer equipped with a 5-kg load cell. The synthesized polymer was compressed into a tablet which was used for the test. The polymer tablet was fixed to a cylindrical probe of the texture analyzer. A porcine cheek pouch was exploited as the model mucosal tissue for the mucoadhesion test. After the cheek pouch was excised and trimmed evenly, it was washed in simulated saliva (2.38 g Na_2HPO_4 , 0.19 g KH_2PO_4 , and 8 g of NaCl per liter of distilled water adjusted with phosphoric acid to a pH of 6.8 ± 0.05) and then used immediately. During the measurement, 500 μL of simulated saliva was

dispersed on the tissue. The probe was the moving down at a speed of 2 mm/s to contact the tissue at a force of 0.3 N for 15 s. The force used to detach the tablets from the tissue was recorded as the mucoadhesion force.

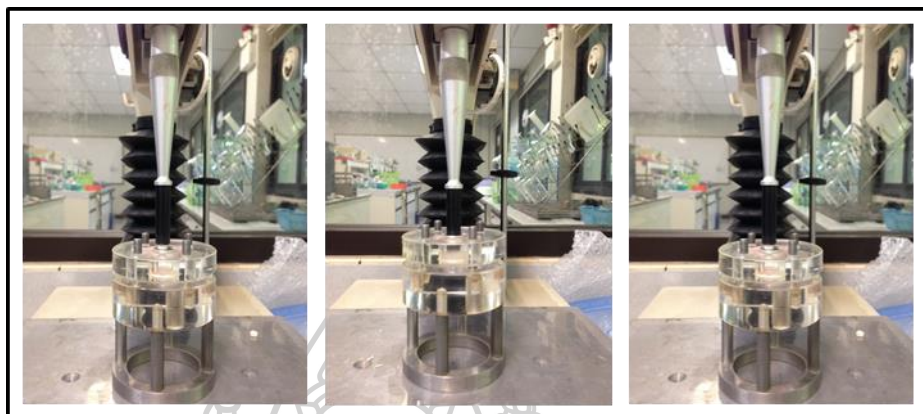


Figure 20 Mucoadhesion test using a texture analyzer with a tissue holder.

3.3.5 Cytotoxicity of the synthesized polymers on normal cells

The biocompatibility of the synthesized polymers was investigated by assessment of the cytotoxicity on HGF cells using an MTT assay. The HGF cells were cultured in 100 μ L of Dulbecco's modified Eagle's medium (DMEM) supplemented with 10% FBS, 2 mM L-glutamine, 1% non-essential amino acids, and 0.1% penicillin-streptomycin before being distributed at 10,000 cells/well in 96-well plates. The cells were then incubated under an appropriate condition used for cell growth (5% CO₂, 95% air, 37°C) until confluence. The cells were treated with the synthesized polymers at various concentrations ranging from 0.01-10 mg/mL in DMEM medium (pH 7.4) without serum and further incubated for 24 h. After treatment, the serum-free medium containing the polymers was discarded and the cells were exposed to 100 μ L of DMEM medium containing MTT (1 mg/mL) for 4 h. After that, the medium was discarded followed by washing the cells with a PBS (pH 7.4). The formazan crystals that created in the living cells were liquified by adding 100 μ L/well of DMSO. The relative viability (%) was computed from the absorbance at 550 nm measured using a microplate reader (Universal Microplate Analyzer, Model AOPUS01, and AI53601, Packard BioScience, CT, USA). The viability of non-treated control cells was arbitrarily defined as 100%.

$$\text{Relative cell viability (\%)} = \frac{[\text{OD}_{550, \text{sample}} - \text{OD}_{550, \text{blank}}]}{[\text{OD}_{550, \text{control}} - \text{OD}_{550, \text{blank}}]} \times 100 \quad (2)$$

3.3.6 Preparation of the mucoadhesive NPs

3.3.6.1 Cat-Alg NPs

The Cat-Alg solution in water was prepared at the concentration of 0.05%. Then, the NPs were formed by adding the Cat-Alg solution in 0.008125% calcium chloride solution at a slow dropping rate (0.15 mL/min) with vigorous stirring and sonication at an amplitude of 40% for 1 h. The NPs were collected after freeze dried.

3.3.6.2 MHA-CS and Cys-CS NPs

The MHA-CS and CS-Cys NPs were prepared by dissolving the MHA-CS or Cys-CS in 1% v/v acetic acid at the polymer concentration of 0.05%. The NPs were formed by dropping 0.05% sodium tripolyphosphate (TPP) solution into the polymer solutions at a slow dropping rate (0.15 mL/min) under vigorous stirring and sonication at an amplitude of 40% for 1 h. The NPs were collected after freeze dried.

3.3.6.3 MHA-CS-Alg-Cat NPs

The MHA-CS-Alg-Cat NPs were generated by the ionotropic gelation method. MHA-CS solution in 1% acetic acid was made at the polymer concentrations of 0.025%, 0.05% and 0.075%. In the meantime, the Cat-Alg solution was prepared in DI water at the polymer concentrations of 0.025%, 0.05%, and 0.075%. Then the NPs were formed by slowly adding the Cat-Alg solution into the MHA-CS solution at a slow dropping rate (0.15 mL/min) under vigorous stirring along with sonication at an amplitude of 40% for 1 h.

3.3.7 Evaluation of NPs

3.3.7.1 DLS measurements

The size and surface charge of the NPs were evaluated by DLS using a Zetasizer Nano ZS (Malvern Instruments Ltd, Malvern, UK). The NPs were filtered

through a 0.45- μm membrane filter and diluted in deionized water prior to the measurement. All analyses were performed in three replications at 25 °C.

3.3.7.2 Morphology of the NPs

The particle size and shape assessment of the NPs were conducted using a transmission electron microscope (TEM). The sample was diluted with deionized water, followed by bath sonication for 30 min. Then, the sample was placed onto a carbon-coated copper grid, and the size and shape of the particles were observed using a 200 kV TEM microscope (Philips CM 20, UK).

3.3.7.3 Mucoadhesive properties of the NPs

3.3.7.3.1 Porcine bowel mucosa

The mucoadhesive features of the NPs on *ex vivo* porcine bowel mucosa were demonstrated using a procedure reported in a published article (Tonglairoum et al., 2016). In this study, fluorescein sodium was loaded into the NPs during the nanoparticle preparation. Aqueous suspensions of the fluorescein-loaded NPs (1 mg/mL in deionized water) were prepared in simulated intestinal fluid. A sample (20 μL) was dropped onto a 1 \times 1 cm² piece of *ex vivo* porcine bowel mucosa, which was located on a sloping channel. The tissue was then rinsed with simulated intestinal fluid at a flow rate of 1 mL/min using a syringe pump. At different time points, images of the whole tissue were taken using a Leica MZ10F fluorescence stereomicroscope fitted with a GFP filter. Then, the fluorescence intensity of the images were determined using Image J software. The fluorescence intensity of the images was directly associated with the quantity of the NPs presented on the tissue. The fluorescence intensity of the blank tissue was subtracted from the pixel intensity of the samples. The data was displayed as a percent of NPs retained on the mucosal tissue with the rinsing time. The experiments were carried out in three replications.

3.3.7.3.2 Porcine bladder mucosa

The mucoadhesive capacities of the NPs on *ex vivo* porcine bladder mucosal tissue were demonstrated using the same method as described in section 3.3.7.3.1. However, the tissue was then rinsed with artificial urine (AU) pH 6.2.

3.3.8 GM extract-loaded NPs

3.3.8.1 Standardization and assay of GM extract

The GM extract used in this study was standardized with the standard α -mangostin to determine the α -mangostin content in the extract. The standard stock solution (1 mg/mL) of standard α -mangostin was made by dissolving an accurately weighed α -mangostin in methanol. Several concentrations of the standard solution α -mangostin (250, 200, 150, 100, and 50 μ g/mL) were prepared from the stock solution by dilution with methanol. Then, the analysis was performed by an HPLC method modified from the procedure reported by Pothitirat et al. (2009) using a VertiSep[®] AQS C18 column (250 mm \times 4.6 mm, 5 μ m particle size) as the stationary phase. The elution was accomplished at room temperature using a gradient system consisting of acetonitrile (mobile A) and 0.1% v/v orthophosphoric acid (mobile B). The flow rate of the mobile phase was 1 mL/min. The gradient systems was as follows: 70% A for 0-15 min, 70% A to 75% A in 3 min, 75% A to 80% A in 1 min, constant at 80% A for 6 min, and 80% A to 70% A in 1 min. The detection was performed using a UV-visible spectrophotometer at the wavelength of 320 nm (Pothitirat et al., 2009). Standard curve was plotted between area under the curve and α -mangostin concentration. The content of α -mangostin in the GM extract was analyzed by HPLC as mentioned above. The content of α -mangostin was reported as g of α -mangostin /100 g of the extract.

3.3.8.2 Preparation of GM extract-loaded NPs

GM extract was loaded into the NPs by entrapment method. Briefly, GM extract solutions in ethanol (1, 5 and 10 mg/mL) 500 μ L were added slowly into the polymer solution under magnetic stirring before adding the polymer solution into the crosslinking agent (CaCl₂, TPP). The NPs were obtained after centrifugation and freeze-dried.

3.3.8.3 Determination of percentage loading efficiency (LE) and loading capacity (LC)

The drug content in the NPs was assessed using HPLC. Briefly, the freeze-dried powder of the NPs (5 mg) was dispersed in 1 mL methanol in an Eppendorf tube. The mixture was then mixed using a vortex mixer for 5 min before

being centrifuged at 14,800 rpm for 30 min. The amount of α -mangostin was analyzed using HPLC using the analytical condition mentioned above.

$$\text{LE (\%)} = \frac{\text{Amount of drug on the NPs}}{\text{Amount of initial drug used}} \times 100 \quad (3)$$

$$\text{LC} = \frac{\text{Amount of drug on the NPs}}{\text{Amount of polymer used}} \quad (4)$$

3.3.8.4 Release of GM-extract loaded NPs

The *in vitro* release of α -mangostin from the GM extract-loaded NPs was studied using a dialysis method modified from previously reported procedure (Brannigan and Khutoryanskiy, 2017). Briefly, 2 mL of the GM extract-loaded NPs (50 mg) in a simulated intestinal fluid was contained in a dialysis bag. The dialysis bag was placed in 30 mL of simulated colonic fluid (pH 7.4) which was used as the release medium. The release study was conducted at 37°C using a shaking incubator shaken at 150 rpm for 24 h. At predetermined time intervals, 5.0-mL samples of the medium were taken out and used for drug content analysis. Same volume of the fresh medium was added to maintain the initial volume. The released α -mangostin in each withdrawn sample was quantified by HPLC. The release kinetics was also calculated.

3.3.9 DOX-loaded NPs

3.3.9.1 Preparation of DOX-loaded NPs

DOX was incorporated into the MHA-CS-Alg-Cat NPs by adsorption method at various ratios of NPs: DOX (1: 0.25, 1: 0.5, and 1: 1) to get the right dosage by weighing the DOX and the NPs. After that, dissolve the DOX in the deionized water at pH 8.0 before mixing in various ratios and freeze-dried.

3.3.9.2 DOX assay

The content of DOX in the DOX-loaded MHA-CS-Alg-Cat NPs was determined using a UV/Vis spectrophotometer at the wavelength of 470 nm. The amount of DOX in the NPs was then calculated. Briefly, an accurately weighed sample of the NPs (5 mg) was added to Eppendorf tubes comprising 1 mL of deionized water, followed by mixing overnight to take out the DOX from the NPs.

The drug content was quantified by measuring the fluorescent intensity of DOX using a fluorescent spectrometer (Thermo Scientific™ Fluoroskan Ascent FL) at the excitation and emission wavelengths of 485 nm and 538 nm, respectively, and the percentages of LE and LC were computed according to Equations 3 and 4, respectively.

3.3.9.3 Release of DOX-loaded NPs

The *in vitro* release of DOX from the DOX-loaded MHA-CS-Alg-Cat NPs was investigated in AU (pH 6.2). Briefly, Exact amount (3 mg) of DOX-loaded NPs was placed into a dialysis bag comprising 1 mL of AU. The dialysis bag was subsequently placed into a glass bottle comprising 20 mL of AU. The release experiment was carried out at 37 °C in a shaking incubator shaken at 80 rpm. At different time intervals (5, 10, 15, 30, 60, 120, 240, 480, 720, and 1440 min), a sample of the release medium (1 mL) was withdrawn and used for the content analysis using a fluorescent spectrometer (Thermo Scientific™ Fluoroskan Ascent FL) at the excitation and emission wavelengths of 485 nm and 538 nm, respectively, and the percentages of cumulative release at different time points were then calculated.

3.3.10 Anticancer activity on cancer cells

To demonstrate the anticancer activities of the GM extract-loaded NPs, the cytotoxicity of the GM extract, the blank NPs, and GM extract-loaded NPs were investigated against HT29 cells using MTT assay as described in section 3.3.5.

The anticancer activity of the DOX-loaded NPs and free DOX was investigated against MB49 cells using an MTT assay as described in section 3.3.5.

3.3.11 Cellular uptake analysis

The uptake of DOX-loaded NPs to the cancer cells (MB49 cells) was evaluated. The cells dispersed in DMEM were grown in a 24-well plate with a cell density of 100,000 cells/well under a specified condition (5% CO₂, and 95% air at 37 °C) for 24 h. After that, the cells were exposed to DOX or DOX-loaded NPs samples having DOX concentration equaled to the IC₅₀ value for 24 h. Afterwards, the cells were subsequently cleansed two times by PBS. Then, trypsin was included to detach the cells from the plate, and add 4% formaldehyde prepared in PBS was used to fix

the cells. The cell suspension was combined with the formaldehyde solution and stored at 4 °C until the investigation by flow cytometry. Flow cytometry was performed using an Attune[®] NxT Flow Cytometer POC measuring the mean fluorescence intensity (MFI) of DOX within the cells.

3.3.12 Confocal laser scanning microscopy (CLSM) analysis

The accumulation of DOX-loaded NPs in MB49 cells was also assessed by CLSM. In brief, MB49 cells were cultured on sterile coverslips placed in a well of a 24-well plate at a cell density of 30,000 cells/well for 24 h. Then, the cells were incubated with DOX or DOX-loaded NPs samples having DOX concentration equaled to the IC₅₀ for 24 h. Afterward, the cells were washed three times with PBS, and 5 µg/mL of Hoechst 33342 prepared in the medium was subsequently added to the cells (200 µL/well) and incubated for 15 min for plasma membrane and nucleus staining. After that, the cells were subsequently rinsed with PBS before being fixed with 4% formaldehyde in PBS for 15 min. The cell-containing coverslips were removed from the well and air-dried before affixing on a glass slide using a ProLong[™] Diamond Antifade Mountant. Then, cell imaging was performed using an Olympus FV10i confocal laser scanning microscope with a 60x oil immersion objective lens.

3.3.13 Statistical analysis

All experimental measurements were gathered in triplicate. Data were presented as mean standard deviation (SD). Statistical significance of differences was determined using a one-way analysis of variance (ANOVA) (SPSS version 16.0 for Windows (SPSS Inc., USA)).

CHAPTER 4

RESULTS AND DISCUSSION

- 4.1 Chemical characterization of the synthesized polymers
 - 4.1.1 Synthesis of Cys-CS
 - 4.1.2 Synthesis of MHA-CS
 - 4.1.3 Synthesis of Cat-Alg
 - 4.1.4 Molecular weight determination of the synthesized polymers
- 4.2 Mucoadhesive properties
 - 4.2.1 Polymer-mucin interaction
 - 4.2.2 *Ex-vivo* mucoadhesion assay (Tensile testing method)
- 4.3 Biocompatibility of the synthesized polymers
- 4.4 Development of the mucoadhesive NPs
 - 4.4.1 Particle size, size distribution and zeta potential measurements
 - 4.4.2 Morphology of the NPs
 - 4.4.3 Mucoadhesive properties of the NPs on *ex vivo* porcine bowel mucosa
 - 4.4.4 Mucoadhesive properties of the NPs on *ex vivo* porcine bladder mucosa
- 4.5 Development of GM extract-loaded NPs
 - 4.5.1 Extraction and standardization of GM extract
 - 4.5.2 Particle size, size distribution and zeta potential measurements
 - 4.5.3 Determination of drug loading and drug content
 - 4.5.4 Release studies
 - 4.5.5 Cytotoxicity on cancer cells
- 4.6 Development of DOX-loaded NPs
 - 4.6.1 Particle size, size distribution and zeta potential measurements
 - 4.6.2 Determination of drug loading and drug content
 - 4.6.3 Release of DOX-loaded NPs
 - 4.6.4 *In vitro* cytotoxicity using MTT assay
 - 4.6.5 Cellular uptake of the NPs
 - 4.6.6 Confocal laser scanning microscopy (CLSM) analysis of the NPs

4.1 Chemical characterization of the synthesized polymers

4.1.1 Synthesis of Cys-CS

The Cys-CS was obtained from the reaction between CS and L-cysteine with the presence of EDAC as a catalyst. The synthetic route of Cys-CS is displayed in Figure 21.

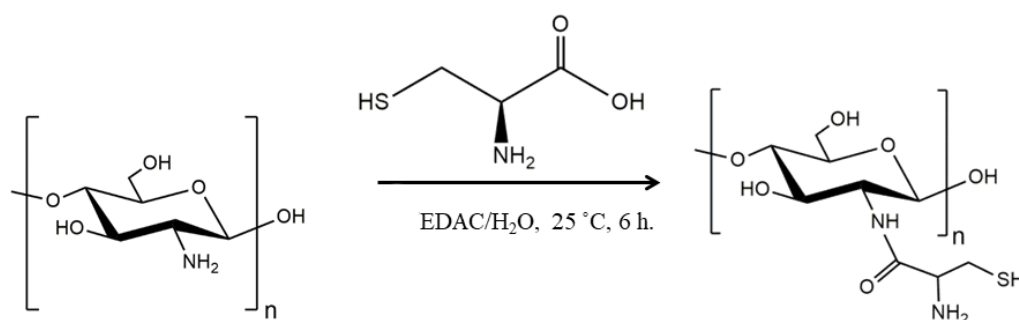


Figure 21 Synthetic route of Cys-CS.

The synthesized Cys-CS was used as control mucoadhesive polymer for comparison of mucoadhesive properties with other synthesized polymers. The obtained polymer was characterized by ^1H NMR and FT-IR, and the results are presented in Figures 22 and 23, respectively. The ^1H NMR spectrum of CS presented a peak at around 3.1-3.3 ppm which is the attribute of hydrogen-bonded to the C2 glucosamine ring. The peaks at around 3.4 and 4.1 ppm corresponds to the hydrogen-bonded to the carbon atoms C3, C4, C5 and C6 of the glucopyranose ring. After conjugating with cysteine, there is an appearance of new signals at 3.35 ppm of methine CH proton and 2.91 ppm of diastereotopic methylene CH_2 protons of L-cysteine. These peaks were not seen in the ^1H NMR spectrum of CS. The FT-IR spectrum of CS and Cys-CS exhibited the broadband at 3385 cm^{-1} which is attributed to $-\text{OH}$ stretching found in both molecular structures of CS and cysteine. The peaks at 2883 and $1075\text{-}1031\text{ cm}^{-1}$ are due to the $\text{C}-\text{H}$ and $\text{C}=\text{O}$ stretchings of the pyranose ring. The carbonyl group of the amide band was observed at 1640 cm^{-1} . The amine, NH_2 , was represented by the band at 1590 cm^{-1} . The presence of cysteine on the backbone of CS was confirmed by the ^1H NMR spectra. The thiol content of the Cys-

CS was quantified using Ellman's assay, and the results revealed that the quantity of thiol group on the synthesized Cys-CS was $253.26 \pm 12.59 \mu\text{mol/g}$.

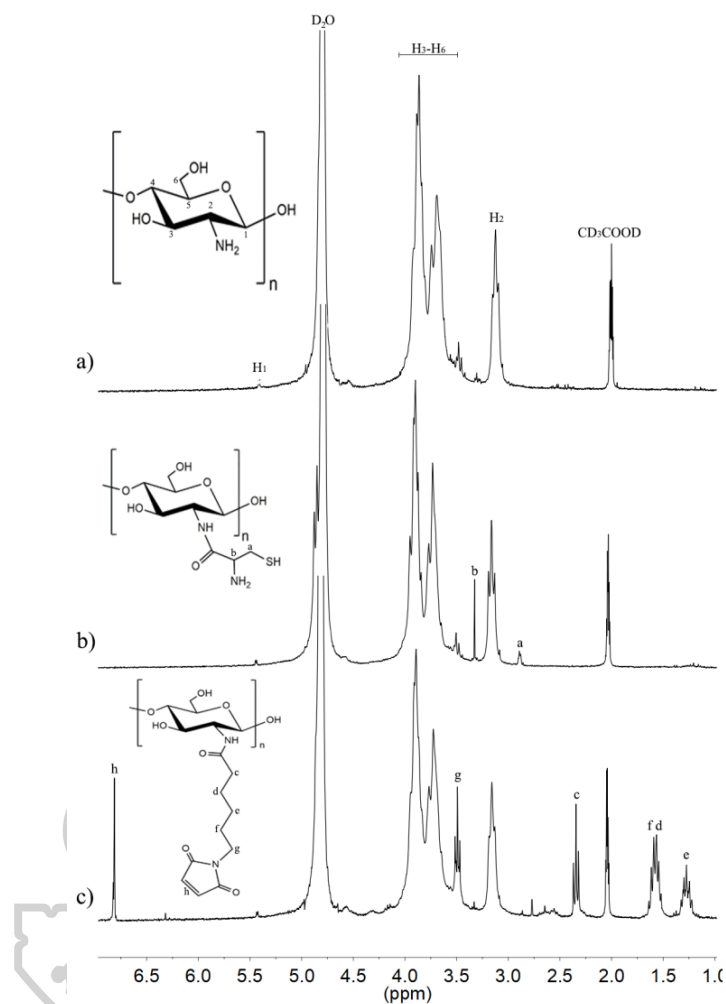


Figure 22 ^1H NMR spectra of a) CS b) Cys-CS and c) MHA-CS in 2% $\text{CD}_3\text{COOD}/\text{D}_2\text{O}$

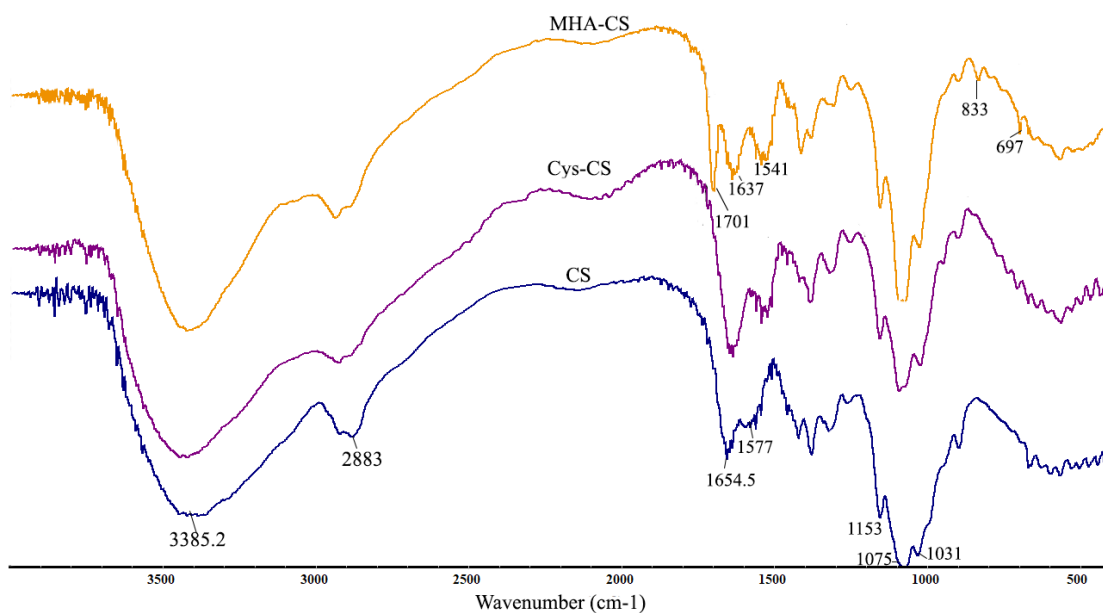


Figure 23 FT-IR spectra of CS, Cys-CS and MHA-CS

4.1.2 Synthesis of MHA-CS

The MHA-CS was obtained by functionalization of MHA onto the CS backbone using a coupling reaction with the aid of EDAC. In the synthesis process, the carboxylic groups of MHA were initially reacted with EDAC making them a higher reactivity. Then, the reactive carboxylic group of MHA reacted with the primary amine of the CS backbone led to successful conjugation. The synthesis reaction was accomplished in aqueous solution pH 5.5 at ambient temperature. The synthetic route of MHA-CS is illustrated in Figure 24.

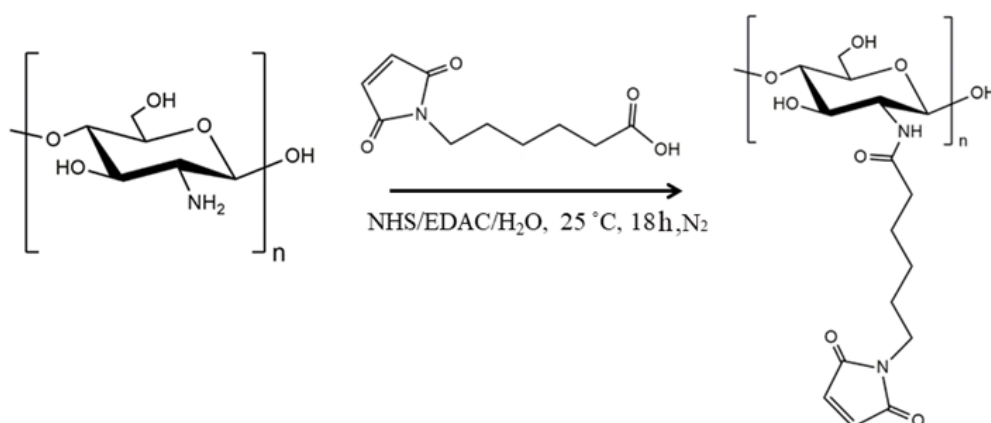


Figure 24 Synthetic route of MHA-CS

The obtained MHA-CS from the synthesis process was assessed by ^1H NMR and FT-IR. The ^1H NMR spectra of CS, MHA and MHA-CS are shown in Figure 22. The interpretation of ^1H NMR spectrum of CS is already described in section 4.1.1. After conjugating CS with MHA, the presence of the signals at 3.46, 2.34, 1.56, and 1.28 ppm which are attributed to the methylene protons of MHA had been noticed. Moreover, There was also a peak at 6.8 ppm which was attributed to the alkenyl protons of the maleimide groups. The FT-IR spectra of CS, Cys-CS and MHA-CS are displayed in Figure 23. The FT-IR spectrum of CS displayed the bands at 2883 and 1075-1031 cm^{-1} due to the C-H and C=O stretchings of the pyranose ring. The carbonyl group of the amide band was observed at 1637 cm^{-1} . The amine (NH_2) is presented by a band at 1541 cm^{-1} . The FT-IR spectrum of MHA-CS is similar to that of CS except for the appearance of additional peaks at 836.6 and 698.3 which are associated with the =CH wag and C-H out of plane vibration of the maleimide groups. The peak at 1703 cm^{-1} corresponds to C=O stretching of the amide bond in the maleimide structure. The presence of new bands together with the shift of the existing peaks in both the ^1H NMR and FT-IR spectra is highly indicative of the fruitful conjugation of MHA onto the CS structure.

Owing to the excessive reactivity of maleimide group to react with thiol groups of mucins by Michael-type addition reaction, the MHA-CS was expected to have strong mucoadhesive properties. Therefore, the amount of maleimide groups available for mucosal attachment was determined using a reverse Ellman's assay as previously mentioned. The finding found that that the maleimide content of the MHA-CS was $466.11 \pm 4.27 \mu\text{mol/g}$.

4.1.3 Synthesis of Cat-Alg

The Cat-Alg conjugate was synthesized by standard a carbodiimide coupling (EDAC/NHS) reaction. In the synthesis reaction, the carboxyl moieties of Alg was actuated with EDAC/NHS. The amine moieties of dopamine were then reacted with the actuated carboxyl moieties of Alg resulted in bond formation. The reaction was conducted in an aqueous solution pH 4-5 at room temperature. The synthetic route of Cat-Alg is illustrated in Figure 25.

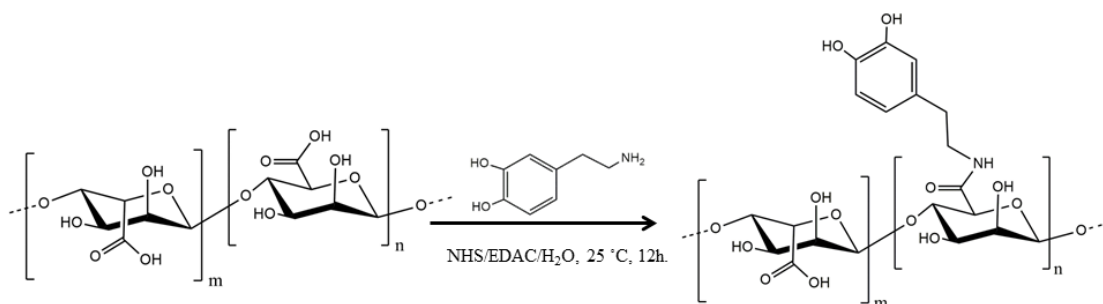


Figure 25 Synthetic route of Cat-Alg

The successful conjugation of dopamine to the structure of alginate chain was assured by the analyses by ^1H NMR and FT-IR. The ^1H NMR spectra of Alg and Cat-Alg are displayed in Figure 26. The ^1H NMR spectrum of alginate showed a signal at around 3.6- 4.2 ppm. The spectrum was presented which clearly shows the signal from three aromatic protons of the dopamine moiety between 6.7 and 7.2 ppm.

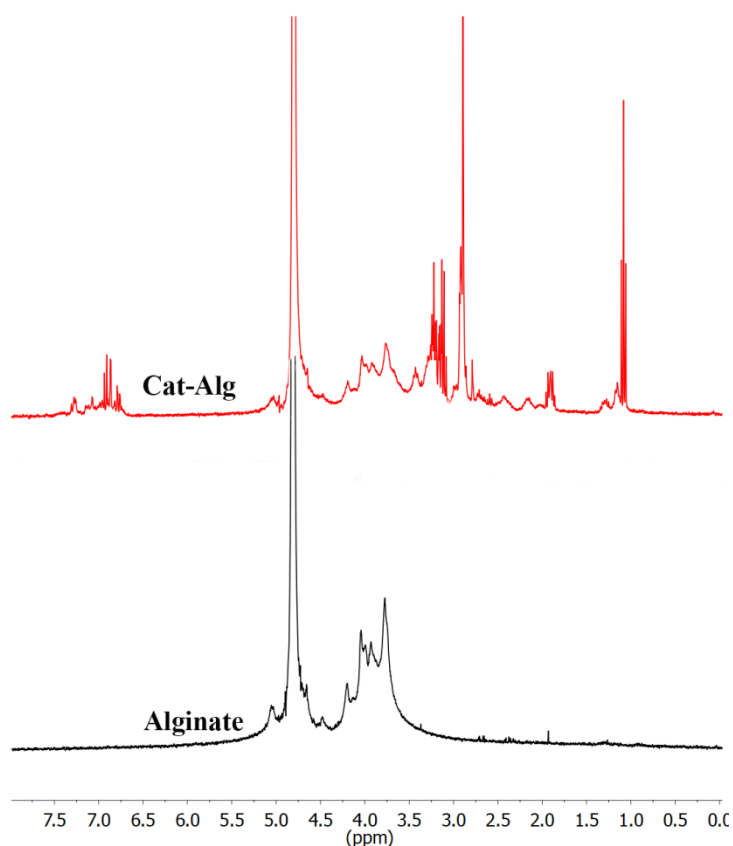


Figure 26 ^1H NMR spectra of Alg and Cat-Alg in D_2O

Figure 27 displays the FT-IR spectra of Alg and Cat-Alg. The FT-IR spectrum of Alg exposes a signal at 3200-3600 cm^{-1} due to the $-\text{OH}$ stretching vibration, and the peak of aliphatic $\text{C}-\text{H}$ stretching appears at 2930 cm^{-1} . The peaks at 1610 and 1421 cm^{-1} correspond to asymmetric and symmetric stretching of carboxylic salt ion, while the peak of the pyranose ring is related to $\text{C}-\text{O}$ stretching at 1035 cm^{-1} . The peak at 938 cm^{-1} is attributed to the $\text{C}-\text{O}$ stretching of uronic acid as a result of $\text{C}-\text{C}-\text{H}$ and $\text{C}-\text{O}-\text{H}$ deformation, and the peak at 885 cm^{-1} is a result of the deformation vibration of $\beta\text{-C1-H}$. After catechol was conjugated to the Alg structure, the bands at 1279 and 780 cm^{-1} (the peaks of the phenolic structure of the catechol groups) appeared. Moreover, the secondary amine peak was witnessed at 3407 cm^{-1} . The occurrence of new peaks in the ^1H NMR and FT-IR spectra is a clue of the successful functionalization of catechol onto the Alg chain. The DS of catechol groups on the Cat-Alg specified by the ^1H NMR spectrum was perceived to be 0.564.

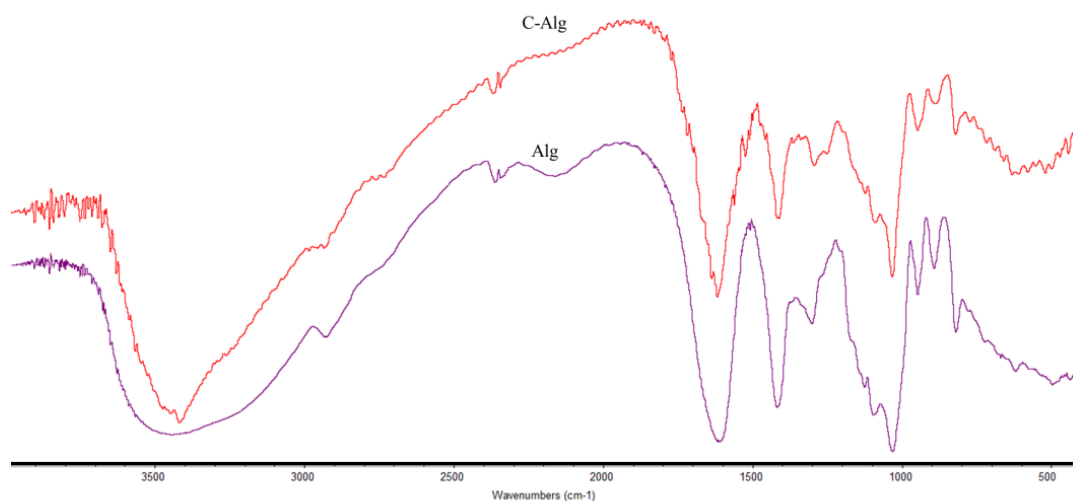


Figure 27 FT-IR spectra of Alg and Cat-Alg

4.1.4 Molecular weight (MW) of the obtained polymers

The MW of the polymers were analyzed using a gel permeation chromatography (GPC) and the findings are listed in Table 1. After the functionalization of cysteine and MHA onto the structure of CS and conjugation of dopamine onto the Alg sidechain, the MWs of the polymers were observed to be

increased. The increased MWs of the obtained polymer may indicate the successful synthesis.

Table 1 The MW and polydispersity of the CS, Alg, Cys-CS, MHA-CS and Cat-Alg

Polymer	M_n	M_w	M_z	Polydispersity
CS	5.0×10^3	8.0×10^3	1.2×10^4	1.6
Alg	1.3×10^5	4.9×10^5	1.2×10^6	3.6
Cys-CS	5.9×10^3	1.0×10^4	1.6×10^4	1.7
MHA-CS	6.1×10^3	1.2×10^3	2.1×10^4	2.0
Cat-Alg	2.1×10^5	4.5×10^5	9.0×10^5	2.1

4.2 Mucoadhesive properties

4.2.1 Polymer-mucin interaction

The mucoadhesive assay using the rheological technique was initiated by Hassan and Gallo by blending polymer dispersion with mucin. Polymers with excellent mucoadhesive capability demonstrated increased viscosity after mixing with mucin (Hassan and Gallo, 1990; Horvát et al., 2015; Shitrit and Bianco-Peled, 2017). Polymers that are able to generate strong interaction with mucin are expected to have a greater viscosity in the mixture of polymer and mucin compared to the summation of polymer and mucin viscosities (Khutoryanskiy, 2011). In this study, the mucoadhesive properties of the synthesized MHA-CS, Cys-CS and Cat-Alg were evaluated using the rheological assay and compared with the unmodified polymers, and the findings are expressed in Figure 28 and Table 2. The findings revealed that the mixtures of the synthesized polymer and mucin exhibited the increased viscosity compared with the viscosity of the polymer or mucin alone, which represents the force of interaction. Increasing the concentration of the polymers in the mixture led to the further increase in the viscosity of the mixture. At the same polymer concentration (5%), the mixture of MHA-CS and mucin exhibited significantly higher viscosity compared to the mixture of Cys-CS and mucin suggesting larger interaction and superior mucoadhesive capability.

This viscosity can represent the mucoadhesive capability of the polymer. According to the mucoadhesive study of Cat-Alg by viscosity evaluation of the polymer-mucin mixture, the results are displayed in Figure 28d and Table 3. As the

shear rate of the test may destroy the physical interactions and disentanglement of the polymer/mucin mixture. Therefore, the highest viscosities determined at a low shear rate were employed to differentiate the mucoadhesive capability of the polymers. It was noticed that the viscosity of Cat-Alg/mucin mixtures was higher than that of mucin and Cat-Alg. This indicated that Cat-Alg could form a strong bond with mucin. It is probably that the interaction of the polymer/mucin was based both on chemical and physical interactions.

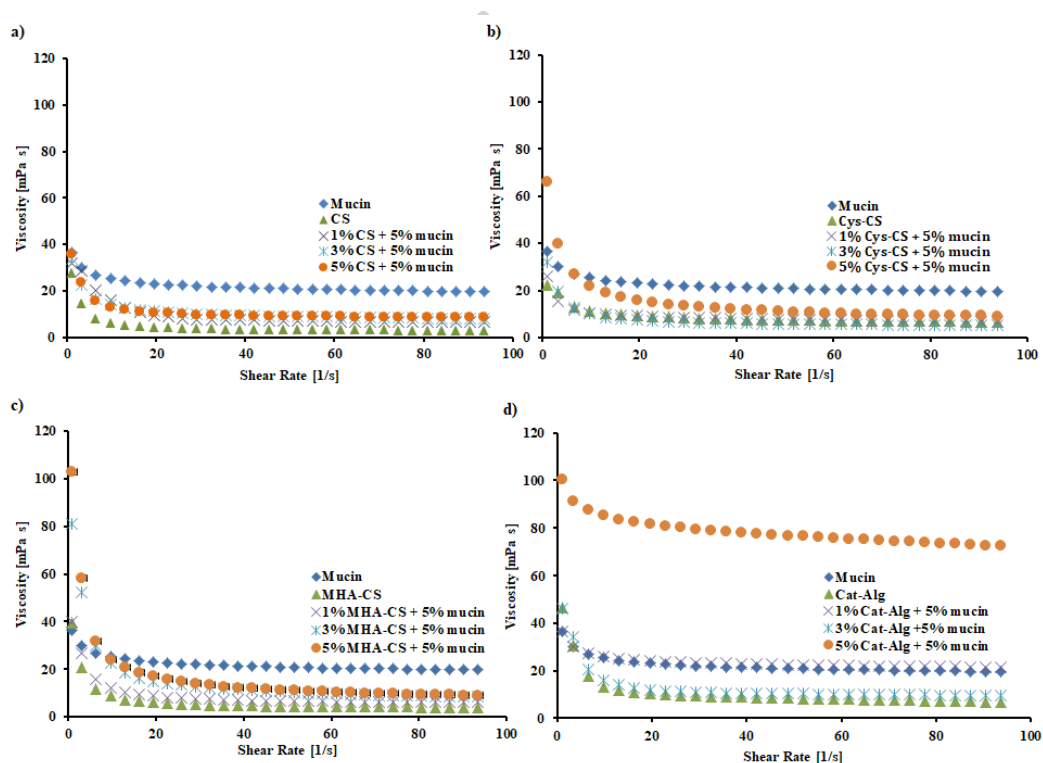


Figure 28 Viscosity of a mixture of a) CS and mucin b) Cys-CS and mucin c) MHA-CS and mucin and d) Cat-Alg and mucin compared with the polymer solution or mucin solution alone.

4.2.2 *Ex-vivo* mucoadhesion assay (Tensile testing method)

In order to conform the results obtained from the rheological study, a tensile testing method was exploited to determine the mucoadhesive capability of the synthesized polymers. In this test, the force of adhesion between the compressed polymer tablets and buccal mucosal tissue was assessed using a texture analyzer. In this experiment, the polymers were compressed to form a tablet. The tablet was then

attached to the probe of a texture analyzer before moving down to contact with porcine buccal mucosa. The force used to separate the tablet from the buccal mucosa was then noted as mucoadhesion force, and the findings are listed in Table 2. The results showed that all the synthesized polymers demonstrated improved mucoadhesive properties compared to the unmodified polymers. MHA-CS exhibited significantly higher mucoadhesion force compared with CS and Cys-CS with roughly 22.4-time and 4.2-time improvement in the force of adhesion, respectively. The findings from this study are harmonized with results from the rheological test which signifies the enhanced mucoadhesive properties of the MHA-CS. The improve in the adhesive capability of the MHA-CS may be associated with the extreme reactivity of maleimide toward the thiol groups presented on the mucosal layer and the ability to form strong bond with the thiol groups through Michael-type addition reaction (Lowe, 2014).

Table 2 Shear viscosity of the polymer-mucin mixture (at the polymer and mucin concentrations of 5%), and the *ex-vivo* mucoadhesive strength of the compressed polymer tablets on a porcine buccal mucosal tissue. *Statistically significant difference from CS (negative control), ** Statistically significant difference from Cys-CS (positive control).

Polymer	Shear viscosity of the polymer-mucin mixture (mPa/s)	<i>Ex-vivo</i> mucoadhesive strength (N)
CS	35.40 ± 11.32	0.027 ± 0.006
Cys-CS	66.37 ± 16.53*	0.145 ± 0.007*
MHA-CS	102.75 ± 9.02 ^{*,**}	0.604 ± 0.018 ^{*,**}

The mucoadhesive properties of Cat-Alg was also investigated by the tensile testing method, and the results are presented in Table 3. As compared to unmodified Alg, the Cat-Alg possessed a considerably better mucoadhesion capacity with an approximately 3.32-time increase in the mucoadhesive force compared with the unmodified polymer. The results of this study are in an agreement with the viscosity measurement which verifies the great mucoadhesive properties of the Cat-Alg. The catechol groups available on the Cat-Alg could generate interact and form strong

bonds with the mucosal layer, and led to an excellent mucoadhesive properties (Moulay, 2018).

Table 3 Shear viscosity of the polymer-mucin mixture (at the polymer and mucin concentrations of 5%), and the *ex-vivo* mucoadhesive strength of the compressed polymer tablets on a porcine buccal mucosa. * Statistically significant difference from Alg (negative control).

Polymer	Shear viscosity of the polymer-mucin mixture (mPa/s)	<i>Ex-vivo</i> mucoadhesive strength (N)
Alg	46.68 ± 9.80	0.076 ± 0.018
Cat-Alg	100.28 ± 5.87*	0.252 ± 0.041*

4.3 Biocompatibility of the synthesized polymers

Since the polymer synthesized in this study were expected to be used as drug delivery carriers, the synthesized polymer should be safe to the human body and biocompatible. Thus, the cytotoxicity of the synthesized polymers (concentration ranging from 0.1-1000 µg/mL) was assessed against HGF cells which are one type of the human normal cells. The percentage cell viability of the HGF cells after exposed to various concentrations of the synthesized polymers is presented in Figure 29a. As compared with CS, no significant cytotoxic effect was observed for MHA-CS and Cys-CS at the tested concentration. Low toxicity of maleimide-bearing materials was also conveyed by Li and Takeoka (2013). They conveyed that modification of materials to have maleimide on the surface of their materials did not affect the biocompatibility of the materials (Li and Takeoka, 2013). Based on the obtained information, the synthesized CS-Cys, MHA-CS may be safe to be applied as carriers for drug delivery to the human body.

Besides the MHA-CS and Cys-CS, the toxicity of Cat-Alg was also investigated. The percentage cell viability of the HGF cells after treatment with Cat-Alg is presented in Figure 29b. As compared with the intact Alg, the Cat-Alg did not show a significant reduction in the cell viability except at the polymer concentration higher than 100 µg/mL. Therefore, the synthesized Cat-Alg was found to be safe to be

applied as a drug delivery material at the low polymer concentration. However, at a higher concentration (100 $\mu\text{g/mL}$), some cytotoxic effect could be observed. Lee (2013) reported that the oxidizing conditions with the increase in pH may result in the rapidly increased cytotoxicity of catechol (Lee et al., 2013). Therefore, the Cat-Alg should be used at a low concentration in the body.

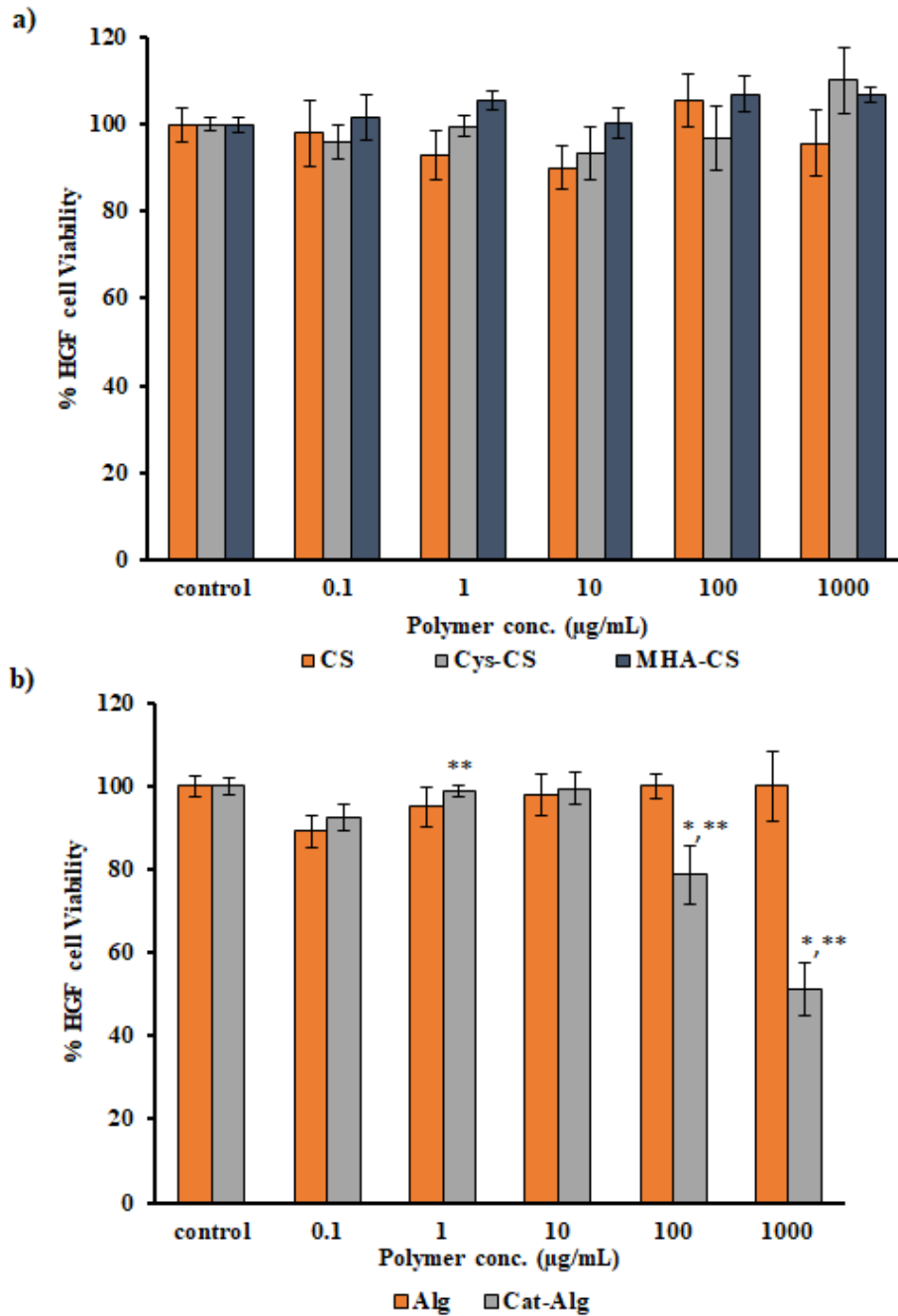


Figure 29 Cytotoxic effect of a) CS, Cys-CS and MHA-CS and b) Alg and Cat-Alg on HGF cells. Data are presented as the mean \pm SD ($n = 5$) *Statistically significant difference from control and **statistically significant difference from Alg ($p < 0.05$).

4.4 Development of the mucoadhesive NPs

4.4.1 Particle size, size distribution and zeta potential measurements

The NPs were prepared from the synthesized polymer by ionic gelation method. The size of NPs was determined by DLS. Table 4 presents the average particle sizes, PDI and zeta potential of the particles. The findings indicated that the particles had a range of diameter between 162-370 nm with an average diameter of 167.07 ± 4.8 nm for Cat-Alg NPs, 270.80 ± 14.42 nm for Cys-CS NPs, 349.87 ± 6.35 nm for MHA-CS NPs and 162.37 ± 1.33 nm for MHA-CS-Alg-Cat NPs. The polydispersity indexes (PDI) of the Alg and Cat-Alg NPs were larger compared with CS NPs.

Table 4 The mean particle size, size distribution and zeta potential of the NPs. Each value is shown as the mean \pm SD of triplicate experiments.

NPs	Particle size (nm)	PDI	zeta potential (mV)
CS	370.63 ± 10.50	0.15 ± 0.03	-0.41 ± 0.06
Alg	218.77 ± 3.76	0.46 ± 0.04	-32.67 ± 1.11
Cat-Alg	167.07 ± 4.48	0.46 ± 0.01	-20.43 ± 1.03
Cys-CS	270.80 ± 14.42	0.39 ± 0.03	-0.85 ± 0.23
MHA-CS	242.53 ± 6.35	0.23 ± 0.01	1.65 ± 2.74
MHA-CS-Alg-Cat	162.37 ± 1.33	0.17 ± 0.02	15.6 ± 0.62

4.4.2 Morphology of the NPs

Investigation by TEM was performed to observe the morphology of the NPs, and the attained images are displayed in Figure 30. The TEM images indicated that the Cys-CS, Cat-Alg, MHA-CS and MHA-CS-Alg-Cat NPs had a circular shape with particle size within the nanometer range. However, the particle sizes obtained from

TEM were a little lesser than those obtained by DLS. This may be due to the different principles and states of the measurement systems. The NPs were observed in a desiccated state during investigation by TEM whereas they were analyzed in the solvated state in the investigation by DLS.

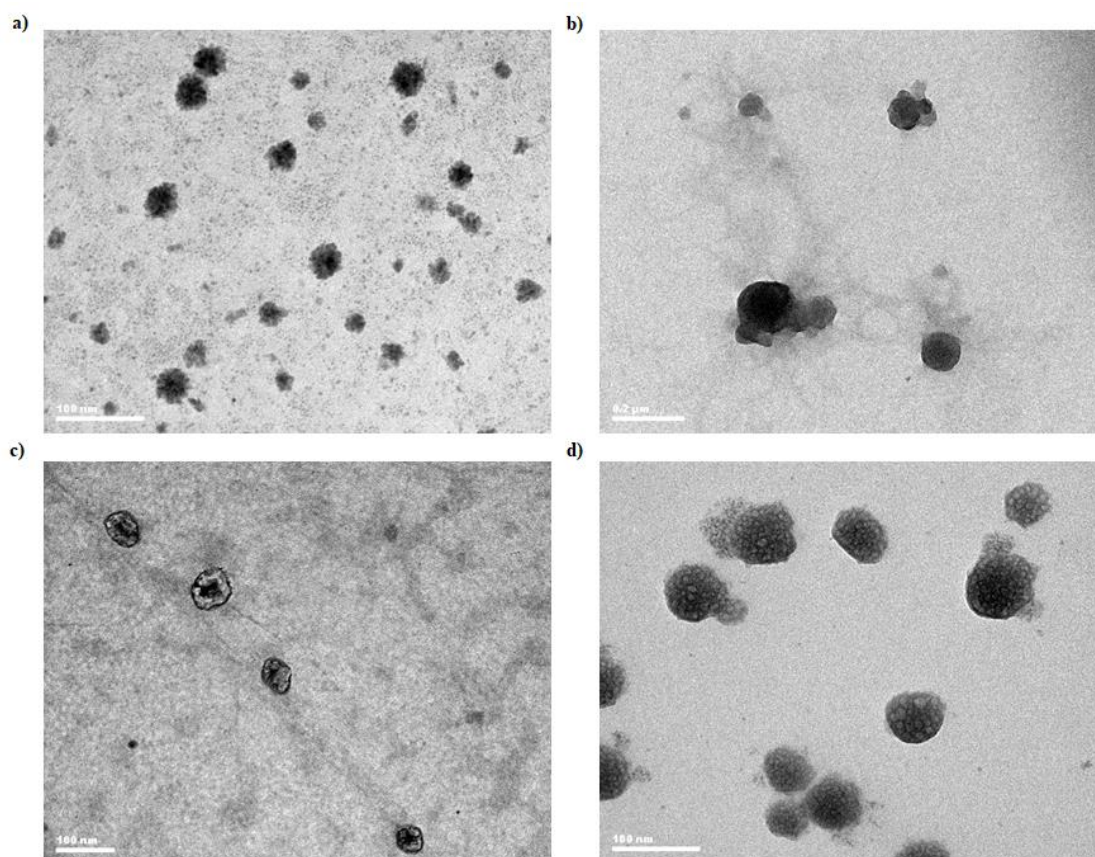


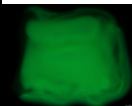
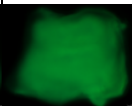
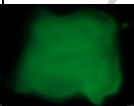



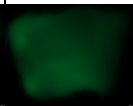

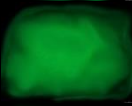
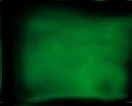
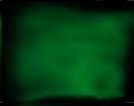





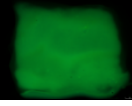
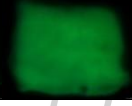



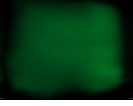


Figure 30 Morphology observed under TEM of a) Cys-CS, b) Cat-Alg, c) MHA-CS and d) MHA-CS-Alg-Cat NPs.

4.3.3 Mucoadhesive properties of the NPs on *ex vivo* porcine bowel mucosa

To demonstrate the mucoadhesive capability of the NPs, the retentive ability of fluorescein sodium (NaFl)-loaded NPs on *ex vivo* porcine bowel mucosa was demonstrated using fluorescence stereo microscopes (Figure 31). CS and Cys-CS were used as controls. The findings suggested that the MHA-CS NPs demonstrated good mucoadhesive properties which were comparable to the mucoadhesive properties of CS and Cys-CS. Approximately 50% of the MHA-CS NPs remained on

the porcine bowel tissue after 1 h of rinsing as compared to 39% of CS and 43% of Cys-CS. Different from CS and Cys-CS, the mucoadhesive properties of the MHA-CS NPs show a substantial improvement in the mucoadhesive capability.

Table 5 Fluorescence images of sodium fluorescein-loaded NPs remained on the porcine bowel mucosa after washing for different intervals. Data are presented as mean \pm SD (n = 3)

NPs	Time (min)							
	0	5	10	20	30	40	50	60
CS								
Cys-CS								
MHA-CS								

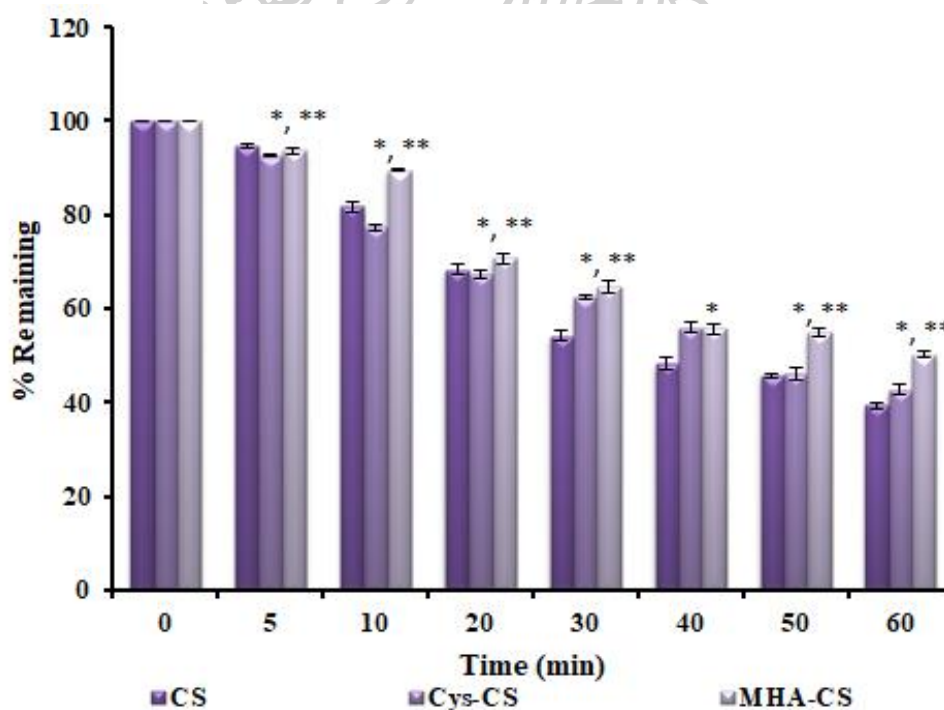
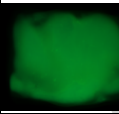
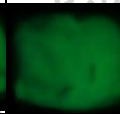
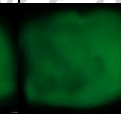
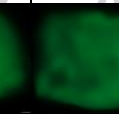
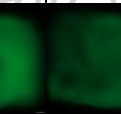
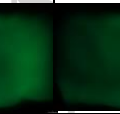
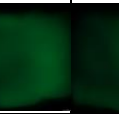
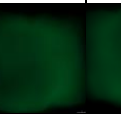
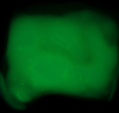
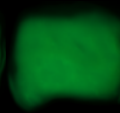

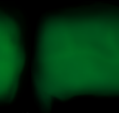
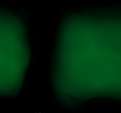
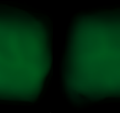
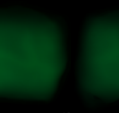
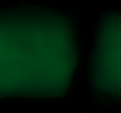


Figure 31 Percentage retention of CS, Cys-CS NPs and MHA-CS NPs on porcine bowel mucosa. Data are shown as mean \pm SD (n = 3). *Statistically significant

difference from CS ($p < 0.05$), **Statistically significant difference from Cys-CS NPs.

The Cat-Alg NPs exhibited good mucoadhesive capability which were comparative to the mucoadhesive capability of Alg. Almost 45% of the Cat-Alg NPs could be retained on the tissue after 1-h rinsing. This investigation ensured the favorable mucoadhesive ability of NPs which can possibly be exploited as mucoadhesive drug delivery carriers. In addition, these MHA-CS NPs and Cat-Alg NPs may be recognized a new class of mucoadhesive DDS.

Table 6 Fluorescence images of sodium fluorescein-loaded NPs remained on the porcine bowel mucosa after washing for different periods. Data are expressed as mean \pm SD ($n = 3$).

NPs	Time (min)							
	0	5	10	20	30	40	50	60
Alg								
Cat-Alg								

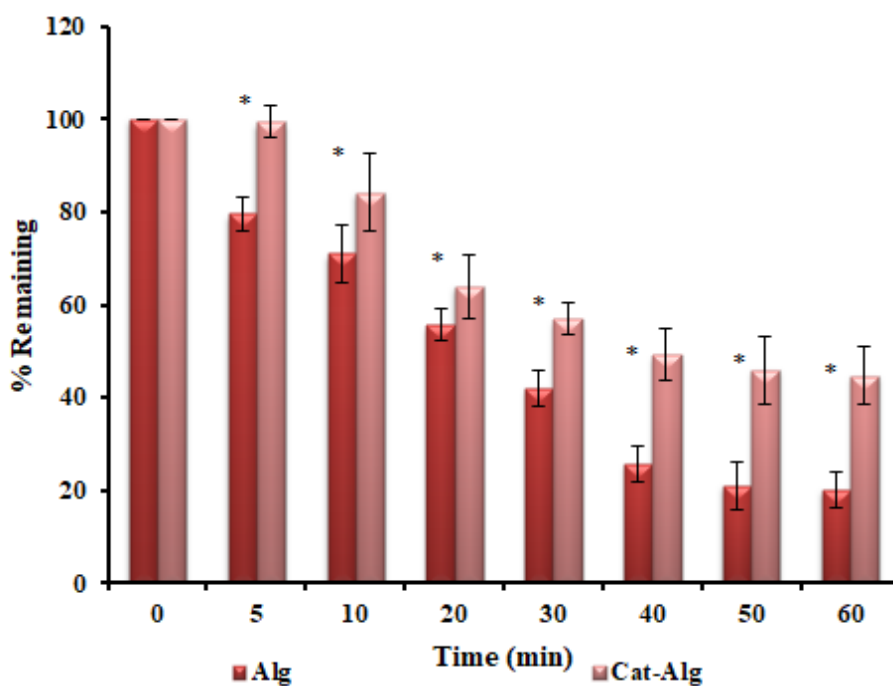
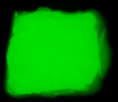
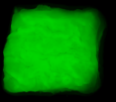
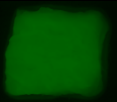
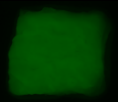
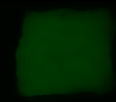
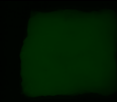


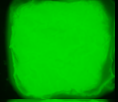
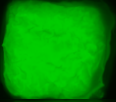
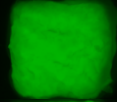
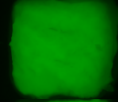
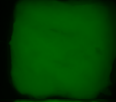
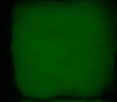


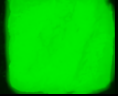
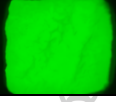
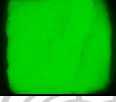
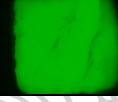
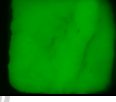
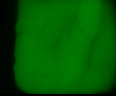
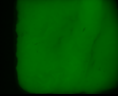
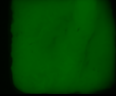


Figure 32 Percentage remaining of Alg and Cat-Alg NPs. Data are expressed as mean \pm SD (n = 3) *statistically significant (p < 0.05).

4.4.4 Mucoadhesive properties of the NPs on *ex vivo* porcine bladder mucosa

Assessment of mucoadhesive properties to demonstrate the mucoadhesive features of dextran, CS-Alg NPs and MHA-CS-Alg-Cat NPs, the existence of fluorescein sodium (NaFl)-loaded NPs on an *ex vivo* porcine bladder mucosa was examined by fluorescence microscopy, and the results are presented in Table 7. Dextran and CS-Alg NPs were used as negative control and positive control, respectively. Dextran-loaded NaFl will be washed off. And the CS-Alg NPs are almost completely washed away After 60 minutes while the cheek is swept at the NPs MHA-CS-Alg-Cat is still able to see the fluorescein intensity even after 60 minutes.

Table 7 Fluorescence images of sodium fluorescein-loaded NPs remained on the porcine bladder mucosa after washing for different periods. Data are expressed as mean \pm SD (n = 3).

Samples	Time (min)							
	0	5	10	20	30	40	50	60
Dextran								
CS-Alg NPs								
MHA-CS-Alg-Cat NPs								

To demonstrate the mucoadhesive features of the dextran, CS-Alg NPs and MHA-CS-Alg-Cat NPs, the existence of sodium fluorescein-loaded NPs on an *ex vivo* porcine bladder mucosa was examined by fluorescence microscopy, and the results are displayed in Figure 33. From the pixel analysis of the photographs derived from fluorescence microscopy, it was found that the MHA-CS-Alg-Cat NPs possessed greater mucoadhesive attributes than that dextran and CS-Alg NPs. Approximately 39% of the MHA-CS-Alg-Cat NPs remained on the porcine bladder tissue even if it was washed by artificial urine (AU) pH 6.2 for one hour. On the other hand, only 14% of CS-Alg NPs remained on the tissue. These findings highlight the favorable mucoadhesive capability of the MHA-CS-Alg-Cat NPs.

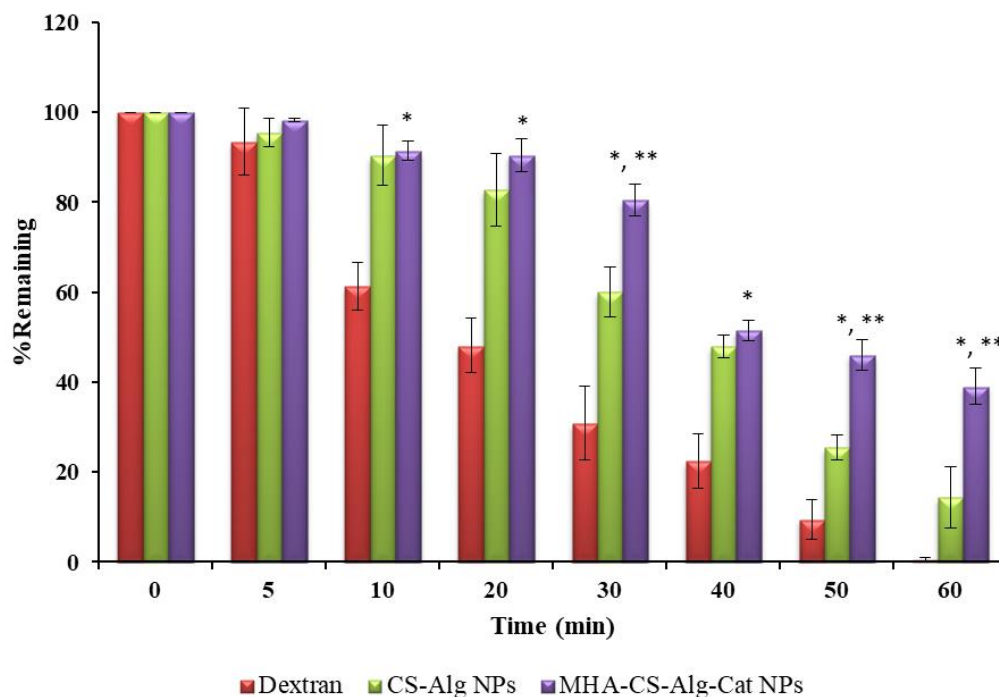


Figure 33 Percentage retention of dextran, CS-Alg NPs and MHA-CS-Alg-Cat NPs on porcine bladder mucosa after washing with AU pH 6.2. Data are expressed as mean \pm SD ($n = 3$). *Statistically significant difference from dextran ($p < 0.05$), **Statistically significant difference from CS-Alg NPs.

4.5 Development of GM extract loaded NPs

4.5.1 Extraction and standardization of GM extract

The ethanolic extract of GM was prepared by the maceration method with a yield of 8.93%. The GM extract was standardized with standard α -mangostin to determine the α -mangostin content in the extract. The α -mangostin content in the GM extract was standardized with the standard α -mangostin. The quantity of α -mangostin in the GM extract was found to be 351.2 mg/g.

4.5.2 Particle size, size distribution and zeta potential measurements

The NPs were prepared by ionotropic gelation under magnetic stirring, followed by sonication at amplitude of 40% for 1 h. The GM extract-loaded NPs were colorless and yellowish. After the drug loading, the particle size was found in Table 8 presents the average particle sizes, PDI, and zeta potential of the particles. The size of

GM extract-loaded Cat-Alg NPs was in the range of 113-117 nm with a negative surface charge (-14 to -25 mV). The size of GM extract-loaded Cys-CS NPs was in the range of 384-434 nm with a slightly negative surface charge (-5 to -9 mV) and the size of GM extract-loaded MHA-CS NPs was in the range of 169-190 nm with a slightly negative surface charge (-3 to -7 mV). The tiny size of the NPs could take part in penetration of the NPs into the bowel tissue. The surface charge of NPs affected their physiological behavior and their stability. The extent of negative surface charge could provide excellent stability of the NPs due to the electrostatic repulsion (French et al., 2009). There was an increment in particle size after GM extract was incorporated into the NPs. The presence of the mucoadhesive functionality, catechol, on the NPs may enhance local adhesion of the NPs and improve the localization and targeting function of the NPs (Mohammed et al., 2017).

Table 8 Particle size, size distribution and zeta potential measurements of GM extract-loaded NPs.

NPs	GM extract (mg/mL)	Particle size (nm)	PDI	Zeta potential (mV)
Cat-Alg	2.5	113.33 ± 0.32	0.13 ± 0.01	-25.9 ± 0.44
	5	119.77 ± 0.47	0.10 ± 0.01	-23.1 ± 1.84
	10	174.50 ± 2.63	0.43 ± 0.01	-14.97 ± 1.22
Cys-CS	2.5	384.33 ± 16.57	0.31 ± 0.04	-9.48 ± 2.05
	5	417.83 ± 71.34	0.44 ± 0.11	-6.85 ± 1.57
	10	434.20 ± 41.71	0.38 ± 0.15	-5.49 ± 0.64
MHA-CS	2.5	169.90 ± 2.60	0.10 ± 0.09	-7.23 ± 0.54
	5	175.97 ± 1.43	0.29 ± 0.02	-5.50 ± 0.64
	10	190.87 ± 4.69	0.29 ± 0.06	-3.44 ± 0.82

4.5.3 Determination of drug loading and drug content

The GM extract was loaded into the NPs by the entrapment method. The amount of GM extract in the GM extract-loaded NPs was reported as %LE and LC (Table 9). The %LE of GM extract in the Cat-Alg, Cys-CS and MHA-CS NPs were calculated to be 71.63%, 10.98% and 12.95%, respectively and the LC value was found to be 292.24, 54.82 and 64.77 µg/mg, respectively. Even though the GM extract has low solubility in water (< 0.5 µg/mL), it could be incorporated into the NPs at a

high extent by the drug loading method. This finding is in concordance with the study by Mulia et al, which demonstrated that the α -mangostin from GM extract could be incorporated into CS microparticles which high loading quantity (Mulia et al., 2020).

Table 9 %Loading efficiency and loading capacity of the drug loading NPs.

NPs	GM extract (mg/mL)	Loading capacity ($\mu\text{g}/\text{mg}$)	Loading efficiency (%)
Cat-Alg	2.5	136.87 ± 3.24	92.48 ± 2.19
	5	212.33 ± 0.19	82.94 ± 0.07
	10	292.24 ± 0.59	71.63 ± 0.15
Cys-CS	2.5	12.68 ± 0.22	6.34 ± 0.11
	5	18.78 ± 0.02	5.62 ± 0.01
	10	54.91 ± 0.10	10.98 ± 0.02
MHA-CS	2.5	17.34 ± 0.06	8.67 ± 0.03
	5	51.82 ± 6.38	15.51 ± 1.91
	10	64.77 ± 0.07	12.95 ± 0.01

4.5.4 Release studies

The release profile of α -mangostin from NPs loaded with GM extract was investigated using HPLC. Figure 34a shows the α -mangostin release characteristics from NPs with different release media including simulated gastric fluid (0.1M HCl pH 1.2) with 2% tween 20 and simulated intestinal fluid (pH 6.8) containing 2% tween 20. The result indicates that in the simulated gastric fluid (0.1M HCl pH 1.2), the α -mangostin was rapidly released. The percentage of cumulative GM extract release from Cys-Cs, MHA-CS and Cat-Alg NPs reached approximately 93%, 88% and 48%, respectively within 1 h. This result reveals that the α -mangostin was burst released from the NPs at an acidic pH. On the other hand, the GM extract was slowly released from the NPs in simulated intestinal fluid (pH 6.8) as presented in Figure 34b. The percentage of the 1-h cumulative release of the extract from Cys-Cs, MHA-CS and Cat-Alg reaches approximately 24%, 31% and 12%, respectively, and the release reached approximately 100% within 4 h. The release of the GM extract from the NPs was completed at 8 h. The slower release of GM extract from the NPs may be because the GM extract loaded in the NPs needed to diffuse through the swollen layer of the polymer matrix. In addition, a constant release could be obtained due to the hydrophobicity of the drug. Drug solubility can be a factor affecting the release of an

active compound from a drug formulation. For drugs with low aqueous solubility, the solubility may become a rate-limiting factor of drug release (Pornpitchanarong et al., 2020b).

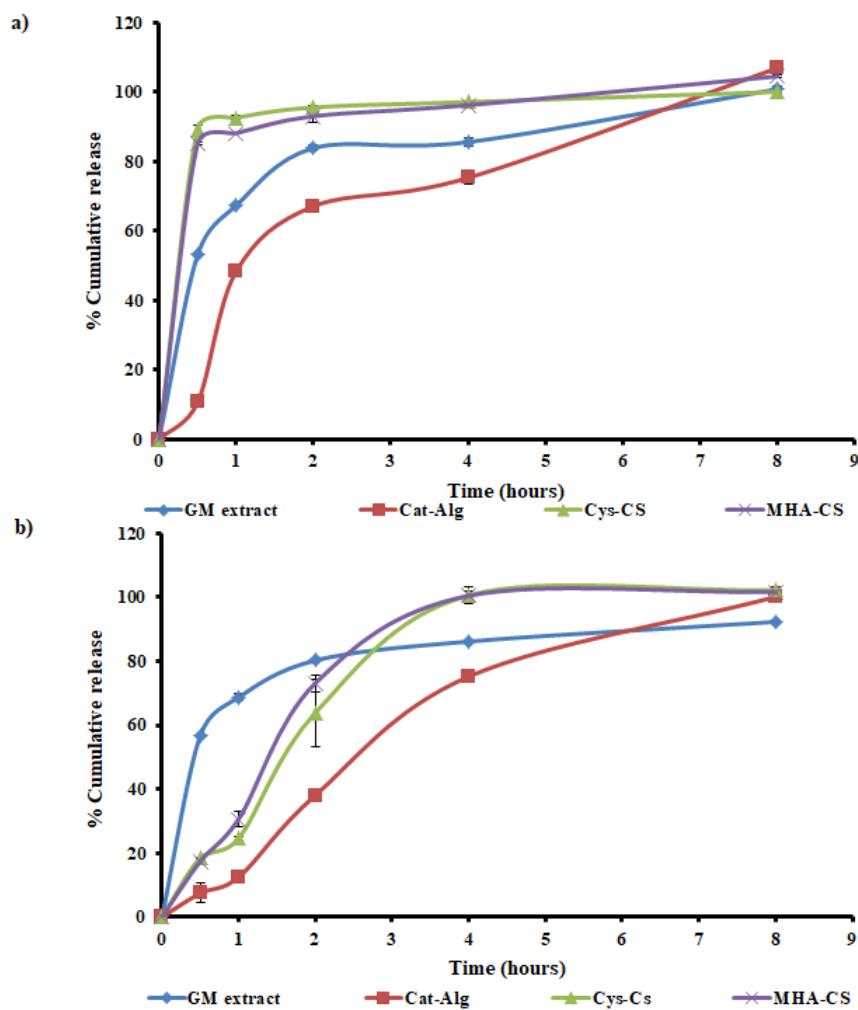


Figure 34 The *in vitro* release of α -mangostin from the GM extract-loaded NPs was studied in two different release media including a) simulated gastric fluid (0.1M HCl pH 1.2) containing 2% tween 20 and b) simulated intestinal fluid (pH 6.8) containing 2% tween 20.

4.5.5 Cytotoxicity on cancer cells

The anticancer activity of the blank NPs and the GM extract-loaded NPs were investigated against HT29 cells compared with GM extract suspension. The cytotoxic effect was presented as the half-maximal inhibitory concentration (IC_{50}), which shows the concentration that kills 50% of the cells. The results indicated that the blank NPs

were not cytotoxic to HT29 cells. On the other hand, GM extract suspension demonstrated a cytotoxic effect on the cells with the IC_{50} of 1.31 $\mu\text{g/mL}$. The GM extract-loaded NPs showed a potent HT29 killing effect with the IC_{50} values 1.60 for Cat-Alg NPs, 1.88 for MHA-CS NPs and 1.95 $\mu\text{g/mL}$ for Cys-CS NPs. The GM extract NPs showed higher IC_{50} values compared to the free GM extract because GM extract from the NPs was slowly released from the drug carrier and later performed its anticancer effect. However, the low IC_{50} value with a sustained-release profile could provide desirable anticancer activity against colon cancer cells.

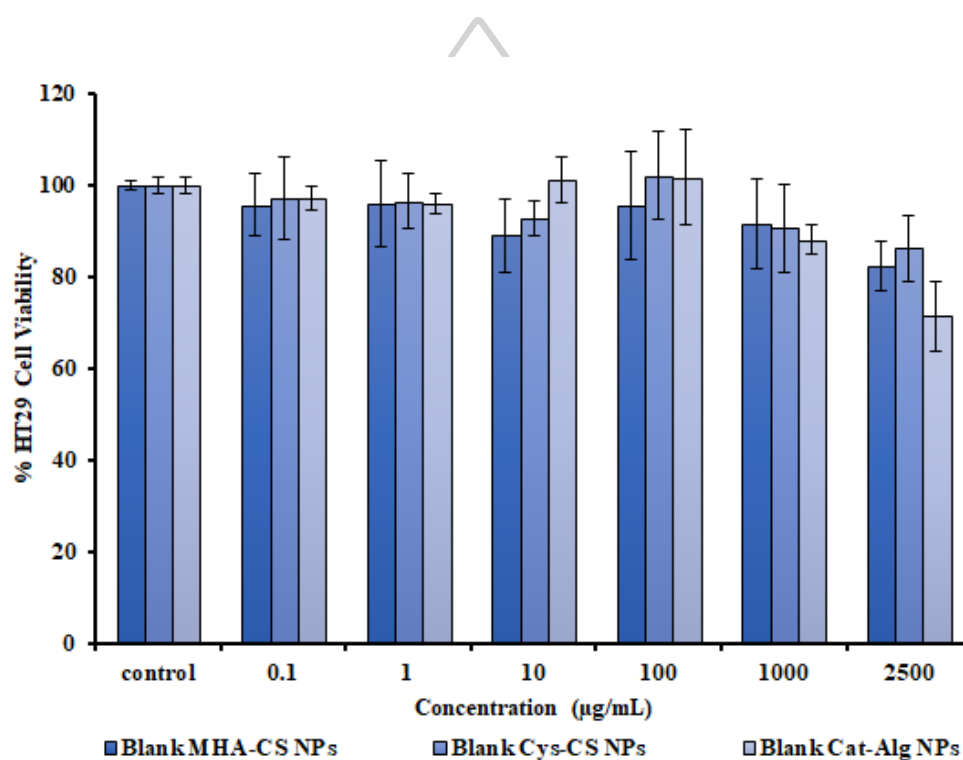


Figure 35 Percentage cell viability of HT29 cells after being treated with the blank MHA-CS NPs, Cys-CS NPs and Cat-Alg NPs.

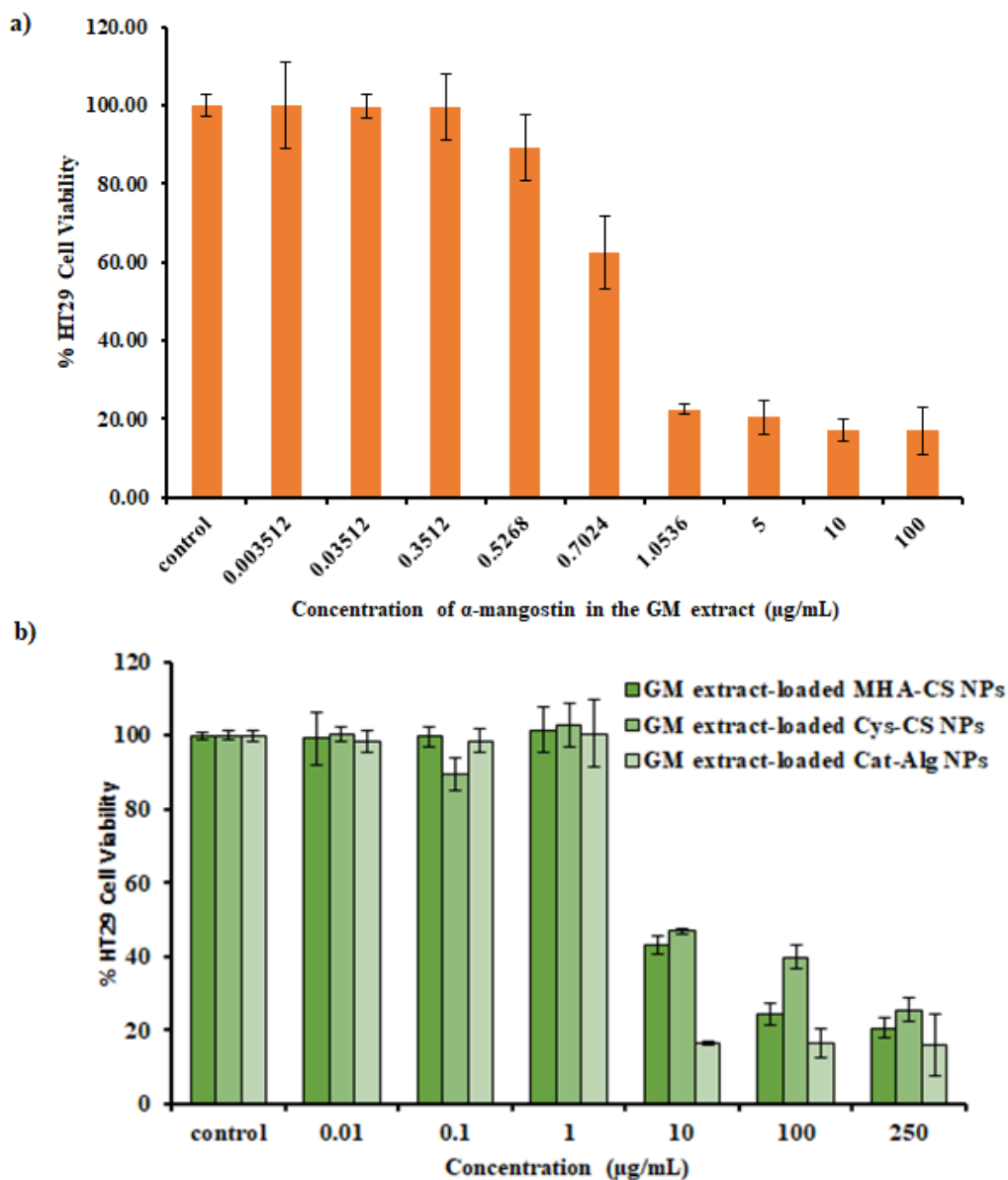


Figure 36 Cytotoxicity of a) free GM extract and b) GM extract-loaded NPs on HT29 cells.

4.6 Development of DOX loaded NPs

4.6.1 DLS measurements

The MHA-CS-Alg-Cat NPs were created by ionic gelation between the Cat-Alg and MHA-CS. Table 10 shows the average particle size, PDI, and zeta potential of the particles. It can be seen that the optimal concentrations of MHA-CS and Cat-Alg for NP formation was 0.05% (MHA-CS: Cat-Alg = 1:1), which offered the

particles with the smallest size lowest PDI value. After the drug loading, the particle size tended to increase compared with the blank NPs. The tiny size of particle may be advantageous for drug delivery as it facilitates penetration of the delivery carriers and accumulation of the delivery systems in the cancer cells. In addition, the surface charge of the NPs were slightly positive, representing the desirable stability of the NPs formulation because it could prevent NPs aggregation due to the strong repulsive forces between particles (Katuwavila et al., 2016; Sorasitthiyankarn et al., 2018).

Table 10 The mean particle size, PDI and zeta potential of the NPs. Each number is displayed as the mean \pm SD from three separated experiments.

NPs	Particle size (nm)	PDI	Zeta potential (mV)
0.025% MHA-CS + 0.075% Cat-Alg	182.43 \pm 10.06	0.50 \pm 0.05	14.40 \pm 0.40
0.050% MHA-CS + 0.050% Cat-Alg	115.80 \pm 0.89	0.20 \pm 0.01	36.17 \pm 1.17
0.075% MHA-CS + 0.025% Cat-Alg	172.90 \pm 4.06	0.36 \pm 0.05	39.63 \pm 2.37
0.050% MHA-CS + 0.025% Cat-Alg	133.13 \pm 2.27	0.32 \pm 0.04	38.23 \pm 0.25

4.6.2 Determination of drug loading and drug content

The DOX was loaded into the MHA-CS-Alg-Cat NPs by adsorption method at various ratios of NPs: DOX. The amount of DOX in the DOX-loaded NPs was reported as %LE and LC (Table 11). The %LE of DOX in the NPs revealed that the drug loading efficiency reaches its limit at the NPs: DOX ratio of 1: 0.5; the %LE was 74%, and the LC value was found to be 249 μ g/mg. Since Cat-Alg is a negatively charged polymer. Hence, the ionic interaction could be created among the drug carriers and the positively charged DOX providing a high loading of the drug on the nanoparticle (Ruggiero et al., 1992). Therefore, this ratio of the NPs: DOX ratio of 1:0.5 was the most suitable condition for DOX loading into NPs.

Table 11 The mean particle size, size distribution, zeta potential, loading efficiency and loading capacity of the DOX loaded mucoadhesive NPs. Data are expressed as mean \pm SD (n = 3).

The ratio of NPs:DOX	Particle size (nm)	PDI	Zeta potential (mV)	Loading capacity ($\mu\text{g}/\text{mg}$)	% loading efficiency
1:0.25	133.87 \pm 1.14	0.26 \pm 0.01	36.87 \pm 1.04	57.3 \pm 0.5	40.9 \pm 0.4
1:0.5	143.27 \pm 0.85	0.25 \pm 0.01	38.07 \pm 1.15	249.0 \pm 0.9	74.7 \pm 0.3
1:1	198.97 \pm 2.83	0.35 \pm 0.04	35.43 \pm 3.32	242.7 \pm 2.2	53.9 \pm 0.5

4.6.3 Release of DOX-loaded NPs

The *in vitro* release of DOX from the DOX-loaded MHA-CS-Alg-Cat NPs was evaluated in AU pH 6.2, which is the pH of the bladder fluid. The cumulative drug release of free DOX and DOX-loaded NPs is presented in Figure 37. It can be observed that DOX was released quickly and depleted in 2 h. Because of the high hydrophilicity of DOX, immediate-release characteristics were witnessed from both DOX and DOX-loaded NPs at the initial stage. In contrast, the drug release from DOX-loaded NPs was found to be increased as time increased. The highest drug release was around 87% at 24 h, suggesting that NPs were able to control the release of DOX. The release characteristics of DOX from the NPs are concordant with a previous study, which reported that a retarded release of DOX could be obtained by incorporation into CS/Alg NPs (Katuwavila et al., 2016).

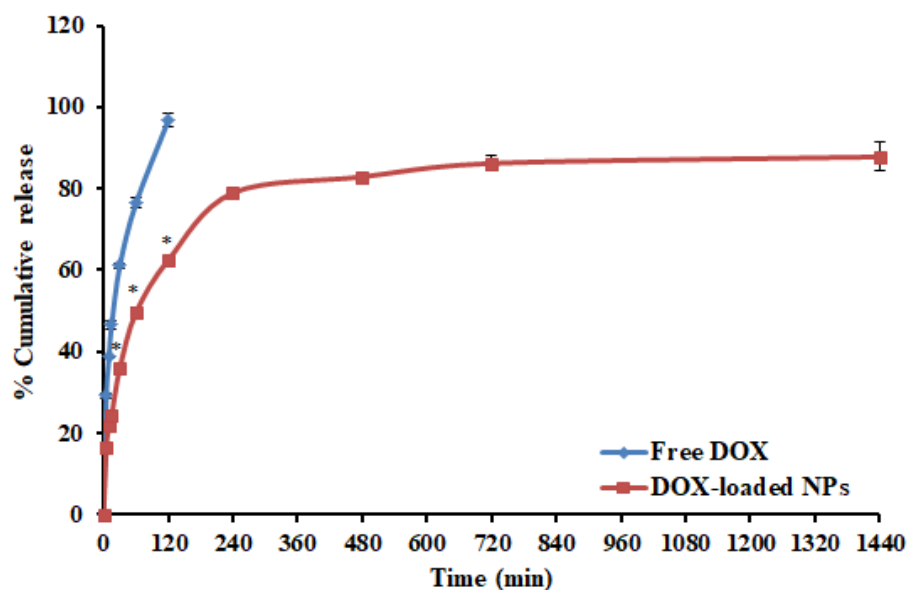


Figure 37 Cumulative release profiles of free DOX and DOX-loaded MHA-CS-Alg-Cat NPs. Data are expressed as mean \pm SD (n = 3) * statistically significant (p < 0.05).

4.6.4 *In vitro* cytotoxicity using MTT assay

The cytotoxic effect of the DOX-loaded MHA-CS-Alg-Cat NPs against bladder cancer cells were investigated against MB49 cells. The *in vitro* anticancer activity of the drug-loaded NPs against bladder cancer was represented by the IC_{50} values, which were the equivalent drug concentration that inhibited 50% of the cells. As it can be seen from Figure 38, the blank NPs exhibited a relative cell viability of greater than 80% indicating that the blank NPs had no cytotoxic effect on the MB49 cells, which was also conveyed by the literature (Bellich et al., 2016; Suárez-Barrio et al., 2019). The IC_{50} values of free DOX and DOX-loaded NPs were determined to be 3.21 and 2.62 $\mu\text{g}/\text{mL}$, respectively. The IC_{50} values of DOX-loaded NPs were lower than the free DOX. These findings indicated that the DOX-loaded NPs eluded quickly from NPs and rapidly released DOX into the cytoplasm, which enhanced the cytotoxicity levels (Tian et al., 2019).

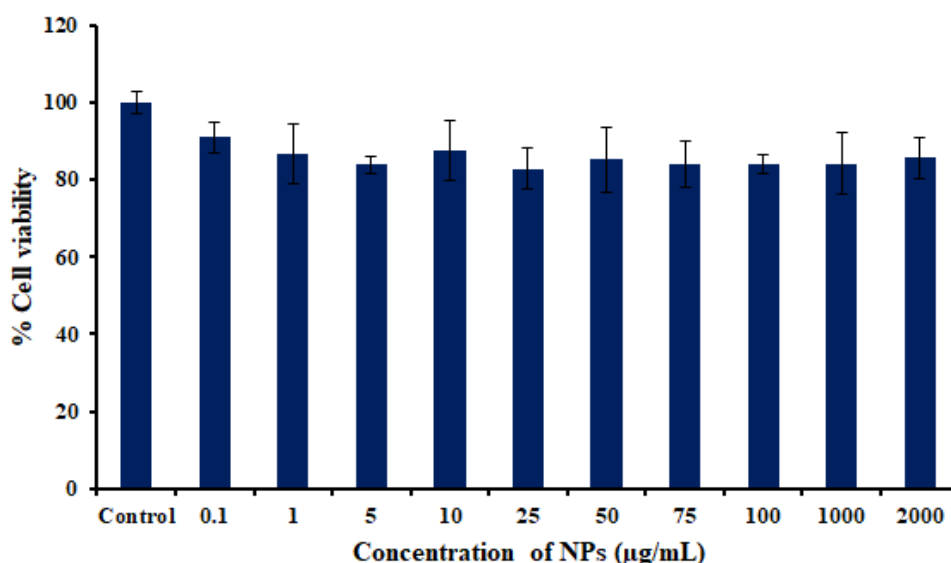


Figure 38 Percentage cell viability of MB49 cells after being treated with the blank NPs.

4.6.5 Cellular Uptake of the NPs

The cellular uptake efficiency at different time points of MHA-CS-Alg-Cat NPs on MB49 cells was investigated by flow cytometry compared with free DOX, and the results are presented in Figure 39. DOX is a fluorescence active compound having a bright red color. MFI from a 10,000-event analysis was reported. The results indicated that DOX-loaded NPs were accumulated into the cancer cells with a relatively greater amount than the free DOX. The findings also indicated that DOX-loaded NPs were continuously deposited into the cells over time. The effective internalization of the NPs could be associated with the positive surface charge of the NPs. A similar finding was conveyed with the *in vitro* cellular uptake of paclitaxel-loaded PEGylated PLGA-based NPs (Danhier et al., 2009). In general, NPs are nonspecifically uptaken into cells through endocytosis or phagocytosis. On the other hand, free DOX pass through the cell membrane by passive diffusion (des Rieux et al., 2006). Morphology observation specified that the cell growth inhibition by DOX-loaded NPs occurs over a longer period than those by the free DOX. From these information, it is suggested that the DOX-loaded NPs sufficiently uptaken into the cells over time.

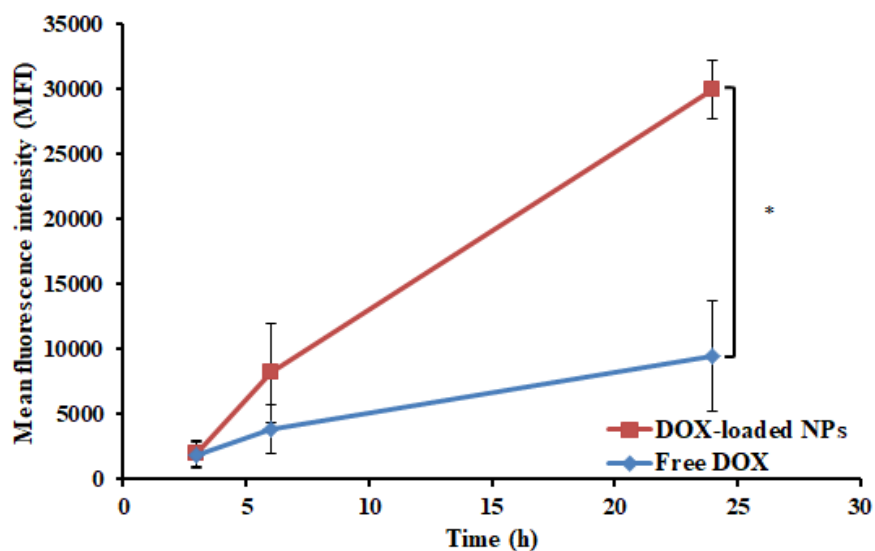


Figure 39 Mean fluorescence intensity (MFI) of free DOX and DOX-loaded MHA-CS-Alg-Cat NPs by flow cytometry. Data are expressed as mean \pm SD (n = 3). *statistically significant (p < 0.05).

4.6.6 Confocal laser scanning microscopy (CLSM) analysis of the NPs

The CLSM images of MB49 cells after exposed to free DOX and the DOX-loaded NPs for 24 h were obtained from Hoechst channel (blue) exciting images at 405 nm, DOX channel (red) excited at 559 nm, and the merged one (Figure 40). The findings revealed that most free DOX are in the nucleus after being uptaken into the cells. However, the DOX-loaded NPs were situated densely enclosing the blue cell nuclei. The obtained data indicated that these NPs could be highly accumulated into the cytoplasm of MB49 cells. Therefore, loading of DOX into NPs were able to improve uptake of the drug into the cancer cells which may lead to the increase in the ability to kill the cancer cells.

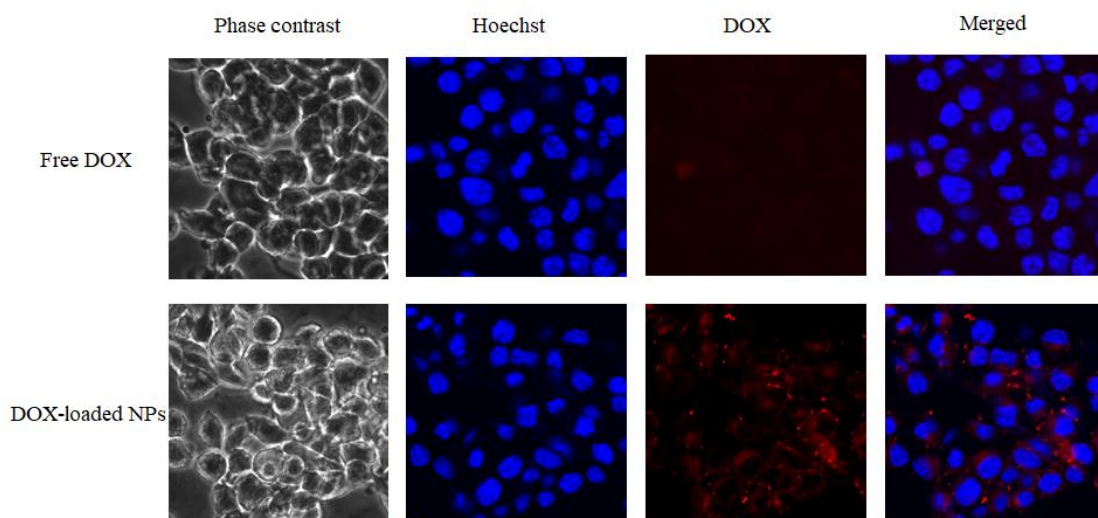
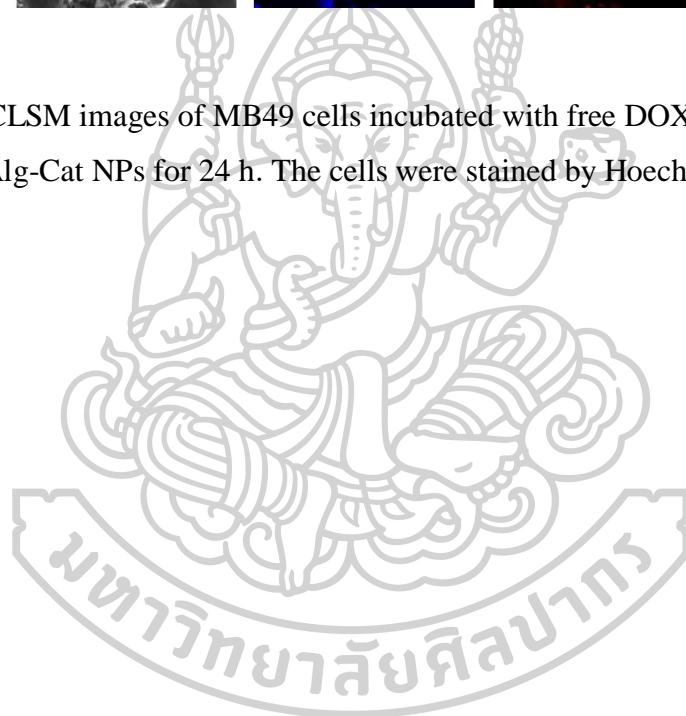


Figure 40 CLSM images of MB49 cells incubated with free DOX, DOX-loaded MHA-CS-Alg-Cat NPs for 24 h. The cells were stained by Hoechst (blue) and DOX (red).



CHAPTER 5

CONCLUSIONS

5.1 Development of Mucoadhesive polymer

The new mucoadhesive polymer, Cat-Alg, Cys-CS and MHA-CS were successfully synthesized. The mucoadhesive polymers were confirmed by FT-IR and NMR. The MHA-CS polymer showed superior mucoadhesive properties compared with Cys-CS and Cat-Alg. In addition, the Cat-Alg, Cys-CS and MHA-CS were found to be non-toxic on the HGF cells. Therefore, the synthesized polymers may be a promising materials for mucoadhesive DDS with enhanced mucoadhesive properties.

5.2 Development of GM extracts loaded mucoadhesive NPs for colon cancer

GM extracts were successfully incorporated into MHA-CS, Cys-CS and Cat-Alg NPs by entrapment method. The particles sizes were in the nanometer range. A large number of drug loading was achieved with optimal %LE. The release of α -mangostin was sustained from the NPs which ensured prolonged action. The GM extracts-loaded NPs exhibited the ability to kill colon cancer cell line with low IC_{50} value. Moreover, the GM extracts-loaded Cat-Alg NPs were able to be deposited inside the colon cancer cells leading to a gradual and continual release of the drug to perform its killing effect.

5.3 Development of DOX loaded mucoadhesive NPs for bladder cancer

The synthesized MHA-CS and Cat-Alg were employed for the fabrication of MHA-CS-Alg-Cat mucoadhesive NPs by the ionotropic gelation method. DOX was incorporated into the NPs through the adsorption method. The particles were in the nanometer range and positive surface charge. The NPs exhibited excellent mucoadhesive properties compared to the CS-Alg NPs and could prolong residence on the mucous tissue. DOX-loaded NPs provided high loading efficiency of DOX. Moreover, the DOX-loaded NPs were able to offer a sustained release profile which is expected to provide a prolonged action. The DOX-loaded NPs could kill the MB49 bladder cancer cells with low IC_{50} . *In in vitro* cellular uptake study indicated that

DOX-loaded NPs could be internalized by MB49 cells and had high targeting efficiency due to specific recognition. Thus, these MHA-CS-Alg-Cat NPs may be a promising mucoadhesive platform for bladder cancer.



REFERENCES

- Ahuja, A., Khar, R.K., Ali, J., 1997. Mucoadhesive drug delivery systems. *Drug Development and Industrial Pharmacy* 23, 489-515. <http://doi.org/10.3109/03639049709148498>.
- Aisha, A.F., Abu-Salah, K.M., Ismail, Z., Majid, A.M., 2012. In vitro and in vivo anti-colon cancer effects of *Garcinia mangostana* xanthenes extract. *MC Complementary and Alternative Medicine* 12, 104. <http://doi.org/10.1186/1472-6882-12-104>.
- Alhusaini, A.M., Fadda, L.M., Alanazi, A.M., Sarawi, W.S., Alomar, H.A., Ali, H.M., Hasan, I.H., Ali, R.A., 2022. Nano-resveratrol: a promising candidate for the treatment of renal toxicity induced by doxorubicin in rats through modulation of beclin-1 and mTOR. *Frontiers in Pharmacology* 13. <http://doi.org/10.3389/fphar.2022.826908>.
- Anitha, A., Sowmya, S., Kumar, P.T.S., Deepthi, S., Chennazhi, K.P., Ehrlich, H., Tsurkan, M., Jayakumar, R., 2014. Chitin and chitosan in selected biomedical applications. *Progress in Polymer Science* 39, 1644-1667. <http://doi.org/https://doi.org/10.1016/j.progpolymsci.2014.02.008>.
- Arcamone, F., Cassinelli, G., Fantini, G., Grein, A., Orezzi, P., Pol, C., Spalla, C., 1969. Adriamycin, 14-hydroxydaunomycin, a new antitumor antibiotic from *S. peuceetius* var. *caesius*. *Biotechnology and Bioengineering* 11, 1101-1110. <http://doi.org/10.1002/bit.260110607>.
- Arnold, M., Sierra, M.S., Laversanne, M., Soerjomataram, I., Jemal, A., Bray, F., 2017. Global patterns and trends in colorectal cancer incidence and mortality. *Gut* 66, 683-691. <http://doi.org/10.1136/gutjnl-2015-310912>.
- Arruebo, M., Vilaboa, N., Sáez-Gutierrez, B., Lambea, J., Tres, A., Valladares, M., González-Fernández, A., 2011. Assessment of the evolution of cancer treatment therapies. *Cancers (Basel)* 3, 3279-3330. <http://doi.org/10.3390/cancers3033279>.
- Badawy, M.E., Rabea, E.I., 2013. Synthesis and structure-activity relationship of N-(cinnamyl) chitosan analogs as antimicrobial agents. *International Journal of Biological Macromolecules* 57, 185-192. <http://doi.org/10.1016/j.ijbiomac.2013.03.028>.

- Bellich, B., D'Agostino, I., Semeraro, S., Gamini, A., Cesàro, A., 2016. "The good, the bad and the ugly" of chitosans. *Marine Drugs* 14. <http://doi.org/10.3390/md14050099>.
- Bernkop-Schnürch, A., 2005. Thiomers: A new generation of mucoadhesive polymers. *Advanced Drug Delivery Reviews* 57, 1569-1582. <http://doi.org/https://doi.org/10.1016/j.addr.2005.07.002>.
- Bernkop-Schnürch, A., Hornof, M., Zoidl, T., 2003. Thiolated polymers—thiomers: synthesis and in vitro evaluation of chitosan–2-iminothiolane conjugates. *International Journal of Pharmaceutics* 260, 229-237. [http://doi.org/https://doi.org/10.1016/S0378-5173\(03\)00271-0](http://doi.org/https://doi.org/10.1016/S0378-5173(03)00271-0).
- Boddupalli, B.M., Mohammed, Z.N., Nath, R.A., Banji, D., 2010. Mucoadhesive drug delivery system: An overview. *Journal of Advanced Pharmaceutical Technology & Research* 1, 381-387. <http://doi.org/10.4103/0110-5558.76436>.
- Brannigan, R.P., Khutoryanskiy, V.V., 2017. Synthesis and evaluation of mucoadhesive acryloyl-quaternized PDMAEMA nanogels for ocular drug delivery. *Colloids and Surfaces B: Biointerfaces* 155, 538-543. <http://doi.org/10.1016/j.colsurfb.2017.04.050>.
- Brannon-Peppas, L., Blanchette, J.O., 2004. Nanoparticle and targeted systems for cancer therapy. *Advanced Drug Delivery Reviews* 56, 1649-1659. <http://doi.org/10.1016/j.addr.2004.02.014>.
- Bullard Dunn, K.M., Rothenberger, D.A., 2015. Colon, Rectum, and Anus, in: Brunnicardi, F.C., Andersen, D.K., Billiar, T.R., Dunn, D.L., Hunter, J.G., Matthews, J.B., Pollock, R.E. (Eds.), *Schwartz's Principles of Surgery*, 10e. McGraw-Hill Education, New York, NY.
- Cascinu, S., Catalano, V., Piga, A., Mattioli, R., Marcellini, M., Pancotti, A., Bascioni, R., Torresi, U., Silva, R.R., Pieroni, V., Giorgi, F., Catalano, G., Cellerino, R., 2003. The role of levamisole in the adjuvant treatment of stage III colon cancer patients: a randomized trial of 5-fluorouracil and levamisole versus 5-fluorouracil alone. *Cancer Investigation* 21, 701-707. <http://doi.org/10.1081/cnv-120023769>.
- Chai, M., Wientjes, M.G., Badalament, R.A., Burgers, J.K., Au, J.L., 1994.

- Pharmacokinetics of intravesical doxorubicin in superficial bladder cancer patients. *the Journal of Urology* 152, 374-378. [http://doi.org/10.1016/s0022-5347\(17\)32742-8](http://doi.org/10.1016/s0022-5347(17)32742-8).
- Chaveli-López, B., Bagán-Sebastián, J.V., 2016. Treatment of oral mucositis due to chemotherapy. *Journal of Clinical and Experimental Dentistry* 8, e201-209. <http://doi.org/10.4317/jced.52917>.
- Chen, C.H., Chan, T.M., Wu, Y.J., Chen, J.J., 2015. Review: application of nanoparticles in urothelial cancer of the urinary bladder. *Journal of Medical and Biological Engineering* 35, 419-427. <http://doi.org/10.1007/s40846-015-0060-5>.
- Chomnawang, M.T., Surassmo, S., Nukoolkarn, V.S., Gritsanapan, W., 2007. Effect of *Garcinia mangostana* on inflammation caused by *propionibacterium acnes*. *Fitoterapia* 78, 401-408. <http://doi.org/10.1016/j.fitote.2007.02.019>.
- Colombel, M., Soloway, M., Akaza, H., Böhle, A., Palou, J., Buckley, R., Lamm, D., Brausi, M., Witjes, J.A., Persad, R., 2008. Epidemiology, staging, grading, and risk stratification of bladder cancer. *European Urology Supplements* 7, 618-626. <http://doi.org/https://doi.org/10.1016/j.eursup.2008.08.002>.
- Cortés-Funes, H., 2007. Present and future roles of bevacizumab in breast cancer. *Breast Cancer Research* 9, S22. <http://doi.org/10.1186/bcr1705>.
- Cui, J., Hu, W., Cai, Z., Liu, Y., Li, S., Tao, W., Xiang, H., 2010. New medicinal properties of mangostins: analgesic activity and pharmacological characterization of active ingredients from the fruit hull of *Garcinia mangostana* L. *Pharmacology Biochemistry and Behavior* 95, 166-172. <http://doi.org/10.1016/j.pbb.2009.12.021>.
- Danhier, F., Lecouturier, N., Vroman, B., Jérôme, C., Marchand-Brynaert, J., Feron, O., Prétat, V., 2009. Paclitaxel-loaded PEGylated PLGA-based nanoparticles: in vitro and in vivo evaluation. *Journal of Controlled Release* 133, 11-17. <http://doi.org/10.1016/j.jconrel.2008.09.086>.
- Davidovich-Pinhas, M., Bianco-Peled, H., 2010. Mucoadhesion: a review of characterization techniques. *Expert Opinion on Drug Delivery* 7, 259-271. <http://doi.org/10.1517/17425240903473134>.
- Davidovich-Pinhas, M., Bianco-Peled, H., 2011. Alginate-PEGAc: a new mucoadhesive

- polymer. *Acta Biomaterialia* 7, 625-633.
<http://doi.org/10.1016/j.actbio.2010.09.021>.
- Davis, M.E., Chen, Z.G., Shin, D.M., 2008. Nanoparticle therapeutics: an emerging treatment modality for cancer. *Nature Reviews Drug Discovery* 7, 771-782.
<http://doi.org/10.1038/nrd2614>.
- De Jong, W.H., Borm, P.J., 2008. Drug delivery and nanoparticles: applications and hazards. *International Journal of Nanomedicine* 3, 133-149.
<http://doi.org/10.2147/ijn.s596>.
- des Rieux, A., Fievez, V., Garinot, M., Schneider, Y.J., Pr at, V., 2006. Nanoparticles as potential oral delivery systems of proteins and vaccines: a mechanistic approach. *Journal of Controlled Release* 116, 1-27.
<http://doi.org/10.1016/j.jconrel.2006.08.013>.
- Dhawan, D., Ramos-Vara, J.A., Naughton, J.F., Cheng, L., Low, P.S., Rothenbuhler, R., Leamon, C.P., Parker, N., Klein, P.J., Vlahov, I.R., Reddy, J.A., Koch, M., Murphy, L., Fourez, L.M., Stewart, J.C., Knapp, D.W., 2013. Targeting folate receptors to treat invasive urinary bladder cancer. *Cancer Research* 73, 875-884.
<http://doi.org/10.1158/0008-5472.Can-12-2101>.
- Din, F.U., Aman, W., Ullah, I., Qureshi, O.S., Mustapha, O., Shafique, S., Zeb, A., 2017. Effective use of nanocarriers as drug delivery systems for the treatment of selected tumors. *International Journal of Nanomedicine* 12, 7291-7309.
<http://doi.org/10.2147/ijn.S146315>.
- Donin, N.M., Lenis, A.T., Holden, S., Drakaki, A., Pantuck, A., Belldegrun, A., Chamie, K., 2017. Immunotherapy for the treatment of urothelial carcinoma. *The Journal of Urology* 197, 14-22. <http://doi.org/10.1016/j.juro.2016.02.3005>.
- Douglass, L., Schoenberg, M., 2016. The future of intravesical drug delivery for non-muscle invasive bladder cancer. *Bladder Cancer* 2, 285-292.
<http://doi.org/10.3233/blc-160056>.
- Duggan, S., Cummins, W., O' Donovan, O., Hughes, H., Owens, E., 2017. Thiolated polymers as mucoadhesive drug delivery systems. *European Journal of Pharmaceutical Sciences* 100. <http://doi.org/10.1016/j.ejps.2017.01.008>.
- Fitzmaurice, C., Allen, C., Barber, R.M., al, e., 2017. Global, regional, and national

- cancer incidence, mortality, years of life lost, years lived with disability, and disability-adjusted life-years for 32 cancer groups, 1990 to 2015: a systematic analysis for the global burden of disease study. *JAMA Oncol* 3, 524-548. <http://doi.org/10.1001/jamaoncol.2016.5688>.
- Fleshman, J., Sargent, D.J., Green, E., Anvari, M., Stryker, S.J., Beart, R.W., Jr., Hellinger, M., Flanagan, R., Jr., Peters, W., Nelson, H., 2007. Laparoscopic colectomy for cancer is not inferior to open surgery based on 5-year data from the COST Study Group trial. *Ann Surg* 246, 655-662; discussion 662-654. <http://doi.org/10.1097/SLA.0b013e318155a762>.
- Folkesson, J., Birgisson, H., Pahlman, L., Cedermark, B., Glimelius, B., Gunnarsson, U., 2005. Swedish rectal cancer trial: long lasting benefits from radiotherapy on survival and local recurrence rate. *Journal of Clinical Oncology* 23, 5644-5650. <http://doi.org/10.1200/jco.2005.08.144>.
- French, R.A., Jacobson, A.R., Kim, B., Isley, S.L., Penn, R.L., Baveye, P.C., 2009. Influence of ionic strength, pH, and cation valence on aggregation kinetics of titanium dioxide nanoparticles. *Environmental Science & Technology* 43, 1354-1359. <http://doi.org/10.1021/es802628n>.
- Fukuokaya, W., Kimura, T., Miki, J., Kimura, S., Watanabe, H., Bo, F., Okada, D., Aikawa, K., Ochi, A., Suzuki, K., Shiga, N., Abe, H., Egawa, S., 2020. Effectiveness of intravesical doxorubicin immediately following resection of primary non-muscle-invasive bladder Cancer: a propensity score-matched analysis. *Clinical Genitourinary Cancer* 18, e55-e61. <http://doi.org/10.1016/j.clgc.2019.09.005>.
- Granados-Romero, J., Valderrama-Treviño, A., Contreras Flores, E., Barrera-Mera, B., Herrera, M., Uriarte-Ruiz, K., Ceballos-Villalva, J.C., Estrada Mata, A., Alvarado, C., Arauz-Peña, G., 2017. Colorectal cancer: a review. *International Journal of Research in Medical Sciences* 5, 4667. <http://doi.org/10.18203/2320-6012.ijrms20174914>.
- Grasso, M., 2008. Bladder Cancer: A major public health issue. *European Urology Supplements* 7, 510-515. <http://doi.org/https://doi.org/10.1016/j.eursup.2008.04.001>.

- GuhaSarkar, S., Banerjee, R., 2010. Intravesical drug delivery: Challenges, current status, opportunities and novel strategies. *Journal of Controlled Release* 148, 147-159. <http://doi.org/10.1016/j.jconrel.2010.08.031>.
- Guillou, P.J., Quirke, P., Thorpe, H., Walker, J., Jayne, D.G., Smith, A.M., Heath, R.M., Brown, J.M., 2005. Short-term endpoints of conventional versus laparoscopic-assisted surgery in patients with colorectal cancer (MRC CLASICC trial): multicentre, randomised controlled trial. *Lancet* 365, 1718-1726. [http://doi.org/10.1016/s0140-6736\(05\)66545-2](http://doi.org/10.1016/s0140-6736(05)66545-2).
- Haruenkit, R., Poovarodom, S., Leontowicz, H., Leontowicz, M., Sajewicz, M., Kowalska, T., Delgado-Licon, E., Rocha-Guzmán, N.E., Gallegos-Infante, J.A., Trakhtenberg, S., Gorinstein, S., 2007. Comparative study of health properties and nutritional value of durian, mangosteen, and snake fruit: experiments in vitro and in vivo. *Journal of Agricultural and Food Chemistry* 55, 5842-5849. <http://doi.org/10.1021/jf070475a>.
- Hassan, E.E., Gallo, J.M., 1990. A simple rheological method for the in vitro assessment of mucin-polymer bioadhesive bond strength. *Pharmaceutical Research* 7, 491-495. <http://doi.org/10.1023/a:1015812615635>.
- Hong, T.S., Clark, J.W., Haigis, K.M., 2012. Cancers of the colon and rectum: identical or fraternal twins? *Cancer Discovery* 2, 117-121. <http://doi.org/10.1158/2159-8290.Cd-11-0315>.
- Horvát, G., Gyarmati, B., Berkó, S., Szabó-Révész, P., Szilágyi, B.Á., Szilágyi, A., Soós, J., Sandri, G., Bonferoni, M.C., Rossi, S., Ferrari, F., Caramella, C., Csányi, E., Budai-Szűcs, M., 2015. Thiolated poly(aspartic acid) as potential in situ gelling, ocular mucoadhesive drug delivery system. *European Journal of Pharmaceutical Sciences* 67, 1-11. <http://doi.org/https://doi.org/10.1016/j.ejps.2014.10.013>.
- Huang, C., Neoh, K.G., Xu, L., Kang, E.T., Chiong, E., 2012. Polymeric nanoparticles with encapsulated superparamagnetic iron oxide and conjugated cisplatin for potential bladder cancer therapy. *Biomacromolecules* 13, 2513-2520. <http://doi.org/10.1021/bm300739w>.
- Ishikawa, T., Watanabe, Y., Takayama, K., Endo, H., Matsumoto, M., 2000. Effect of

- hydroxypropylmethylcellulose (HPMC) on the release profiles and bioavailability of a power water-soluble drug from tablets prepared using macrogol and HPMC. *International journal of pharmaceutics* 202, 173-178. [http://doi.org/10.1016/S0378-5173\(00\)00426-9](http://doi.org/10.1016/S0378-5173(00)00426-9).
- Janes, K.A., Fresneau, M.P., Marazuela, A., Fabra, A., Alonso, M.J., 2001. Chitosan nanoparticles as delivery systems for doxorubicin. *Journal of Controlled Release* 73, 255-267. [http://doi.org/10.1016/s0168-3659\(01\)00294-2](http://doi.org/10.1016/s0168-3659(01)00294-2).
- Kaidar-Person, O., Gil, Z., Billan, S., 2018. Precision medicine in head and neck cancer. *Drug Resistance Updates* 40, 13-16. <http://doi.org/10.1016/j.drug.2018.09.001>.
- Karavana, S.Y., Şenyiğit, Z.A., Çalışkan, Ç., Sevin, G., Özdemir, D., Erzurumlu, Y., Şen, S., Baloğlu, E., 2018. Gemcitabine hydrochloride microspheres used for intravesical treatment of superficial bladder cancer: a comprehensive in vitro/ex vivo/in vivo evaluation. *Drug Design, Development and Therapy* 12, 1959-1975. <http://doi.org/10.2147/dddt.S164704>.
- Katuwavila, N.P., Perera, A.D.L.C., Samarakoon, S.R., Soysa, P., Karunaratne, V., Amaratunga, G.A.J., Karunaratne, D.N., 2016. Chitosan-alginate nanoparticle system efficiently delivers doxorubicin to MCF-7 cells. *Journal of Nanomaterials* 2016, 3178904. <http://doi.org/10.1155/2016/3178904>.
- Kaufman, D.S., 2006. Challenges in the treatment of bladder cancer. *Annals of Oncology* 17 Suppl 5, v106-112. <http://doi.org/10.1093/annonc/mdj963>.
- Kaufman, D.S., Shipley, W.U., Feldman, A.S., 2009. Bladder cancer. *Lancet* 374, 239-249. [http://doi.org/10.1016/s0140-6736\(09\)60491-8](http://doi.org/10.1016/s0140-6736(09)60491-8).
- Keizer, H.G., Pinedo, H.M., Schuurhuis, G.J., Joenje, H., 1990. Doxorubicin (adriamycin): a critical review of free radical-dependent mechanisms of cytotoxicity. *Pharmacology & Therapeutics* 47, 219-231. [http://doi.org/https://doi.org/10.1016/0163-7258\(90\)90088-J](http://doi.org/https://doi.org/10.1016/0163-7258(90)90088-J).
- Khutoryanskiy, V.V., 2011. Advances in mucoadhesion and mucoadhesive polymers. *Macromolecular Bioscience* 11, 748-764. <http://doi.org/10.1002/mabi.201000388>.
- Kim, K., Kim, K., Ryu, J.H., Lee, H., 2015. Chitosan-catechol: a polymer with long-lasting mucoadhesive properties. *Biomaterials* 52, 161-170.

<http://doi.org/10.1016/j.biomaterials.2015.02.010>.

- Korossis, S., Bolland, F., Ingham, E., Fisher, J., Kearney, J., Southgate, J., 2006. Review: tissue engineering of the urinary bladder: considering structure-function relationships and the role of mechanotransduction. *Tissue engineering* 12, 635-644. <http://doi.org/10.1089/ten.2006.12.635>.
- Kumari, A., Yadav, S.K., Yadav, S.C., 2010. Biodegradable polymeric nanoparticles based drug delivery systems. *Colloids and Surfaces B: Biointerfaces* 75, 1-18. <http://doi.org/10.1016/j.colsurfb.2009.09.001>.
- Labianca, R., Beretta, G.D., Kildani, B., Milesi, L., Merlin, F., Mosconi, S., Pessi, M.A., Prochilo, T., Quadri, A., Gatta, G., de Braud, F., Wils, J., 2010. Colon cancer. *Crit Rev Oncol Hematol* 74, 106-133. <http://doi.org/10.1016/j.critrevonc.2010.01.010>.
- Lee, C., Shin, J., Lee, J.S., Byun, E., Ryu, J.H., Um, S.H., Kim, D.I., Lee, H., Cho, S.W., 2013. Bioinspired, calcium-free alginate hydrogels with tunable physical and mechanical properties and improved biocompatibility. *Biomacromolecules* 14, 2004-2013. <http://doi.org/10.1021/bm400352d>.
- Lee, K., Lim, S., Kim, T.H., 2018. Dopamine-conjugated poly(acrylic acid) blended with an electrically conductive polyaniline binder for silicon anode. *Bulletin of the Korean Chemical Society* 39. <http://doi.org/10.1002/bkcs.11492>.
- Lee, S.J., Kim, S.W., Chung, H., Park, Y.T., Choi, Y.W., Cho, Y.H., Yoon, M.S., 2005. Bioadhesive drug delivery system using glyceryl monooleate for the intravesical administration of paclitaxel. *Chemotherapy* 51, 311-318. <http://doi.org/10.1159/000088953>.
- Lehr, C.-M., Bouwstra, J.A., Schacht, E.H., Junginger, H.E., 1992. In vitro evaluation of mucoadhesive properties of chitosan and some other natural polymers. *International Journal of Pharmaceutics* 78, 43-48. [http://doi.org/https://doi.org/10.1016/0378-5173\(92\)90353-4](http://doi.org/https://doi.org/10.1016/0378-5173(92)90353-4).
- Lenis, A.T., Lec, P.M., Chamie, K., Mshs, M.D., 2020. Bladder cancer: a review. *The Journal of the American Medical Association* 324, 1980-1991. <http://doi.org/10.1001/jama.2020.17598>.
- Li, T., Takeoka, S., 2013. A novel application of maleimide for advanced drug delivery:

- in vitro and in vivo evaluation of maleimide-modified pH-sensitive liposomes. *International Journal of Nanomedicine* 8, 3855-3866. <http://doi.org/10.2147/ijn.S47749>.
- Lowe, A.B., 2014. Thiol–ene “click” reactions and recent applications in polymer and materials synthesis: a first update. *Polymer Chemistry* 5, 4820-4870. <http://doi.org/10.1039/C4PY00339J>.
- Lu, Z., Yeh, T.K., Tsai, M., Au, J.L., Wientjes, M.G., 2004. Paclitaxel-loaded gelatin nanoparticles for intravesical bladder cancer therapy. *Clinical Cancer Research* 10, 7677-7684. <http://doi.org/10.1158/1078-0432.Ccr-04-1443>.
- Lu, Z., Yeh, T.K., Wang, J., Chen, L., Lyness, G., Xin, Y., Wientjes, M.G., Bergdall, V., Couto, G., Alvarez-Berger, F., Kosarek, C.E., Au, J.L., 2011. Paclitaxel gelatin nanoparticles for intravesical bladder cancer therapy. *The Journal of Urology* 185, 1478-1483. <http://doi.org/10.1016/j.juro.2010.11.091>.
- Madhav, N.V., Tangri, P., 2011. Formulation and evaluation of zidovudine bio-micro dwarfs using a novel bio-muco resident from *Artocarpus heterophyllus*. *International Journal of PharmTech Research* 3, 169-174.
- Mallikarjuna Setty, C., Sahoo, S.S., Sa, B., 2005. Alginate-coated alginate-polyethyleneimine beads for prolonged release of furosemide in simulated intestinal fluid. *Drug Development and Industrial Pharmacy* 31, 435-446. <http://doi.org/10.1080/03639040500214647>.
- Mármol, I., Sánchez-de-Diego, C., Pradilla Dieste, A., Cerrada, E., Rodriguez Yoldi, M.J., 2017. Colorectal carcinoma: a general overview and future perspectives in colorectal cancer. *International Journal of Molecular Sciences* 18. <http://doi.org/10.3390/ijms18010197>.
- Matsumoto, K., Akao, Y., Yi, H., Ohguchi, K., Ito, T., Tanaka, T., Kobayashi, E., Iinuma, M., Nozawa, Y., 2004. Preferential target is mitochondria in α -mangostin-induced apoptosis in human leukemia HL60 cells. *Bioorganic & Medicinal Chemistry* 12, 5799-5806. <http://doi.org/https://doi.org/10.1016/j.bmc.2004.08.034>.
- Maxwell, M.B., Maher, K.E., 1992. Chemotherapy-induced myelosuppression. *Seminars in Oncology Nursing* 8, 113-123. <http://doi.org/10.1016/0749->

[2081\(92\)90027-z.](#)

- Mehnert, W., Mäder, K., 2001. Solid lipid nanoparticles: production, characterization and applications. *Advanced Drug Delivery Reviews* 47, 165-196. [http://doi.org/10.1016/s0169-409x\(01\)00105-3](http://doi.org/10.1016/s0169-409x(01)00105-3).
- Moertel, C.G., Fleming, T.R., Macdonald, J.S., Haller, D.G., Laurie, J.A., Goodman, P.J., Ungerleider, J.S., Emerson, W.A., Tormey, D.C., Glick, J.H., et al., 1990. Levamisole and fluorouracil for adjuvant therapy of resected colon carcinoma. *The New England Journal of Medicine* 322, 352-358. <http://doi.org/10.1056/nejm199002083220602>.
- Mohammed, M.A., Syeda, J.T.M., Wasan, K.M., Wasan, E.K., 2017. An overview of chitosan nanoparticles and its application in non-parenteral drug delivery. *Pharmaceutics* 9. <http://doi.org/10.3390/pharmaceutics9040053>.
- Moongkarndi, P., Kosem, N., Kaslungka, S., Luanratana, O., Pongpan, N., Neungton, N., 2004. Antiproliferation, antioxidation and induction of apoptosis by *Garcinia mangostana* (mangosteen) on SKBR3 human breast cancer cell line. *Journal of Ethnopharmacology* 90, 161-166. <http://doi.org/10.1016/j.jep.2003.09.048>.
- Mudshinge, S.R., Deore, A.B., Patil, S., Bhalgat, C.M., 2011. Nanoparticles: emerging carriers for drug delivery. *Saudi Pharmaceutical Journal* 19, 129-141. <http://doi.org/10.1016/j.jsps.2011.04.001>.
- Mulia, K., Singarimbun, A.C., Krisanti, E.A., 2020. Optimization of chitosan-alginate microparticles for delivery of mangostins to the colon area using box-behnken experimental design. *International Journal of Molecular Sciences* 21. <http://doi.org/10.3390/ijms21030873>.
- Neutsch, L., Plattner, V.E., Polster-Wildhofen, S., Zidar, A., Chott, A., Borchard, G., Zechner, O., Gabor, F., Wirth, M., 2011. Lectin mediated biorecognition as a novel strategy for targeted delivery to bladder cancer. *The Journal of Urology* 186, 1481-1488. <http://doi.org/10.1016/j.juro.2011.05.040>.
- Ninan, L., Monahan, J., Stroshine, R.L., Wilker, J.J., Shi, R., 2003. Adhesive strength of marine mussel extracts on porcine skin. *Biomaterials* 24, 4091-4099. [http://doi.org/https://doi.org/10.1016/S0142-9612\(03\)00257-6](http://doi.org/https://doi.org/10.1016/S0142-9612(03)00257-6).
- Ovalle-Magallanes, B., Eugenio-Pérez, D., Pedraza-Chaverri, J., 2017a. Medicinal

- properties of mangosteen (*Garcinia mangostana* L.): A comprehensive update. *Food and Chemical Toxicology* 109, 102-122. <http://doi.org/10.1016/j.fct.2017.08.021>.
- Ovalle-Magallanes, B., Eugenio-Pérez, D., Pedraza-Chaverri, J., 2017b. Medicinal properties of mangosteen (*Garcinia mangostana* L.): A comprehensive update. *Food and Chemical Toxicology* 109, 102-122. <http://doi.org/https://doi.org/10.1016/j.fct.2017.08.021>.
- Paques, J.P., van der Linden, E., van Rijn, C.J., Sagis, L.M., 2014. Preparation methods of alginate nanoparticles. *Advances in Colloid and Interface Science* 209, 163-171. <http://doi.org/10.1016/j.cis.2014.03.009>.
- Parveen, S., Misra, R., Sahoo, S.K., 2012. Nanoparticles: a boon to drug delivery, therapeutics, diagnostics and imaging. *Nanomedicine* 8, 147-166. <http://doi.org/10.1016/j.nano.2011.05.016>.
- Parveen, S., Sahoo, S.K., 2008. Polymeric nanoparticles for cancer therapy. *Journal of Drug Targeting* 16, 108-123. <http://doi.org/10.1080/10611860701794353>.
- Patil, S.B., Sawant, K.K., 2009. Development, optimization and in vitro evaluation of alginate mucoadhesive microspheres of carvedilol for nasal delivery. *Journal of Microencapsulation* 26, 432-443. <http://doi.org/10.1080/02652040802456726>.
- Pedraza-Chaverri, J., Cárdenas-Rodríguez, N., Orozco-Ibarra, M., Pérez-Rojas, J.M., 2008. Medicinal properties of mangosteen (*Garcinia mangostana*). *Food and Chemical Toxicology* 46, 3227-3239. <http://doi.org/10.1016/j.fct.2008.07.024>.
- Plattner, V.E., Wagner, M., Ratzinger, G., Gabor, F., Wirth, M., 2008. Targeted drug delivery: binding and uptake of plant lectins using human 5637 bladder cancer cells. *European Journal of Pharmaceutics and Biopharmaceutics* 70, 572-576. <http://doi.org/10.1016/j.ejpb.2008.06.004>.
- Pornpitchanarong, C., Rojanarata, T., Opanasopit, P., Ngawhirunpat, T., Patrojanasophon, P., 2020a. Synthesis of novel N-vinylpyrrolidone/acrylic acid nanoparticles as drug delivery carriers of cisplatin to cancer cells. *Colloids and Surfaces B: Biointerfaces* 185, 110566. <http://doi.org/10.1016/j.colsurfb.2019.110566>.
- Pornpitchanarong, C., Sahatsapan, N., Rojanarata, T., Opanasopit, P., Ngawhirunpat, T.,

- Patrojanasophon, P., 2020b. Curcumin-incorporated thiolated chitosan/alginate nanocarriers: physicochemical properties and release mechanism. *Indian Journal of Pharmaceutical Sciences*.
- Pothitirat, W., Chomnawang, M.T., Supabphol, R., Gritsanapan, W., 2009. Comparison of bioactive compounds content, free radical scavenging and anti-acne inducing bacteria activities of extracts from the mangosteen fruit rind at two stages of maturity. *Fitoterapia* 80, 442-447. <http://doi.org/10.1016/j.fitote.2009.06.005>.
- Prabhu, V., Jasmine, M., 2014. Polymeric nanoparticles- the new face in drug delivery and cancer therapy. *Malaya Journal of Biosciences*, 1-7.
- Putz, A., Burghilea, T., 2009. The solid–fluid transition in a yield stress shear thinning physical gel. *Rheologica Acta* 48, 673-689. <http://doi.org/10.1007/s00397-009-0365-9>.
- Rinaudo, M., 2006. Chitin and chitosan: properties and applications. *Progress in Polymer Science* 31, 603-632. <http://doi.org/https://doi.org/10.1016/j.progpolymsci.2006.06.001>.
- Rositch, A.F., 2020. Global burden of cancer attributable to infections: the critical role of implementation science. *The Lancet Global Health* 8, e153-e154. [http://doi.org/https://doi.org/10.1016/S2214-109X\(20\)30001-2](http://doi.org/https://doi.org/10.1016/S2214-109X(20)30001-2).
- Rossi, J.M., Dunn, N.R., Hogan, B.L., Zaret, K.S., 2001. Distinct mesodermal signals, including BMPs from the septum transversum mesenchyme, are required in combination for hepatogenesis from the endoderm. *Genes & Development* 15, 1998-2009. <http://doi.org/10.1101/gad.904601>.
- Ruggiero, J., Xodo, L.E., Ciana, A., Manzini, G., Quadrifoglio, F., 1992. Charge effect in the interaction of doxorubicin and derivatives with polydeoxynucleotides. *Biochimica et Biophysica Acta (BBA) - Gene Structure and Expression* 1129, 294-302. [http://doi.org/https://doi.org/10.1016/0167-4781\(92\)90506-U](http://doi.org/https://doi.org/10.1016/0167-4781(92)90506-U).
- Sahoo, S., Chakraborti, C., Mishra, S., Nanda, U., 2011. Qualitative analysis of environmentally responsive biodegradable smart carbopol polymer. *International Journal of Pharmaceutical Sciences Review and Research* 9.
- Shaikh, R., Raj Singh, T.R., Garland, M.J., Woolfson, A.D., Donnelly, R.F., 2011. Mucoadhesive drug delivery systems. *Journal of Pharmacy and Bioallied*

- Sciences 3, 89-100. <http://doi.org/10.4103/0975-7406.76478>.
- Shen, Z., Shen, T., Wientjes, M.G., O'Donnell, M.A., Au, J.L., 2008. Intravesical treatments of bladder cancer: review. *Pharmaceutical Research* 25, 1500-1510. <http://doi.org/10.1007/s11095-008-9566-7>.
- Shibata, M.A., Iinuma, M., Morimoto, J., Kurose, H., Akamatsu, K., Okuno, Y., Akao, Y., Otsuki, Y., 2011. α -Mangostin extracted from the pericarp of the mangosteen (*Garcinia mangostana* Linn) reduces tumor growth and lymph node metastasis in an immunocompetent xenograft model of metastatic mammary cancer carrying a p53 mutation. *BMC Med* 9, 69. <http://doi.org/10.1186/1741-7015-9-69>.
- Shitrit, Y., Bianco-Peled, H., 2017. Acrylated chitosan for mucoadhesive drug delivery systems. *International Journal of Pharmaceutics* 517, 247-255. <http://doi.org/10.1016/j.ijpharm.2016.12.023>.
- Siefker-Radtke, A.O., Apolo, A.B., Bivalacqua, T.J., Spiess, P.E., Black, P.C., 2018. Immunotherapy with checkpoint blockade in the treatment of urothelial carcinoma. *The Journal of Urology* 199, 1129-1142. <http://doi.org/https://doi.org/10.1016/j.juro.2017.10.041>.
- Singla, A.K., Chawla, M., 2001. Chitosan: some pharmaceutical and biological aspects--an update. *Journal of Pharmacy and Pharmacology* 53, 1047-1067. <http://doi.org/10.1211/0022357011776441>.
- Soares, L.B.M., Lima, A.P.B., Melo, A.S., Almeida, T.C., de Medeiros Teixeira, L.F., da Silva, G.N., 2022. Additive effects of resveratrol and doxorubicin on bladder cancer cells. *Anti-Cancer Drugs* 33, e389-e397. <http://doi.org/10.1097/cad.0000000000001218>.
- Soler, R., Bruschini, H., Martins, J.R., Dreyfuss, J.L., Camara, N.O., Alves, M.T., Leite, K.R., Truzzi, J.C., Nader, H.B., Srougi, M., Ortiz, V., 2008. Urinary glycosaminoglycans as biomarker for urothelial injury: is it possible to discriminate damage from recovery? *Urology* 72, 937-942. <http://doi.org/10.1016/j.urology.2008.01.028>.
- Sorasitthyanukarn, F.N., Muangnoi, C., Ratnatilaka Na Bhuket, P., Rojsitthisak, P., Rojsitthisak, P., 2018. Chitosan/alginate nanoparticles as a promising approach for oral delivery of curcumin diglutaric acid for cancer treatment. *Materials*

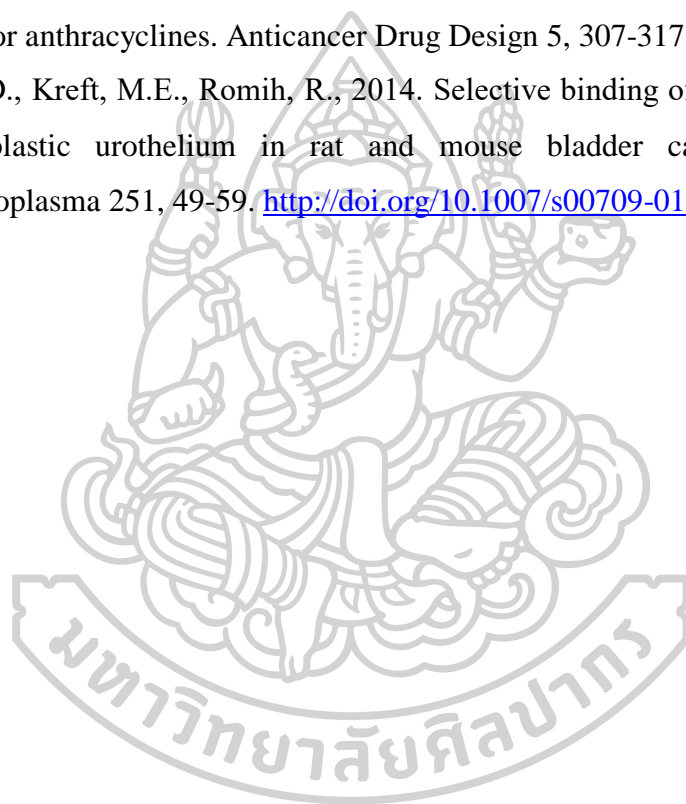
- Science & Engineering, C: Materials for Biological Applications 93, 178-190.
<http://doi.org/10.1016/j.msec.2018.07.069>.
- Sosnik, A., das Neves, J., Sarmiento, B., 2014. Mucoadhesive polymers in the design of nano-drug delivery systems for administration by non-parenteral routes: A review. *Progress in Polymer Science* 39, 2030-2075.
<http://doi.org/https://doi.org/10.1016/j.progpolymsci.2014.07.010>.
- Suárez-Barrio, C., Etxebarria, J., Hernáez-Moya, R., Del Val-Alonso, M., Rodríguez-Astigarraga, M., Urkaregi, A., Freire, V., Morales, M.C., Durán, J.A., Vicario, M., Molina, I., Herrero-Vanrell, R., Andollo, N., 2019. Hyaluronic acid combined with serum rich in growth factors in corneal epithelial defects. *International Journal of Molecular Sciences* 20.
<http://doi.org/10.3390/ijms20071655>.
- Sun, J., Tan, H., 2013. Alginate-based biomaterials for regenerative medicine applications. *Materials (Basel)* 6, 1285-1309. <http://doi.org/10.3390/ma6041285>.
- Sundaram, B.M., Gopalakrishnan, C., Subramanian, S., Shankaranarayanan, D., Kameswaran, L., 1983. Antimicrobial activities of *Garcinia mangostana*. *Planta Med* 48, 59-60. <http://doi.org/10.1055/s-2007-969882>.
- Taber, A., Christensen, E., Lamy, P., Nordentoft, I., Prip, F., Lindskrog, S.V., Birkenkamp-Demtröder, K., Okholm, T.L.H., Knudsen, M., Pedersen, J.S., Steiniche, T., Agerbæk, M., Jensen, J.B., Dyrskjöt, L., 2020. Molecular correlates of cisplatin-based chemotherapy response in muscle invasive bladder cancer by integrated multi-omics analysis. *Nature Communications* 11, 4858.
<http://doi.org/10.1038/s41467-020-18640-0>.
- Tahara, K., Yamamoto, K., Nishihata, T., 1995. Overall mechanism behind matrix sustained release (SR) tablets prepared with hydroxypropyl methylcellulose 2910. *Journal of Controlled Release* 35, 59-66.
[http://doi.org/https://doi.org/10.1016/0168-3659\(95\)00021-Y](http://doi.org/https://doi.org/10.1016/0168-3659(95)00021-Y).
- Takata, R., Katagiri, T., Kanehira, M., Tsunoda, T., Shuin, T., Miki, T., Namiki, M., Kohri, K., Matsushita, Y., Fujioka, T., Nakamura, Y., 2005. Predicting response to methotrexate, vinblastine, doxorubicin, and cisplatin neoadjuvant chemotherapy for bladder cancers through genome-wide gene expression

- profiling. *Clinical Cancer Research* 11, 2625-2636. <http://doi.org/10.1158/1078-0432.Ccr-04-1988>.
- Thorn, C.F., Oshiro, C., Marsh, S., Hernandez-Boussard, T., McLeod, H., Klein, T.E., Altman, R.B., 2011. Doxorubicin pathways: pharmacodynamics and adverse effects. *Pharmacogenetics and Genomics* 21, 440-446. <http://doi.org/10.1097/FPC.0b013e32833ffb56>.
- Tian, G., Sun, X., Bai, J., Dong, J., Zhang, B., Gao, Z., Wu, J., 2019. Doxorubicin-loaded dual-functional hyaluronic acid nanoparticles: Preparation, characterization and antitumor efficacy in vitro and in vivo. *Molecular Medicine Reports* 19, 133-142. <http://doi.org/10.3892/mmr.2018.9687>.
- Tonglairoum, P., Brannigan, R.P., Opanasopit, P., Khutoryanskiy, V.V., 2016. Maleimide-bearing nanogels as novel mucoadhesive materials for drug delivery. *Journal of Materials Chemistry B* 4, 6581-6587. <http://doi.org/10.1039/c6tb02124g>.
- Tyagi, P., Kashyap, M., Hensley, H., Yoshimura, N., 2016. Advances in intravesical therapy for urinary tract disorders. *Expert Opinion on Drug Delivery* 13, 71-84. <http://doi.org/10.1517/17425247.2016.1100166>.
- Vyas, R., Gupta, N., Nimesh, S., 2016. Chapter 9 - Chitosan nanoparticles for efficient and targeted delivery of anticancer drugs, in: Grumezescu, A.M. (Ed.), *Nanobiomaterials in Cancer Therapy*. William Andrew Publishing, pp. 281-306.
- Waite, J.H., 1985. Catechol oxidase in the byssus of the common mussel, *mytilus edulis* L. *Journal of the Marine Biological Association of the United Kingdom* 65, 359-371. <http://doi.org/10.1017/S0025315400050487>.
- Wang, F., Yang, S., Yuan, J., Gao, Q., Huang, C., 2016. Effective method of chitosan-coated alginate nanoparticles for target drug delivery applications. *Journal of Biomaterials Applications* 31, 3-12. <http://doi.org/10.1177/0885328216648478>.
- Werle, M., Takeuchi, H., Bernkop-Schnürch, A., 2009. Modified chitosans for oral drug delivery. *Journal of Pharmaceutical Sciences* 98, 1643-1656. <http://doi.org/10.1002/jps.21550>.
- Wilczewska, A.Z., Niemirowicz, K., Markiewicz, K.H., Car, H., 2012. Nanoparticles as drug delivery systems. *Pharmacological Reports* 64, 1020-1037.

[http://doi.org/10.1016/s1734-1140\(12\)70901-5](http://doi.org/10.1016/s1734-1140(12)70901-5).

- Wirth, M., Plattner, V.E., Gabor, F., 2009. Strategies to improve drug delivery in bladder cancer therapy. *Expert Opinion on Drug Delivery* 6, 727-744. <http://doi.org/10.1517/17425240903022758>.
- Wissing, S.A., Müller, R.H., 2003. The influence of solid lipid nanoparticles on skin hydration and viscoelasticity--in vivo study. *European Journal of Pharmaceutics and Biopharmaceutics* 56, 67-72. [http://doi.org/10.1016/s0939-6411\(03\)00040-7](http://doi.org/10.1016/s0939-6411(03)00040-7).
- Woraphatphadung, T., Sajomsang, W., Gonil, P., Saesoo, S., Opanasopit, P., 2015. Synthesis and characterization of pH-responsive N-naphthyl-N,O-succinyl chitosan micelles for oral meloxicam delivery. *Carbohydrate Polymers* 121, 99-106. <http://doi.org/10.1016/j.carbpol.2014.12.039>.
- Xu, J., Strandman, S., Zhu, J.X., Barralet, J., Cerruti, M., 2015. Genipin-crosslinked catechol-chitosan mucoadhesive hydrogels for buccal drug delivery. *Biomaterials* 37, 395-404. <http://doi.org/10.1016/j.biomaterials.2014.10.024>.
- Xu, J., Tam, M., Samaei, S., Lerouge, S., Barralet, J., Stevenson, M.M., Cerruti, M., 2017. Mucoadhesive chitosan hydrogels as rectal drug delivery vessels to treat ulcerative colitis. *Acta Biomater* 48, 247-257. <http://doi.org/10.1016/j.actbio.2016.10.026>.
- Yan, X., Al-Hayek, S., Huang, H., Zhu, Z., Zhu, W., Guo, H., 2013. Photodynamic effect of 5-aminolevulinic acid-loaded nanoparticles on bladder cancer cells: a preliminary investigation. *Scandinavian Journal of Urology* 47, 145-151. <http://doi.org/10.3109/00365599.2012.713000>.
- Yoo, H.S., Lee, K.H., Oh, J.E., Park, T.G., 2000. In vitro and in vivo anti-tumor activities of nanoparticles based on doxorubicin-PLGA conjugates. *Journal of Controlled Release* 68, 419-431. [http://doi.org/10.1016/s0168-3659\(00\)00280-7](http://doi.org/10.1016/s0168-3659(00)00280-7).
- Yoo, J., Park, C., Yi, G., Lee, D., Koo, H., 2019. Active targeting strategies using biological ligands for nanoparticle drug delivery systems. *Cancers (Basel)* 11. <http://doi.org/10.3390/cancers11050640>.
- Zargar, H., Aning, J., Ischia, J., So, A., Black, P., 2014. Optimizing intravesical mitomycin C therapy in non-muscle-invasive bladder cancer. *Nature Reviews Urology* 11, 220-230. <http://doi.org/10.1038/nrurol.2014.52>.

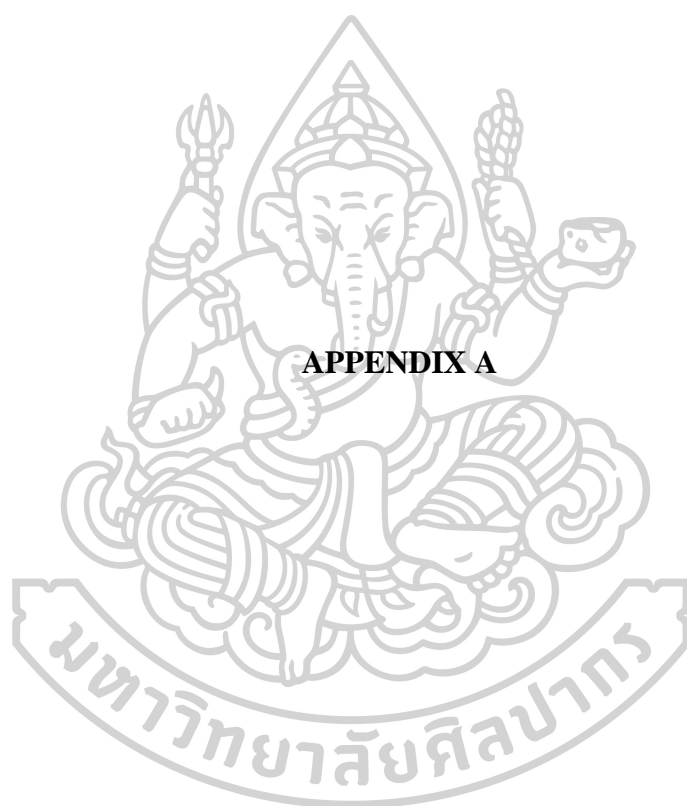
- Zeng, Q., Wen, H., Wen, Q., Chen, X., Wang, Y., Xuan, W., Liang, J., Wan, S., 2013. Cucumber mosaic virus as drug delivery vehicle for doxorubicin. *Biomaterials* 34, 4632-4642. <http://doi.org/10.1016/j.biomaterials.2013.03.017>.
- Zhong, C., Wu, J., Reinhart-King, C.A., Chu, C.C., 2010. Synthesis, characterization and cytotoxicity of photo-crosslinked maleic chitosan–polyethylene glycol diacrylate hybrid hydrogels. *Acta Biomaterialia* 6, 3908-3918. <http://doi.org/https://doi.org/10.1016/j.actbio.2010.04.011>.
- Zunino, F., Capranico, G., 1990. DNA topoisomerase II as the primary target of anti-tumor anthracyclines. *Anticancer Drug Design* 5, 307-317.
- Zupančič, D., Kreft, M.E., Romih, R., 2014. Selective binding of lectins to normal and neoplastic urothelium in rat and mouse bladder carcinogenesis models. *Protoplasma* 251, 49-59. <http://doi.org/10.1007/s00709-013-0524-9>.





APPENDIX

มหาวิทยาลัยศิลปากร



1. Synthesized polymers

Table 12 The amount of thiol groups on the Cys-CS

No.	Thiol group ($\mu\text{mol/g}$)
1	247.02
2	245.01
3	267.75
mean	253.26
SD	12.59

Table 13 The amount of maleimide groups on the MHA-CS

No.	Maleimide group ($\mu\text{mol/g}$)
1	470.21
2	466.42
3	461.69
mean	466.11
SD	4.27



2. Mucoadhesive properties

2.1 *Ex-vivo* mucoadhesion assay (Tensile testing method)

Table 14 The *ex vivo* mucoadhesive strength of the compressed tablets made of the polymers after being contacted with a porcine buccal mucosa.

Sample	No.	Force (N)	mean	SD
CS	1	0.021	0.027	0.006
	2	0.033		
	3	0.027		
Alg	1	0.088	0.076	0.018
	2	0.084		
	3	0.055		
Cys-CS	1	0.144	0.145	0.007
	2	0.138		
	3	0.152		
MHA-CS	1	0.605	0.604	0.018
	2	0.585		
	3	0.621		
Cat-Alg	1	0.238	0.252	0.041
	2	0.298		
	3	0.219		



2.2 Polymer-mucin interaction

Table 15 Viscosity of 5% mucin solution

Point Index	Shear rate (s ⁻¹)	Shear viscosity(mPa s)			mean	SD
		n=1	n=2	n=3		
1	1.007	3.64E+01	3.66E+01	3.69E+01	3.67E+01	0.247857
2	3.273	3.01E+01	2.83E+01	3.12E+01	2.99E+01	1.463637
3	6.513	2.68E+01	2.56E+01	2.68E+01	2.64E+01	0.736139
4	9.834	2.54E+01	2.41E+01	2.56E+01	2.50E+01	0.827103
5	13.07	2.42E+01	2.32E+01	2.50E+01	2.42E+01	0.902663
6	16.29	2.37E+01	2.26E+01	2.37E+01	2.34E+01	0.614898
7	19.52	2.31E+01	2.22E+01	2.34E+01	2.29E+01	0.657445
8	22.74	2.27E+01	2.18E+01	2.28E+01	2.24E+01	0.53799
9	25.96	2.23E+01	2.15E+01	2.25E+01	2.21E+01	0.50362
10	29.18	2.21E+01	2.13E+01	2.22E+01	2.18E+01	0.488672
11	32.41	2.18E+01	2.11E+01	2.19E+01	2.16E+01	0.44238
12	35.63	2.16E+01	2.09E+01	2.17E+01	2.14E+01	0.446019
13	38.85	2.14E+01	2.07E+01	2.15E+01	2.12E+01	0.413562
14	42.09	2.12E+01	2.06E+01	2.13E+01	2.10E+01	0.378462
15	45.39	2.11E+01	2.04E+01	2.11E+01	2.09E+01	0.383145
16	48.62	2.09E+01	2.03E+01	2.10E+01	2.07E+01	0.372693
17	51.84	2.08E+01	2.02E+01	2.08E+01	2.06E+01	0.349333
18	55.06	2.06E+01	2.01E+01	2.07E+01	2.05E+01	0.354448
19	58.29	2.06E+01	2.00E+01	2.06E+01	2.04E+01	0.363639
20	61.51	2.05E+01	1.99E+01	2.05E+01	2.03E+01	0.348712
21	64.73	2.04E+01	1.98E+01	2.05E+01	2.02E+01	0.354448
22	67.96	2.03E+01	1.97E+01	2.04E+01	2.01E+01	0.356791
23	71.18	2.02E+01	1.96E+01	2.03E+01	2.00E+01	0.365923
24	74.4	2.02E+01	1.95E+01	2.02E+01	2.00E+01	0.367469
25	77.62	2.00E+01	1.95E+01	2.01E+01	1.99E+01	0.347707
26	80.85	2.00E+01	1.94E+01	2.00E+01	1.98E+01	0.344432
27	84.07	1.99E+01	1.93E+01	1.99E+01	1.97E+01	0.341223
28	87.29	1.98E+01	1.93E+01	1.99E+01	1.96E+01	0.340783
29	90.52	1.98E+01	1.92E+01	1.98E+01	1.96E+01	0.349619
30	93.74	1.97E+01	1.92E+01	1.98E+01	1.96E+01	0.352184

Table 16 Viscosity of 5% CS solution

Point Index	Shear rate (s ⁻¹)	Shear viscosity(mPa s)			mean	SD
		n=1	n=2	n=3		
1	1.129	2.68E+01	2.83E+01	2.85E+01	2.79E+01	0.923598
2	3.439	1.31E+01	1.50E+01	1.57E+01	1.46E+01	1.316067
3	6.663	7.96E+00	8.10E+00	8.19E+00	8.08E+00	0.115832
4	9.885	6.21E+00	5.89E+00	5.97E+00	6.02E+00	0.164695
5	13.11	5.36E+00	5.16E+00	5.22E+00	5.25E+00	0.100817
6	16.33	4.83E+00	4.58E+00	4.62E+00	4.68E+00	0.134768
7	19.55	4.48E+00	4.21E+00	4.24E+00	4.31E+00	0.148665
8	22.78	4.24E+00	4.00E+00	4.03E+00	4.09E+00	0.130001
9	26	4.05E+00	3.79E+00	3.82E+00	3.88E+00	0.145351
10	29.22	3.90E+00	3.65E+00	3.68E+00	3.75E+00	0.13593
11	32.44	3.79E+00	3.54E+00	3.57E+00	3.63E+00	0.135249
12	35.67	3.71E+00	3.45E+00	3.48E+00	3.55E+00	0.137784
13	38.89	3.62E+00	3.38E+00	3.40E+00	3.47E+00	0.132095
14	42.11	3.57E+00	3.32E+00	3.34E+00	3.41E+00	0.139173
15	45.34	3.51E+00	3.26E+00	3.28E+00	3.35E+00	0.139747
16	48.56	3.45E+00	3.21E+00	3.23E+00	3.30E+00	0.137197
17	51.78	3.43E+00	3.17E+00	3.20E+00	3.26E+00	0.139328
18	55.01	3.39E+00	3.14E+00	3.16E+00	3.23E+00	0.141552
19	58.23	3.36E+00	3.10E+00	3.13E+00	3.20E+00	0.140522
20	61.45	3.35E+00	3.08E+00	3.13E+00	3.19E+00	0.143572
21	64.67	3.34E+00	3.10E+00	3.09E+00	3.17E+00	0.140735
22	67.9	3.32E+00	3.07E+00	3.07E+00	3.15E+00	0.145547
23	71.12	3.32E+00	3.05E+00	3.05E+00	3.14E+00	0.155597
24	74.34	3.30E+00	3.03E+00	3.03E+00	3.12E+00	0.155336
25	77.57	3.27E+00	3.02E+00	3.01E+00	3.10E+00	0.145496
26	80.79	3.23E+00	3.00E+00	2.98E+00	3.07E+00	0.139576
27	84.01	3.19E+00	2.94E+00	2.95E+00	3.02E+00	0.142693
28	87.23	3.18E+00	2.93E+00	2.95E+00	3.02E+00	0.141938
29	90.46	3.17E+00	2.91E+00	2.93E+00	3.01E+00	0.14238
30	93.68	3.16E+00	2.91E+00	2.91E+00	2.99E+00	0.142084

Table 17 Viscosity of 1% CS solution/5% mucin mixtures

Point Index	Shear rate (s ⁻¹)	Shear viscosity(mPa s)			mean	SD
		n=1	n=2	n=3		
1	1.129	3.14E+01	3.27E+01	3.17E+01	3.19E+01	0.650231
2	3.439	2.59E+01	2.60E+01	2.40E+01	2.53E+01	1.113927
3	6.663	2.57E+01	2.52E+01	2.42E+01	2.51E+01	0.772528
4	9.885	1.91E+01	2.87E+01	2.57E+01	2.45E+01	4.922208
5	13.11	1.60E+01	2.15E+01	2.25E+01	2.00E+01	3.5
6	16.33	1.45E+01	1.53E+01	1.56E+01	1.52E+01	0.571664
7	19.55	1.37E+01	1.41E+01	1.42E+01	1.40E+01	0.293655
8	22.78	1.38E+01	1.52E+01	1.54E+01	1.48E+01	0.905152
9	26	1.46E+01	1.57E+01	1.51E+01	1.51E+01	0.565361
10	29.22	1.54E+01	1.45E+01	1.47E+01	1.49E+01	0.478226
11	32.44	1.82E+01	1.44E+01	1.42E+01	1.56E+01	2.238489
12	35.67	2.31E+01	1.35E+01	1.37E+01	1.68E+01	5.516965
13	38.89	1.96E+01	1.10E+01	1.12E+01	1.40E+01	4.9111
14	42.11	1.15E+01	1.11E+01	1.11E+01	1.12E+01	0.259808
15	45.34	9.25E+00	1.11E+01	1.11E+01	1.05E+01	1.046736
16	48.56	8.11E+00	1.00E+01	1.09E+01	9.66E+00	1.403924
17	51.78	7.74E+00	9.35E+00	9.38E+00	8.82E+00	0.93858
18	55.01	7.59E+00	8.80E+00	8.81E+00	8.40E+00	0.702351
19	58.23	7.41E+00	8.51E+00	8.59E+00	8.17E+00	0.659774
20	61.45	7.25E+00	8.26E+00	8.36E+00	7.96E+00	0.615181
21	64.67	7.18E+00	8.18E+00	8.19E+00	7.85E+00	0.578218
22	67.9	7.18E+00	8.16E+00	8.17E+00	7.83E+00	0.567861
23	71.12	7.19E+00	8.12E+00	8.13E+00	7.81E+00	0.538676
24	74.34	7.14E+00	7.96E+00	7.96E+00	7.68E+00	0.474005
25	77.57	7.04E+00	7.79E+00	7.72E+00	7.52E+00	0.415683
26	80.79	6.96E+00	7.91E+00	7.91E+00	7.59E+00	0.549638
27	84.01	6.87E+00	7.93E+00	7.94E+00	7.58E+00	0.615769
28	87.23	6.84E+00	7.76E+00	7.66E+00	7.42E+00	0.503054
29	90.46	6.84E+00	7.66E+00	7.56E+00	7.35E+00	0.445068
30	93.68	6.84E+00	7.62E+00	7.52E+00	7.33E+00	0.425914

Table 18 Viscosity of 3% CS solution/5% mucin mixtures

Point Index	Shear rate (s ⁻¹)	Shear viscosity(mPa s)			mean	SD
		n=1	n=2	n=3		
1	1.129	3.37E+01	3.89E+01	2.87E+01	3.38E+01	5.095596
2	3.439	2.62E+01	2.79E+01	1.37E+01	2.26E+01	7.73936
3	6.663	2.01E+01	1.80E+01	1.18E+01	1.66E+01	4.351785
4	9.885	1.71E+01	1.52E+01	1.03E+01	1.42E+01	3.518442
5	13.11	1.50E+01	1.38E+01	9.28E+00	1.27E+01	3.021859
6	16.33	1.39E+01	1.27E+01	8.87E+00	1.18E+01	2.60347
7	19.55	1.29E+01	1.20E+01	8.72E+00	1.12E+01	2.186374
8	22.78	1.22E+01	1.16E+01	8.46E+00	1.07E+01	2.008279
9	26	1.17E+01	1.12E+01	8.07E+00	1.03E+01	1.956945
10	29.22	1.13E+01	1.09E+01	7.91E+00	1.00E+01	1.841207
11	32.44	1.09E+01	1.07E+01	7.78E+00	9.80E+00	1.756498
12	35.67	1.07E+01	1.05E+01	7.65E+00	9.61E+00	1.697197
13	38.89	1.05E+01	1.03E+01	7.57E+00	9.44E+00	1.623404
14	42.11	1.03E+01	1.01E+01	7.49E+00	9.29E+00	1.558591
15	45.34	1.01E+01	9.95E+00	7.41E+00	9.16E+00	1.518763
16	48.56	9.98E+00	9.82E+00	7.36E+00	9.05E+00	1.466867
17	51.78	9.83E+00	9.69E+00	7.31E+00	8.94E+00	1.415814
18	55.01	9.68E+00	9.58E+00	7.24E+00	8.83E+00	1.381808
19	58.23	9.57E+00	9.46E+00	7.22E+00	8.75E+00	1.323894
20	61.45	9.46E+00	9.37E+00	7.17E+00	8.67E+00	1.293541
21	64.67	9.33E+00	9.30E+00	7.16E+00	8.60E+00	1.248052
22	67.9	9.23E+00	9.22E+00	7.11E+00	8.52E+00	1.220545
23	71.12	9.14E+00	9.13E+00	7.10E+00	8.46E+00	1.174632
24	74.34	9.04E+00	9.09E+00	7.09E+00	8.41E+00	1.142828
25	77.57	8.93E+00	8.99E+00	7.02E+00	8.31E+00	1.118237
26	80.79	8.86E+00	8.94E+00	6.98E+00	8.26E+00	1.108044
27	84.01	8.76E+00	8.86E+00	6.95E+00	8.19E+00	1.076765
28	87.23	8.69E+00	8.79E+00	6.93E+00	8.14E+00	1.048554
29	90.46	8.60E+00	8.74E+00	6.90E+00	8.08E+00	1.025965
30	93.68	8.56E+00	8.68E+00	6.90E+00	8.05E+00	0.998372

Table 19 Viscosity of 5% CS solution/5% mucin mixtures

Point Index	Shear rate (s ⁻¹)	Shear viscosity(mPa s)			mean	SD
		n=1	n=2	n=3		
1	1.129	2.26E+01	4.41E+01	3.96E+01	3.54E+01	11.32027
2	3.439	2.42E+01	2.11E+01	2.53E+01	2.35E+01	2.189094
3	6.663	1.48E+01	1.51E+01	1.62E+01	1.54E+01	0.718401
4	9.885	1.23E+01	1.29E+01	1.35E+01	1.29E+01	0.615819
5	13.11	1.12E+01	1.18E+01	1.22E+01	1.17E+01	0.529937
6	16.33	1.04E+01	1.11E+01	1.14E+01	1.10E+01	0.50362
7	19.55	9.98E+00	1.07E+01	1.09E+01	1.05E+01	0.486746
8	22.78	9.65E+00	1.04E+01	1.05E+01	1.02E+01	0.457122
9	26	9.35E+00	1.02E+01	1.01E+01	9.88E+00	0.457371
10	29.22	9.15E+00	9.96E+00	9.90E+00	9.67E+00	0.449603
11	32.44	8.99E+00	9.81E+00	9.71E+00	9.50E+00	0.447246
12	35.67	8.86E+00	9.69E+00	9.56E+00	9.37E+00	0.446516
13	38.89	8.74E+00	9.57E+00	9.41E+00	9.24E+00	0.439389
14	42.11	8.65E+00	9.49E+00	9.30E+00	9.15E+00	0.440453
15	45.34	8.58E+00	9.40E+00	9.20E+00	9.06E+00	0.432043
16	48.56	8.50E+00	9.32E+00	9.11E+00	8.98E+00	0.428188
17	51.78	8.45E+00	9.27E+00	9.07E+00	8.93E+00	0.427226
18	55.01	8.39E+00	9.20E+00	9.00E+00	8.86E+00	0.422018
19	58.23	8.34E+00	9.14E+00	8.95E+00	8.81E+00	0.417307
20	61.45	8.31E+00	9.12E+00	8.89E+00	8.77E+00	0.418409
21	64.67	8.27E+00	9.05E+00	8.87E+00	8.73E+00	0.410322
22	67.9	8.26E+00	9.02E+00	8.85E+00	8.71E+00	0.399049
23	71.12	8.20E+00	8.98E+00	8.82E+00	8.66E+00	0.412564
24	74.34	8.20E+00	8.96E+00	8.78E+00	8.65E+00	0.393672
25	77.57	8.16E+00	8.91E+00	8.74E+00	8.61E+00	0.392768
26	80.79	8.12E+00	8.89E+00	8.72E+00	8.57E+00	0.404307
27	84.01	8.09E+00	8.85E+00	8.69E+00	8.54E+00	0.399152
28	87.23	8.08E+00	8.80E+00	8.68E+00	8.52E+00	0.388754
29	90.46	8.06E+00	8.77E+00	8.65E+00	8.49E+00	0.381301
30	93.68	8.04E+00	8.74E+00	8.62E+00	8.47E+00	0.377194

Table 20 Viscosity of 5% Cys-CS

Point Index	Shear rate (s ⁻¹)	Shear viscosity(mPa s)			mean	SD
		n=1	n=2	n=3		
1	1.009	2.25E+01	2.60E+01	2.58E+01	2.48E+01	1.989129
2	3.274	1.91E+01	1.90E+01	2.11E+01	1.98E+01	1.188234
3	6.498	1.31E+01	1.55E+01	1.85E+01	1.57E+01	2.71
4	9.72	1.12E+01	1.37E+01	1.44E+01	1.31E+01	1.642752
5	12.94	1.03E+01	1.28E+01	1.38E+01	1.23E+01	1.795893
6	16.17	9.73E+00	1.21E+01	1.33E+01	1.17E+01	1.796033
7	19.39	9.39E+00	1.15E+01	1.29E+01	1.13E+01	1.747447
8	22.63	9.14E+00	1.11E+01	1.26E+01	1.10E+01	1.744987
9	25.95	8.84E+00	1.08E+01	1.22E+01	1.06E+01	1.684075
10	29.19	8.53E+00	1.05E+01	1.17E+01	1.02E+01	1.602994
11	32.41	8.29E+00	1.03E+01	1.12E+01	9.90E+00	1.462491
12	35.63	8.12E+00	1.00E+01	1.10E+01	9.71E+00	1.451236
13	38.85	7.98E+00	9.84E+00	1.10E+01	9.60E+00	1.52034
14	42.08	7.85E+00	9.63E+00	1.08E+01	9.43E+00	1.496591
15	45.3	7.73E+00	9.41E+00	1.07E+01	9.27E+00	1.469204
16	48.52	7.63E+00	9.24E+00	1.05E+01	9.13E+00	1.454346
17	51.75	7.55E+00	9.07E+00	1.04E+01	9.01E+00	1.43629
18	54.97	7.46E+00	8.91E+00	1.03E+01	8.89E+00	1.425047
19	58.19	7.37E+00	8.77E+00	1.02E+01	8.77E+00	1.407008
20	61.41	7.31E+00	8.65E+00	1.01E+01	8.68E+00	1.378256
21	64.64	7.27E+00	8.55E+00	1.00E+01	8.61E+00	1.362803
22	67.86	7.21E+00	8.46E+00	9.91E+00	8.53E+00	1.34775
23	71.08	7.15E+00	8.37E+00	9.80E+00	8.44E+00	1.322824
24	74.31	7.10E+00	8.30E+00	9.71E+00	8.37E+00	1.307433
25	77.53	7.05E+00	8.21E+00	9.64E+00	8.30E+00	1.297723
26	80.75	7.00E+00	8.14E+00	8.64E+00	7.93E+00	0.84285
27	83.97	6.94E+00	8.06E+00	8.74E+00	7.91E+00	0.906083
28	87.2	6.91E+00	8.00E+00	8.44E+00	7.78E+00	0.786575
29	90.42	6.87E+00	7.93E+00	6.74E+00	7.18E+00	0.655161
30	93.64	6.83E+00	7.90E+00	6.66E+00	7.13E+00	0.673636

Table 21 Viscosity of 1% Cys-CS/5% mucin mixtures

Point Index	Shear rate (s ⁻¹)	Shear viscosity(mPa s)			mean	SD
		n=1	n=2	n=3		
1	1.009	2.06E+01	2.04E+01	3.75E+01	2.61E+01	9.82441
2	3.274	1.37E+01	1.37E+01	1.90E+01	1.55E+01	3.036862
3	6.497	1.17E+01	1.16E+01	1.24E+01	1.19E+01	0.448813
4	9.72	1.08E+01	1.07E+01	1.03E+01	1.06E+01	0.28746
5	12.94	1.04E+01	1.02E+01	9.30E+00	9.96E+00	0.57672
6	16.17	1.01E+01	9.89E+00	8.77E+00	9.59E+00	0.714942
7	19.39	9.74E+00	9.59E+00	8.39E+00	9.24E+00	0.743616
8	22.69	9.49E+00	9.32E+00	8.04E+00	8.95E+00	0.794035
9	25.96	9.29E+00	9.14E+00	7.83E+00	8.75E+00	0.800233
10	29.18	9.14E+00	9.02E+00	7.62E+00	8.59E+00	0.848127
11	32.41	9.03E+00	8.92E+00	7.44E+00	8.46E+00	0.88871
12	35.63	8.89E+00	8.80E+00	7.33E+00	8.34E+00	0.878098
13	38.85	8.76E+00	8.68E+00	7.20E+00	8.21E+00	0.875865
14	42.08	8.60E+00	8.54E+00	7.09E+00	8.08E+00	0.853385
15	45.3	8.44E+00	8.39E+00	6.97E+00	7.93E+00	0.836812
16	48.52	8.32E+00	8.26E+00	6.84E+00	7.81E+00	0.836386
17	51.75	8.19E+00	8.15E+00	6.74E+00	7.69E+00	0.828515
18	54.97	8.08E+00	8.03E+00	6.62E+00	7.57E+00	0.825139
19	58.19	8.00E+00	7.94E+00	6.53E+00	7.49E+00	0.828971
20	61.42	7.92E+00	7.88E+00	6.45E+00	7.42E+00	0.837474
21	64.64	7.85E+00	7.80E+00	6.38E+00	7.34E+00	0.836103
22	67.86	7.77E+00	7.75E+00	6.32E+00	7.28E+00	0.833754
23	71.08	7.70E+00	7.70E+00	6.26E+00	7.22E+00	0.833986
24	74.31	7.66E+00	7.63E+00	6.21E+00	7.17E+00	0.824559
25	77.53	7.59E+00	7.57E+00	6.17E+00	7.11E+00	0.811521
26	80.75	7.51E+00	7.51E+00	6.12E+00	7.05E+00	0.798768
27	83.97	7.46E+00	7.46E+00	6.04E+00	6.99E+00	0.821859
28	87.2	7.42E+00	7.42E+00	6.01E+00	6.95E+00	0.813199
29	90.42	7.36E+00	7.37E+00	5.97E+00	6.90E+00	0.807158
30	93.64	7.34E+00	7.36E+00	5.93E+00	6.87E+00	0.821031

Table 22 Viscosity of 3% Cys-CS/5% mucin mixtures

Point Index	Shear rate (s ⁻¹)	Shear viscosity(mPa s)			mean	SD
		n=1	n=2	n=3		
1	1.011	3.19E+01	3.59E+01	2.83E+01	3.20E+01	3.787642
2	3.274	2.31E+01	1.95E+01	1.64E+01	1.97E+01	3.344792
3	6.497	1.60E+01	1.22E+01	1.02E+01	1.28E+01	2.932968
4	9.72	1.24E+01	9.76E+00	8.40E+00	1.02E+01	2.01717
5	12.94	9.82E+00	8.57E+00	7.47E+00	8.62E+00	1.172778
6	16.17	8.88E+00	7.93E+00	6.87E+00	7.89E+00	1.004432
7	19.39	8.49E+00	7.51E+00	6.51E+00	7.50E+00	0.992014
8	22.61	7.79E+00	7.15E+00	6.21E+00	7.05E+00	0.793529
9	25.83	7.56E+00	6.93E+00	6.00E+00	6.83E+00	0.787775
10	29.06	7.17E+00	6.76E+00	5.83E+00	6.58E+00	0.688057
11	32.28	6.90E+00	6.61E+00	5.69E+00	6.40E+00	0.631153
12	35.5	6.75E+00	6.46E+00	5.60E+00	6.27E+00	0.598503
13	38.8	6.58E+00	6.34E+00	5.51E+00	6.14E+00	0.562936
14	42.08	6.48E+00	6.27E+00	5.42E+00	6.06E+00	0.559387
15	45.3	6.32E+00	6.18E+00	5.35E+00	5.95E+00	0.525635
16	48.52	6.19E+00	6.10E+00	5.29E+00	5.86E+00	0.499706
17	51.75	6.13E+00	6.05E+00	5.24E+00	5.81E+00	0.490339
18	54.97	6.04E+00	6.00E+00	5.20E+00	5.74E+00	0.472119
19	58.19	5.95E+00	5.94E+00	5.14E+00	5.68E+00	0.463665
20	61.41	5.93E+00	5.90E+00	5.13E+00	5.65E+00	0.456626
21	64.64	5.87E+00	5.85E+00	5.09E+00	5.60E+00	0.441487
22	67.86	5.82E+00	5.82E+00	5.06E+00	5.57E+00	0.439666
23	71.08	5.76E+00	5.80E+00	5.06E+00	5.54E+00	0.414662
24	74.31	5.74E+00	5.75E+00	5.02E+00	5.50E+00	0.421804
25	77.53	5.71E+00	5.73E+00	4.96E+00	5.46E+00	0.439755
26	80.75	5.65E+00	5.66E+00	4.94E+00	5.41E+00	0.41167
27	83.97	5.59E+00	5.62E+00	4.89E+00	5.37E+00	0.412195
28	87.2	5.55E+00	5.60E+00	4.87E+00	5.34E+00	0.406789
29	90.42	5.53E+00	5.57E+00	4.85E+00	5.32E+00	0.403275
30	93.64	5.50E+00	5.54E+00	4.82E+00	5.29E+00	0.402772

Table 23 Viscosity of 5% Cys-CS/5% mucin mixtures

Point Index	Shear rate (s ⁻¹)	Shear viscosity(mPa s)			mean	SD
		n=1	n=2	n=3		
1	1.128	8.53E+01	5.48E+01	5.90E+01	6.64E+01	16.49282
2	3.439	6.00E+01	2.60E+01	3.40E+01	4.00E+01	17.74601
3	6.663	3.48E+01	1.90E+01	2.77E+01	2.72E+01	7.924155
4	9.885	2.58E+01	1.55E+01	2.48E+01	2.20E+01	5.672604
5	13.11	2.11E+01	1.37E+01	2.30E+01	1.92E+01	4.934332
6	16.33	1.85E+01	1.28E+01	2.10E+01	1.74E+01	4.201099
7	19.55	1.71E+01	1.21E+01	1.90E+01	1.61E+01	3.557035
8	22.78	1.60E+01	1.15E+01	1.76E+01	1.50E+01	3.118659
9	26	1.50E+01	1.11E+01	1.66E+01	1.43E+01	2.830377
10	29.22	1.44E+01	1.08E+01	1.61E+01	1.37E+01	2.695206
11	32.45	1.38E+01	1.05E+01	1.53E+01	1.32E+01	2.466097
12	35.67	1.33E+01	1.03E+01	1.46E+01	1.27E+01	2.208265
13	38.89	1.29E+01	1.00E+01	1.40E+01	1.23E+01	2.020503
14	42.11	1.26E+01	9.84E+00	1.35E+01	1.20E+01	1.891867
15	45.34	1.22E+01	9.63E+00	1.30E+01	1.16E+01	1.745592
16	48.56	1.17E+01	9.41E+00	1.26E+01	1.12E+01	1.641991
17	51.78	1.12E+01	9.24E+00	1.22E+01	1.09E+01	1.502841
18	55.01	1.10E+01	9.07E+00	1.19E+01	1.06E+01	1.425617
19	58.23	1.10E+01	8.91E+00	1.16E+01	1.05E+01	1.409282
20	61.45	1.08E+01	8.77E+00	1.14E+01	1.03E+01	1.373047
21	64.67	1.07E+01	8.65E+00	1.11E+01	1.01E+01	1.323293
22	67.9	1.05E+01	8.55E+00	1.09E+01	1.00E+01	1.276919
23	71.12	1.04E+01	8.46E+00	1.08E+01	9.89E+00	1.252729
24	74.34	1.03E+01	8.37E+00	1.07E+01	9.78E+00	1.232429
25	77.57	1.02E+01	8.30E+00	1.05E+01	9.65E+00	1.184444
26	80.79	1.01E+01	8.21E+00	1.03E+01	9.54E+00	1.158551
27	84.01	1.00E+01	8.14E+00	1.02E+01	9.44E+00	1.129184
28	87.23	9.91E+00	8.06E+00	1.01E+01	9.34E+00	1.117875
29	90.46	9.80E+00	8.00E+00	9.98E+00	9.26E+00	1.095144
30	93.68	9.71E+00	7.93E+00	9.88E+00	9.17E+00	1.07739

Table 24 Viscosity of 5% MHA-CS

Point Index	Shear rate (s ⁻¹)	Shear viscosity(mPa s)			mean	SD
		n=1	n=2	n=3		
1	1.009	3.97E+01	4.03E+01	3.84E+01	3.95E+01	0.954795
2	3.275	2.08E+01	2.64E+01	2.76E+01	2.49E+01	3.622172
3	6.496	1.17E+01	1.59E+01	1.48E+01	1.41E+01	2.174887
4	9.721	8.82E+00	1.25E+01	1.11E+01	1.08E+01	1.860753
5	12.94	7.15E+00	1.08E+01	9.88E+00	9.28E+00	1.897848
6	16.17	6.53E+00	9.72E+00	8.78E+00	8.34E+00	1.638554
7	19.39	6.08E+00	9.03E+00	8.14E+00	7.75E+00	1.513434
8	22.61	5.56E+00	8.51E+00	7.73E+00	7.27E+00	1.528302
9	25.83	5.38E+00	8.16E+00	7.34E+00	6.96E+00	1.428028
10	29.06	5.16E+00	7.90E+00	7.13E+00	6.73E+00	1.413117
11	32.28	5.01E+00	7.63E+00	6.86E+00	6.50E+00	1.346055
12	35.5	4.86E+00	7.44E+00	6.67E+00	6.32E+00	1.324344
13	38.73	4.70E+00	7.27E+00	6.53E+00	6.17E+00	1.322827
14	41.95	4.65E+00	7.14E+00	6.37E+00	6.05E+00	1.274846
15	45.25	4.55E+00	7.02E+00	6.28E+00	5.95E+00	1.267246
16	48.52	4.46E+00	6.92E+00	6.20E+00	5.86E+00	1.264217
17	51.75	4.40E+00	6.85E+00	6.11E+00	5.79E+00	1.256339
18	54.97	4.36E+00	6.76E+00	6.02E+00	5.71E+00	1.229539
19	58.19	4.32E+00	6.69E+00	5.96E+00	5.66E+00	1.213768
20	61.42	4.29E+00	6.65E+00	5.92E+00	5.62E+00	1.208512
21	64.64	4.26E+00	6.61E+00	5.87E+00	5.58E+00	1.201541
22	67.86	4.26E+00	6.55E+00	5.80E+00	5.54E+00	1.167378
23	71.08	4.21E+00	6.50E+00	5.78E+00	5.50E+00	1.170515
24	74.31	4.21E+00	6.50E+00	5.76E+00	5.49E+00	1.168516
25	77.53	4.20E+00	6.45E+00	5.70E+00	5.45E+00	1.146083
26	80.75	4.13E+00	6.36E+00	5.65E+00	5.38E+00	1.139136
27	83.97	4.08E+00	6.34E+00	5.61E+00	5.34E+00	1.153589
28	87.2	4.07E+00	6.29E+00	5.56E+00	5.31E+00	1.131139
29	90.42	4.05E+00	6.28E+00	5.54E+00	5.29E+00	1.135388
30	93.64	4.03E+00	6.25E+00	5.51E+00	5.26E+00	1.130697

Table 25 Viscosity of 1% MHA-CS/5% mucin mixtures

Point Index	Shear rate (s ⁻¹)	Shear viscosity(mPa s)			mean	SD
		n=1	n=2	n=3		
1	1.129	4.03E+01	3.84E+01	4.05E+01	3.98E+01	1.155177
2	3.439	2.64E+01	2.76E+01	2.68E+01	2.69E+01	0.589435
3	6.663	1.59E+01	1.48E+01	1.62E+01	1.56E+01	0.750489
4	9.885	1.25E+01	1.11E+01	1.27E+01	1.21E+01	0.837377
5	13.11	1.08E+01	9.88E+00	1.09E+01	1.05E+01	0.545909
6	16.33	9.72E+00	8.78E+00	9.72E+00	9.40E+00	0.545309
7	19.55	9.03E+00	8.14E+00	9.04E+00	8.74E+00	0.514749
8	22.78	8.51E+00	7.73E+00	8.56E+00	8.27E+00	0.467799
9	26	8.16E+00	7.34E+00	8.20E+00	7.90E+00	0.486938
10	29.22	7.90E+00	7.13E+00	7.93E+00	7.65E+00	0.45374
11	32.44	7.63E+00	6.86E+00	7.69E+00	7.39E+00	0.465479
12	35.67	7.44E+00	6.67E+00	7.50E+00	7.20E+00	0.46331
13	38.89	7.27E+00	6.53E+00	7.33E+00	7.05E+00	0.447809
14	42.11	7.14E+00	6.37E+00	7.20E+00	6.90E+00	0.459973
15	45.34	7.02E+00	6.28E+00	7.07E+00	6.79E+00	0.445579
16	48.56	6.92E+00	6.20E+00	6.96E+00	6.69E+00	0.431744
17	51.78	6.85E+00	6.11E+00	6.89E+00	6.62E+00	0.440754
18	55.01	6.76E+00	6.02E+00	6.81E+00	6.53E+00	0.440651
19	58.23	6.69E+00	5.96E+00	6.73E+00	6.46E+00	0.432732
20	61.45	6.65E+00	5.92E+00	6.66E+00	6.41E+00	0.424114
21	64.67	6.61E+00	5.87E+00	6.62E+00	6.37E+00	0.431322
22	67.9	6.55E+00	5.80E+00	6.57E+00	6.31E+00	0.439157
23	71.12	6.50E+00	5.78E+00	6.51E+00	6.26E+00	0.420931
24	74.34	6.50E+00	5.76E+00	6.50E+00	6.25E+00	0.427535
25	77.57	6.45E+00	5.70E+00	6.46E+00	6.20E+00	0.431322
26	80.79	6.36E+00	5.65E+00	6.38E+00	6.13E+00	0.415512
27	84.01	6.34E+00	5.61E+00	6.34E+00	6.10E+00	0.420614
28	87.23	6.29E+00	5.56E+00	6.29E+00	6.05E+00	0.423786
29	90.46	6.28E+00	5.54E+00	6.26E+00	6.02E+00	0.421584
30	93.68	6.25E+00	5.51E+00	6.22E+00	6.00E+00	0.418039

Table 26 Viscosity of 3% MHA-CS/5% mucin mixtures

Point Index	Shear rate (s ⁻¹)	Shear viscosity(mPa s)			mean	SD
		n=1	n=2	n=3		
1	1.129	4.23E+01	6.96E+01	1.31E+02	8.10E+01	45.61659
2	3.439	3.80E+01	4.90E+01	7.04E+01	5.24E+01	16.49006
3	6.663	2.20E+01	2.69E+01	4.05E+01	2.98E+01	9.567102
4	9.886	1.70E+01	1.97E+01	3.08E+01	2.25E+01	7.296623
5	13.11	1.38E+01	1.61E+01	2.51E+01	1.83E+01	5.98321
6	16.33	1.19E+01	1.45E+01	2.20E+01	1.61E+01	5.247822
7	19.55	1.10E+01	1.41E+01	2.01E+01	1.50E+01	4.640607
8	22.78	1.02E+01	1.37E+01	1.84E+01	1.41E+01	4.098004
9	26	9.66E+00	1.33E+01	1.73E+01	1.34E+01	3.798055
10	29.22	9.25E+00	1.30E+01	1.63E+01	1.28E+01	3.505668
11	32.45	8.94E+00	1.26E+01	1.55E+01	1.23E+01	3.286949
12	35.67	8.69E+00	1.22E+01	1.48E+01	1.19E+01	3.056275
13	38.89	8.49E+00	1.19E+01	1.42E+01	1.15E+01	2.860495
14	42.11	8.33E+00	1.15E+01	1.37E+01	1.12E+01	2.692182
15	45.34	8.20E+00	1.11E+01	1.32E+01	1.08E+01	2.521126
16	48.56	8.07E+00	1.08E+01	1.28E+01	1.06E+01	2.378573
17	51.78	7.96E+00	1.05E+01	1.25E+01	1.03E+01	2.250789
18	55.01	7.86E+00	1.03E+01	1.21E+01	1.01E+01	2.136736
19	58.23	7.74E+00	1.00E+01	1.18E+01	9.86E+00	2.037102
20	61.45	7.64E+00	9.83E+00	1.15E+01	9.66E+00	1.938381
21	64.68	7.59E+00	9.65E+00	1.13E+01	9.50E+00	1.845297
22	67.9	7.50E+00	9.47E+00	1.10E+01	9.32E+00	1.759702
23	71.12	7.43E+00	9.30E+00	1.08E+01	9.17E+00	1.674427
24	74.34	7.35E+00	9.18E+00	1.06E+01	9.04E+00	1.619025
25	77.57	7.28E+00	9.04E+00	1.04E+01	8.89E+00	1.545516
26	80.79	7.20E+00	8.89E+00	1.02E+01	8.75E+00	1.477934
27	84.01	7.14E+00	8.76E+00	9.97E+00	8.62E+00	1.419467
28	87.23	7.07E+00	8.63E+00	9.78E+00	8.50E+00	1.359487
29	90.46	7.02E+00	8.53E+00	9.63E+00	8.39E+00	1.307002
30	93.68	6.97E+00	8.44E+00	9.50E+00	8.30E+00	1.272987

Table 27 Viscosity of 5% MHA-CS/5% mucin mixtures

Point Index	Shear rate (s ⁻¹)	Shear viscosity(mPa s)			mean	SD
		n=1	n=2	n=3		
1	1.129	93.97	112.40	1.02E+02	1.03E+02	9.024817
2	3.44	44.85	68.66	6.18E+01	5.84E+01	12.24931
3	6.662	20.19	36.85	3.84E+01	3.18E+01	10.09589
4	9.885	14.20	25.77	3.19E+01	2.40E+01	9.001513
5	13.11	12.14	21.57	2.85E+01	2.07E+01	8.188156
6	16.33	11.03	19.38	2.58E+01	1.87E+01	7.410756
7	19.55	10.38	17.74	2.36E+01	1.72E+01	6.628969
8	22.78	9.76	16.38	2.18E+01	1.60E+01	6.024618
9	26	9.17	15.62	2.02E+01	1.50E+01	5.558077
10	29.22	8.75	15.05	1.86E+01	1.41E+01	4.986793
11	32.44	8.41	14.52	1.72E+01	1.34E+01	4.490787
12	35.67	8.18	14.02	1.63E+01	1.28E+01	4.184465
13	38.89	8.01	13.58	1.55E+01	1.24E+01	3.892641
14	42.11	7.88	13.20	1.48E+01	1.20E+01	3.640785
15	45.34	7.80	12.86	1.43E+01	1.16E+01	3.396255
16	48.56	7.73	12.53	1.38E+01	1.14E+01	3.197687
17	51.78	7.68	12.24	1.34E+01	1.11E+01	3.031892
18	55.01	7.64	11.96	1.30E+01	1.09E+01	2.856471
19	58.23	7.57	11.68	1.27E+01	1.06E+01	2.707007
20	61.45	7.55	11.41	1.24E+01	1.04E+01	2.551261
21	64.67	7.55	11.17	1.21E+01	1.03E+01	2.401613
22	67.9	7.51	10.92	1.18E+01	1.01E+01	2.268037
23	71.12	7.47	10.73	1.16E+01	9.93E+00	2.175082
24	74.34	7.44	10.55	1.14E+01	9.79E+00	2.073218
25	77.57	7.37	10.37	1.12E+01	9.63E+00	1.998376
26	80.79	7.29	10.18	1.09E+01	9.47E+00	1.921421
27	84.01	7.26	10.01	1.08E+01	9.35E+00	1.847193
28	87.23	7.19	9.85	1.06E+01	9.21E+00	1.786529
29	90.46	7.15	9.73	1.04E+01	9.11E+00	1.73077
30	93.68	7.10	9.60	1.03E+01	9.00E+00	1.681517

Table 28 Viscosity of 5% Cat-Alg

Point Index	Shear rate (s ⁻¹)	Shear viscosity(mPa s)			mean	SD
		n=1	n=2	n=3		
1	1.129	4.67E+01	4.80E+01	4.38E+01	4.61E+01	2.145934
2	3.439	3.05E+01	3.27E+01	2.95E+01	3.09E+01	1.64807
3	6.663	1.78E+01	2.00E+01	1.73E+01	1.84E+01	1.457086
4	9.885	1.34E+01	1.57E+01	1.43E+01	1.45E+01	1.155177
5	13.11	1.16E+01	1.38E+01	1.31E+01	1.28E+01	1.107535
6	16.33	1.11E+01	1.27E+01	1.19E+01	1.19E+01	0.790527
7	19.55	1.03E+01	1.20E+01	1.11E+01	1.11E+01	0.835125
8	22.78	9.81E+00	1.15E+01	1.06E+01	1.06E+01	0.867357
9	26	9.61E+00	1.13E+01	1.02E+01	1.04E+01	0.844595
10	29.22	9.43E+00	1.11E+01	9.94E+00	1.02E+01	0.848995
11	32.45	9.30E+00	1.10E+01	9.73E+00	1.00E+01	0.884313
12	35.67	9.18E+00	1.10E+01	9.57E+00	9.93E+00	0.96824
13	38.89	9.02E+00	1.11E+01	9.42E+00	9.83E+00	1.080044
14	42.11	8.86E+00	1.11E+01	9.30E+00	9.76E+00	1.197222
15	45.34	8.71E+00	1.12E+01	9.21E+00	9.70E+00	1.306435
16	48.56	8.54E+00	1.12E+01	9.11E+00	9.62E+00	1.393345
17	51.78	8.41E+00	1.12E+01	9.05E+00	9.55E+00	1.456448
18	55.01	8.26E+00	1.12E+01	8.98E+00	9.46E+00	1.506486
19	58.23	8.10E+00	1.11E+01	8.89E+00	9.36E+00	1.545617
20	61.45	7.98E+00	1.10E+01	8.85E+00	9.29E+00	1.570636
21	64.67	7.86E+00	1.10E+01	8.79E+00	9.21E+00	1.594371
22	67.9	7.72E+00	1.09E+01	8.78E+00	9.14E+00	1.625399
23	71.12	7.63E+00	1.09E+01	8.72E+00	9.07E+00	1.643968
24	74.34	7.53E+00	1.08E+01	8.67E+00	9.01E+00	1.671122
25	77.57	7.42E+00	1.08E+01	8.64E+00	8.94E+00	1.695118
26	80.79	7.30E+00	1.07E+01	8.61E+00	8.87E+00	1.715462
27	84.01	7.19E+00	1.06E+01	8.57E+00	8.79E+00	1.725872
28	87.23	7.08E+00	1.06E+01	8.54E+00	8.72E+00	1.749646
29	90.46	6.99E+00	1.05E+01	8.51E+00	8.67E+00	1.769895
30	93.68	6.91E+00	1.05E+01	8.47E+00	8.62E+00	1.786399

Table 29 Viscosity of 1% Cat-Alg/5% mucin mixtures

Point Index	Shear rate (s ⁻¹)	Shear viscosity(mPa s)			mean	SD
		n=1	n=2	n=3		
1	1.008	3.75E+01	3.80E+01	3.40E+01	3.65E+01	2.196657
2	3.274	3.00E+01	3.23E+01	2.79E+01	3.01E+01	2.207585
3	6.516	2.68E+01	2.96E+01	2.57E+01	2.74E+01	2.059393
4	9.837	2.52E+01	2.78E+01	2.45E+01	2.59E+01	1.740527
5	13.07	2.43E+01	2.70E+01	2.39E+01	2.50E+01	1.737824
6	16.29	2.37E+01	2.66E+01	2.34E+01	2.45E+01	1.7591
7	19.52	2.32E+01	2.61E+01	2.30E+01	2.41E+01	1.741302
8	22.74	2.29E+01	2.58E+01	2.27E+01	2.38E+01	1.740153
9	25.96	2.26E+01	2.56E+01	2.25E+01	2.36E+01	1.74463
10	29.18	2.24E+01	2.54E+01	2.23E+01	2.34E+01	1.735291
11	32.41	2.22E+01	2.52E+01	2.22E+01	2.32E+01	1.749629
12	35.63	2.20E+01	2.50E+01	2.20E+01	2.30E+01	1.740776
13	38.85	2.19E+01	2.49E+01	2.19E+01	2.29E+01	1.737939
14	42.1	2.18E+01	2.48E+01	2.18E+01	2.28E+01	1.73208
15	45.39	2.16E+01	2.46E+01	2.16E+01	2.26E+01	1.720504
16	48.62	2.15E+01	2.45E+01	2.16E+01	2.25E+01	1.714759
17	51.84	2.14E+01	2.44E+01	2.15E+01	2.24E+01	1.708986
18	55.06	2.13E+01	2.43E+01	2.14E+01	2.23E+01	1.711909
19	58.29	2.13E+01	2.42E+01	2.13E+01	2.23E+01	1.694707
20	61.51	2.12E+01	2.41E+01	2.12E+01	2.22E+01	1.694589
21	64.73	2.11E+01	2.41E+01	2.12E+01	2.21E+01	1.691902
22	67.96	2.10E+01	2.40E+01	2.11E+01	2.20E+01	1.68334
23	71.18	2.10E+01	2.39E+01	2.10E+01	2.20E+01	1.671496
24	74.4	2.09E+01	2.39E+01	2.10E+01	2.19E+01	1.674585
25	77.62	2.08E+01	2.38E+01	2.09E+01	2.18E+01	1.691902
26	80.85	2.08E+01	2.37E+01	2.08E+01	2.18E+01	1.68334
27	84.07	2.07E+01	2.36E+01	2.08E+01	2.17E+01	1.680565
28	87.29	2.06E+01	2.36E+01	2.07E+01	2.16E+01	1.674794
29	90.52	2.06E+01	2.35E+01	2.06E+01	2.16E+01	1.669022
30	93.74	2.05E+01	2.35E+01	2.06E+01	2.15E+01	1.66325

Table 30 Viscosity of 3% Cat-Alg/5% mucin mixtures

Point Index	Shear rate (s ⁻¹)	Shear viscosity(mPa s)			mean	SD
		n=1	n=2	n=3		
1	1.13	4.38E+01	3.50E+01	6.00E+01	4.62E+01	12.68025
2	3.439	2.61E+01	3.27E+01	4.38E+01	3.42E+01	8.948525
3	6.663	1.73E+01	2.00E+01	2.40E+01	2.04E+01	3.404179
4	9.885	1.43E+01	1.57E+01	1.74E+01	1.58E+01	1.562402
5	13.11	1.31E+01	1.38E+01	1.50E+01	1.39E+01	0.955528
6	16.33	1.19E+01	1.27E+01	1.37E+01	1.28E+01	0.904728
7	19.55	1.11E+01	1.20E+01	1.29E+01	1.20E+01	0.895228
8	22.78	1.06E+01	1.15E+01	1.24E+01	1.15E+01	0.920163
9	26	1.02E+01	1.13E+01	1.21E+01	1.12E+01	0.928278
10	29.22	9.94E+00	1.11E+01	1.17E+01	1.09E+01	0.913119
11	32.44	9.73E+00	1.10E+01	1.15E+01	1.07E+01	0.90013
12	35.67	9.57E+00	1.10E+01	1.13E+01	1.06E+01	0.909124
13	38.89	9.42E+00	1.11E+01	1.11E+01	1.05E+01	0.946277
14	42.11	9.30E+00	1.11E+01	1.09E+01	1.04E+01	0.99749
15	45.34	9.21E+00	1.12E+01	1.08E+01	1.04E+01	1.046803
16	48.56	9.11E+00	1.12E+01	1.07E+01	1.03E+01	1.086273
17	51.78	9.05E+00	1.12E+01	1.06E+01	1.03E+01	1.108815
18	55.01	8.98E+00	1.12E+01	1.05E+01	1.02E+01	1.11801
19	58.23	8.89E+00	1.11E+01	1.04E+01	1.01E+01	1.126623
20	61.45	8.85E+00	1.10E+01	1.04E+01	1.01E+01	1.117748
21	64.67	8.79E+00	1.10E+01	1.03E+01	1.00E+01	1.118106
22	67.9	8.78E+00	1.09E+01	1.03E+01	9.98E+00	1.093273
23	71.12	8.72E+00	1.09E+01	1.02E+01	9.92E+00	1.091713
24	74.34	8.67E+00	1.08E+01	1.01E+01	9.87E+00	1.095548
25	77.57	8.64E+00	1.08E+01	1.01E+01	9.83E+00	1.084595
26	80.79	8.61E+00	1.07E+01	1.00E+01	9.77E+00	1.062725
27	84.01	8.57E+00	1.06E+01	9.97E+00	9.72E+00	1.047856
28	87.23	8.54E+00	1.06E+01	9.91E+00	9.67E+00	1.033904
29	90.46	8.51E+00	1.05E+01	9.87E+00	9.63E+00	1.027762
30	93.68	8.47E+00	1.05E+01	9.82E+00	9.59E+00	1.020125

Table 31 Viscosity of 5% Cat-Alg/5% mucin mixtures

Point Index	Shear rate (s ⁻¹)	Shear viscosity(mPa s)			mean	SD
		n=1	n=2	n=3		
1	1.127	9.46E+01	1.06E+02	1.00E+02	1.00E+02	5.875494
2	3.439	8.70E+01	9.53E+01	9.20E+01	9.14E+01	4.223944
3	6.663	8.38E+01	9.04E+01	8.86E+01	8.76E+01	3.419961
4	9.886	8.19E+01	8.76E+01	8.69E+01	8.55E+01	3.117841
5	13.11	8.06E+01	8.59E+01	8.49E+01	8.38E+01	2.831325
6	16.34	7.95E+01	8.46E+01	8.37E+01	8.26E+01	2.716843
7	19.63	7.87E+01	8.35E+01	8.28E+01	8.16E+01	2.610102
8	22.86	7.80E+01	8.27E+01	8.21E+01	8.09E+01	2.540794
9	26.08	7.74E+01	8.19E+01	8.14E+01	8.02E+01	2.479335
10	29.31	7.68E+01	8.13E+01	8.08E+01	7.96E+01	2.433947
11	32.53	7.64E+01	8.07E+01	8.03E+01	7.91E+01	2.403525
12	35.75	7.59E+01	8.02E+01	7.98E+01	7.86E+01	2.373233
13	38.98	7.55E+01	7.97E+01	7.94E+01	7.82E+01	2.343075
14	42.2	7.50E+01	7.92E+01	7.89E+01	7.77E+01	2.33093
15	45.42	7.46E+01	7.88E+01	7.85E+01	7.73E+01	2.313641
16	48.65	7.43E+01	7.84E+01	7.81E+01	7.69E+01	2.295764
17	51.91	7.39E+01	7.80E+01	7.77E+01	7.65E+01	2.287408
18	55.15	7.35E+01	7.76E+01	7.74E+01	7.62E+01	2.290589
19	58.38	7.32E+01	7.73E+01	7.70E+01	7.58E+01	2.278472
20	61.6	7.29E+01	7.70E+01	7.67E+01	7.55E+01	2.259875
21	64.82	7.26E+01	7.66E+01	7.63E+01	7.52E+01	2.221441
22	68.05	7.23E+01	7.63E+01	7.60E+01	7.49E+01	2.217664
23	71.27	7.20E+01	7.60E+01	7.57E+01	7.46E+01	2.202453
24	74.49	7.17E+01	7.56E+01	7.54E+01	7.43E+01	2.195776
25	77.72	7.14E+01	7.53E+01	7.51E+01	7.39E+01	2.177315
26	80.94	7.11E+01	7.50E+01	7.47E+01	7.36E+01	2.157437
27	84.16	7.08E+01	7.47E+01	7.44E+01	7.33E+01	2.151674
28	87.38	7.06E+01	7.44E+01	7.41E+01	7.30E+01	2.131815
29	90.61	7.03E+01	7.41E+01	7.39E+01	7.28E+01	2.131815
30	93.83	7.01E+01	7.39E+01	7.36E+01	7.25E+01	2.09981



APPENDIX B

Development of the mucoadhesive nanoparticles (NPs)

1. Particle size and surface charge

Table 32 Particle size, size distribution, and surface charge of the NPs.

NPs	NO	Particle size (nm)			PDI			zeta potential (mV)		
			mean	SD		mean	SD		mean	SD
CS	1	361.7	370.63	10.50	0.163	0.148	0.03	-0.479	-0.408	0.06
	2	368.0			0.167			-0.375		
	3	382.2			0.114			-0.369		
Alg	1	216.3	218.76	3.76	0.498	0.457	0.04	-31.5	-32.67	1.11
	2	216.9			0.434			-33.7		
	3	223.1			0.44			-32.8		
Cat-Alg	1	171.2	167.07	4.48	0.44	0.457	0.01	-21.3	-20.43	1.03
	2	162.3			0.464			-20.7		
	3	167.7			0.466			-19.3		
Cys-CS	1	260.6	273.63	11.32	0.417	0.377	0.04	-1.01	-0.82	0.17
	2	281			0.373			-0.683		
	3	279.3			0.342			-0.762		
MHA-CS	1	246.3	242.53	6.35	0.21	0.225	0.01	0.137	1.65	2.74
	2	246.1			0.227			0.00377		
	3	235.2			0.238			4.81		
0.025% MHA-CS + 0.075% Cat-Alg	1	181.8	182.43	10.06	0.483	0.50	0.05	14.8	14.40	0.40
	2	172.7			0.553			14.4		
	3	192.8			0.457			14		
0.050% MHA-CS + 0.050% Cat-Alg	1	115.1	115.80	0.89	0.195	0.20	0.00	34.9	36.17	1.17
	2	116.8			0.192			36.4		
	3	115.5			0.2			37.2		
0.075% MHA-CS + 0.025% Cat-Alg	1	176.5	172.90	4.06	0.376	0.36	0.05	36.9	39.63	2.37
	2	173.7			0.394			40.9		
	3	168.5			0.304			41.1		
0.050% MHA-CS + 0.025% Cat-Alg	1	135.2	133.13	2.27	0.298	0.32	0.04	38.2	38.23	0.25
	2	133.5			0.297			38		
	3	130.7			0.361			38.5		

2. Mucoadhesive properties of the NPs on *ex vivo* porcine bowel mucosa**Table 33** Percentage remaining of CS, Cys-CS NPs and MHA-CS NPs on porcine bowel mucosa.

Sample	Time (min)	% Remaining			mean	SD
		n=1	n=2	n=3		
CS	0	100	100	100	100	0
	5	95.69	95.49	94.62	95.27	0.57
	10	82.63	83.42	81.31	82.45	1.07
	20	68.64	68.19	70.07	68.97	0.98
	30	54.40	54.32	55.98	54.90	0.94
	40	47.47	49.92	49.23	48.87	1.26
	50	46.94	46.49	45.99	46.48	0.475
	60	39.13	40.04	40.65	39.94	0.76
Cys-CS NPs	0	100	100	100	100	0
	5	92.14	91.71	91.67	91.84	0.26
	10	77.01	75.68	76.81	76.50	0.72
	20	67.40	66.55	65.78	66.58	0.81
	30	61.37	61.51	62.00	61.63	0.33
	40	56.33	54.32	55.07	55.24	1.02
	50	46.95	44.51	44.74	45.40	1.35
	60	42.57	40.53	42.87	41.99	1.28
MHA-CS NPs	0	100	100	100	100	0
	5	93.44	94.51	93.18	93.71	0.70
	10	89.50	89.20	89.85	89.52	0.33
	20	71.22	69.19	71.45	70.62	1.28
	30	63.97	63.75	66.21	64.64	1.36
	40	56.03	56.31	54.41	55.58	1.03
	50	54.25	54.71	55.66	54.86	0.73
	60	49.48	51.04	50.28	50.27	0.78

Table 34 Percentage remaining of Alg and Cat-Alg NPs on porcine bowel mucosa.

Sample	Time (min)	% Remaining			mean	SD
		n=1	n=2	n=3		
Alg	0	100	100	100	100	0
	5	80.11	80.10	80.20	80.13	0.06
	10	71.66	71.12	71.34	71.37	0.27
	20	56.03	55.12	55.30	55.48	0.48
	30	41.46	41.66	42.00	41.71	0.28
	40	25.79	26.58	26.05	26.14	0.40
	50	20.94	20.87	21.29	21.03	0.22
	60	20.04	20.09	19.88	20.00	0.11
Cat-Alg NPs	0	100	100	100	100	0
	5	99.15	98.31	98.73	98.73	0.42
	10	85.78	83.28	83.37	84.14	1.42
	20	64.47	64.03	63.38	63.96	0.55
	30	57.3516	55.76	57.89	56.99	1.11
	40	49.13	48.95	49.52	49.20	0.29
	50	46.47	44.32	46.30	45.70	1.19
	60	44.30	44.53	44.82	44.55	0.26



3. Mucoadhesive properties of the NPs on *ex vivo* porcine bladder mucosa**Table 35** Percentage remaining of dextran, CS-Alg NPs and MHA-CS-Alg-Cat NPs on bladder mucosa.

Sample	Time (min)	% Remaining			mean	SD
		n=1	n=2	n=3		
Dextran	0	100	100	100	100	0
	5	99.51	95.70	85.04	93.41	7.50
	10	67.16	57.03	59.67	61.29	5.26
	20	49.04	53.60	41.62	48.09	6.05
	30	27.09	40.15	25.20	30.81	8.14
	40	23.13	28.08	16.05	22.42	6.05
	50	7.77	14.50	6.05	9.44	4.46
	60	0.24	1.07	0.50	0.61	0.43
CS-Alg NPs	0	100	100	100	100	0
	5	99.07	94.47	92.88	95.47	3.21
	10	97.08	83.77	90.18	90.35	6.66
	20	92.12	78.31	77.94	82.79	8.08
	30	56.85	66.52	56.67	60.01	5.63
	40	45.14	50.39	48.19	47.91	2.64
	50	22.45	28.12	25.80	25.46	2.85
	60	6.77	19.62	16.84	14.41	6.76
MHA-CS-Alg-Cat NPs	0	100	100	100	100	0
	5	98.45	98.39	97.83	98.22	0.34
	10	93.01	92.10	89.04	91.38	2.08
	20	91.91	93.30	86.30	90.50	3.71
	30	81.38	83.55	76.48	80.47	3.62
	40	51.65	48.99	53.69	51.44	2.36
	50	43.37	44.88	49.80	46.02	3.37
	60	40.75	34.38	41.99	39.04	4.09



APPENDIX C

Development of GM extract loaded NPs

1. Particle size and surface charge

Table 36 Particle size, size distribution, and surface charge of the GM extract loaded NPs.

NPs	GM extract (mg/mL)	NO.	Particle size (nm)			PDI			zeta potential (mV)		
				mean	SD		mean	SD		mean	SD
Cat-Alg	2.5	1	113.7	113.33	0.32	0.124	0.129	0.01	-26.1	-25.9	0.44
		2	113.1			0.117			-25.4		
		3	113.2			0.145			-26.2		
	5	1	119.6	119.77	0.47	0.09	0.095	0.01	-21	-23.1	1.84
		2	119.4			0.103			-23.9		
		3	120.3			0.092			-24.4		
	10	1	176.4	174.5	2.63	0.419	0.426	0.01	-16.3	-14.97	1.22
		2	171.5			0.429			-13.9		
		3	175.6			0.43			-14.7		
Cys-CS	2.5	1	378.2	384.33	16.57	0.263	0.310	0.04	-11.7	-9.48	2.05
		2	371.7			0.32			-7.67		
		3	403.1			0.348			-9.07		
	5	1	499.7	417.83	71.34	0.453	0.443	0.11	-8.47	-6.85	1.57
		2	369			0.326			-5.33		
		3	384.8			0.549			-6.75		
	10	1	482.3	434.20	41.71	0.302	0.384	0.15	-6.09	-5.49	0.64
		2	412.3			0.291			-4.82		
		3	408			0.558			-5.58		
MHA-CS	2.5	1	171.3	169.90	2.60	0.209	0.095	0.10	-7.64	-7.23	0.54
		2	171.5			0.05			-6.62		
		3	166.9			0.026			-7.43		
	5	1	177.2	175.97	1.43	0.256	0.235	0.02	-5.58	-5.50	0.64
		2	174.4			0.213			-4.82		
		3	176.3			0.237			-6.09		
	10	1	186.6	190.87	4.70	0.221	0.296	0.06	-4.33	-3.44	0.82
		2	190.1			0.329			-3.29		
		3	195.9			0.337			-2.71		

High performance liquid chromatography (HPLC) condition

Column: 250×4.6 nm C18
Flow rate: 1.00 mL/min
Injection volume: 20 µL
Detector: UV-Vis detector
Wavelength: 320 nm
Mobile phase: Acetonitrile and 0.1% orthophosphoric acid

Table 37 Volume ratios of acetonitrile and 0.1% orthophosphoric acid use as a mobile phase for HPLC

Time (min)	Acetonitrile	0.1% Orthophosphoric acid
0	70%	30%
15	70%	30%
18	75%	25%
19	80%	20%
25	80%	30%
26	70%	30%
30	70%	30%

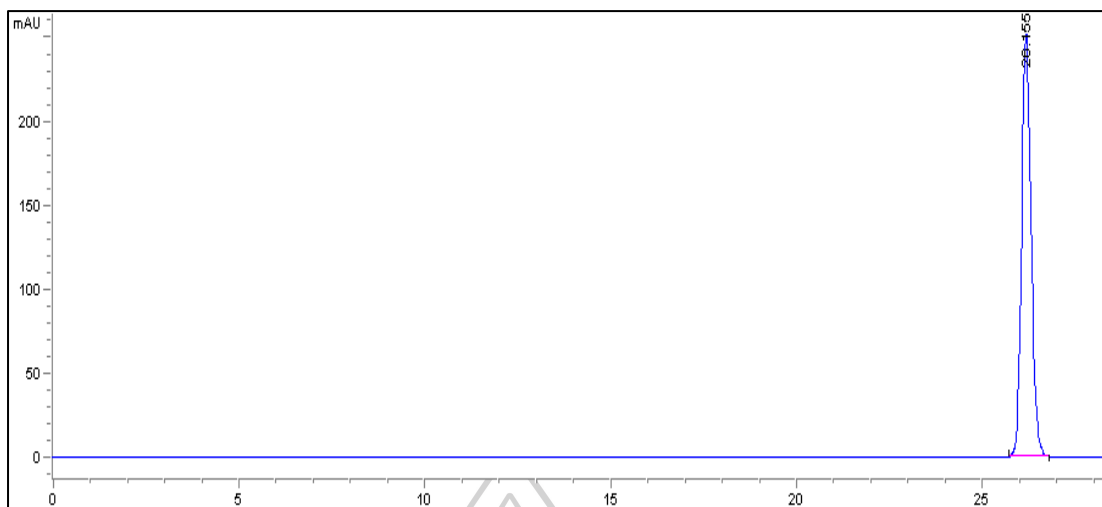


Figure 41 Chromatogram of standard α -mangostin.

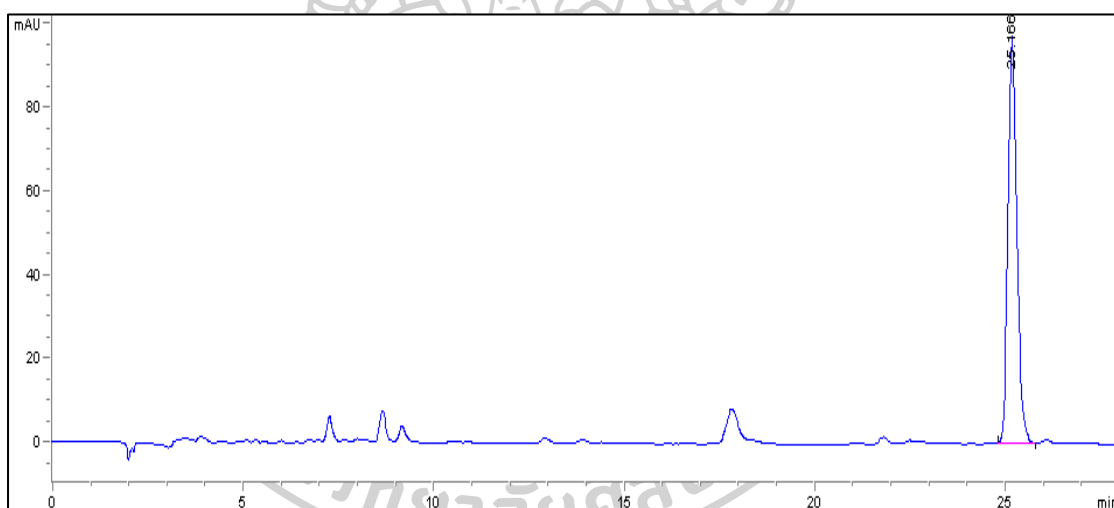
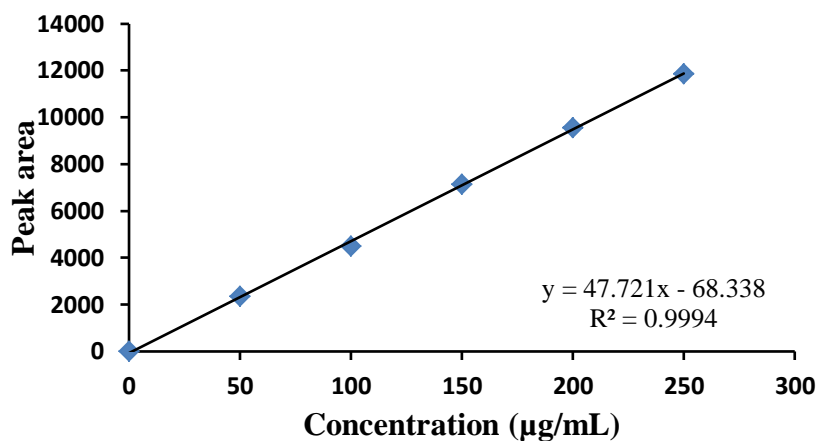
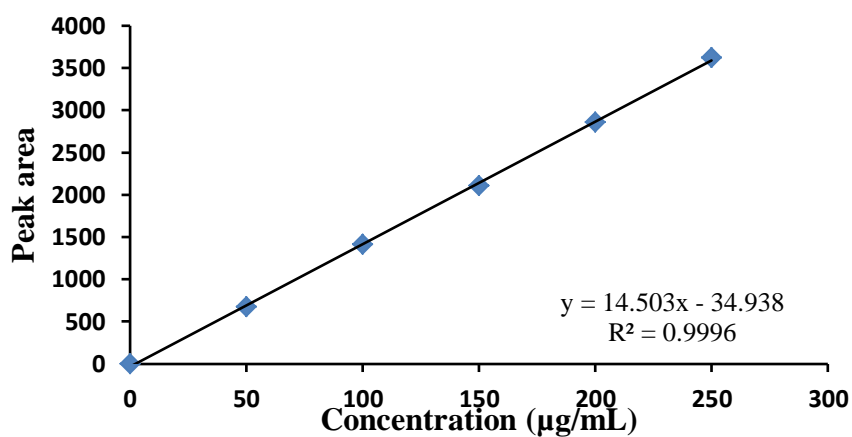


Figure 42 Chromatogram of GM extract.

Standard curve**Standard:** α -mangostin**Method:** High performance liquid chromatography (HPLC)**Wavelength:** 320 nm**Figure 43** Standard curve of α -mangostin.**Standard:** GM extract**Method:** High performance liquid chromatography (HPLC)**Wavelength:** 320 nm**Figure 44** Standard curve of GM extract.

3. Drug loading

Table 38 GM extract content in the NPs.

NPs	GM extract (mg/mL)	NO.	Loading capacity ($\mu\text{g}/\text{mg}$)			Loading efficiency (%)		
				mean	SD		mean	SD
Cat-Alg	2.5	1	134.58	136.87	3.24	90.93	92.48	2.19
		2	139.16			94.03		
		3	82.76			55.92		
	5	1	212.85	212.33	0.19	83.14	82.94	0.07
		2	212.46			82.99		
		3	212.19			82.89		
	10	1	292.50	292.24	0.59	71.69	71.63	0.15
		2	291.56			71.46		
		3	292.66			71.73		
Cys-CS	2.5	1	12.43	12.68	0.22	6.21	6.34	0.11
		2	12.76			6.38		
		3	12.85			6.42		
	5	1	18.72	18.78	0.02	5.61	5.62	0.01
		2	18.76			5.62		
		3	18.80			5.63		
	10	1	54.97	54.91	0.10	10.99	10.98	0.02
		2	54.98			10.99		
		3	54.84			10.97		
MHA-CS	2.5	1	17.27	17.34	0.06	8.64	8.67	0.03
		2	17.38			8.69		
		3	17.37			8.69		
	5	1	59.18	51.82	6.38	17.72	15.51	1.91
		2	47.74			14.29		
		3	48.54			14.53		
	10	1	64.84	64.77	0.07	12.97	12.95	0.01
		2	64.77			12.95		
		3	64.69			12.94		

3. Drug release

Table 39 GM extract release from the NPs at different time point (Simulated Gastric (0.1M HCl pH 1.2)).

Free GM extract	%Release			mean	SD
	n=1	n=2	n=3		
Time (hours)					
0	0	0	0	0	0
0.5	53.23	53.31	52.94	53.16	0.20
1	67.36	67.03	67.85	67.41	0.42
2	82.96	84.70	84.06	83.90	0.88
4	87.06	84.91	84.96	85.64	1.23
8	101.76	101.02	99.78	100.85	1.00
Cat-Alg NPs	%Release			mean	SD
Time (hours)	n=1	n=2	n=3		
0	0	0	0	0	0
0.5	10.87	9.51	11.64	10.67	1.08
1	48.12	48.61	48.54	48.42	0.26
2	68.70	65.85	66.89	67.15	1.67
4	76.33	73.41	76.29	75.34	1.67
8	104.54	107.72	108.46	106.91	2.08
Cys-CS NPs	%Release			mean	SD
Time (hours)	n=1	n=2	n=3		
0	0	0	0	0	0
0.5	90.21	87.92	89.81	89.31	1.22
1	93.53	92.19	93.05	92.62	0.68
2	95.04	95.80	96.05	95.63	0.53
4	97.02	97.46	97.02	97.17	0.25
8	101.03	98.45	100.76	100.08	1.42
MHA-CS NPs	%Release			mean	SD
Time (hours)	n=1	n=2	n=3		
0	0	0	0	0	0
0.5	85.08	85.43	84.75	85.09	0.34
1	88.04	88.12	88.44	88.20	0.21
2	90.94	94.66	93.61	93.07	1.92
4	96.47	96.35	96.03	96.28	0.22
8	104.58	104.86	104.28	104.57	0.29

Table 40 GM extract release from the NPs at different time point (Simulated Intestinal Fluid (pH 6.8))

Free GM extract	%Release			mean	SD
	n=1	n=2	n=3		
Time (hours)					
0	0	0	0	0	0
0.5	56.69	56.60	56.61	56.63	0.05
1	57.42	59.42	59.22	58.69	1.10
2	80.50	80.38	79.83	80.24	0.35
4	86.15	85.98	86.18	86.18	0.11
8	91.71	92.77	92.55	92.34	0.56
Cat-Alg NPs	%Release			mean	SD
Time (hours)	n=1	n=2	n=3		
0	0	0	0	0	0
0.5	8.91	3.97	9.56	7.48	3.06
1	12.16	12.62	12.58	12.45	0.25
2	37.67	38.47	38.14	38.09	0.40
4	75.83	73.58	76.29	72.23	1.45
8	99.96	100.15	100.29	100.13	0.16
Cys-CS NPs	%Release			mean	SD
Time (hours)	n=1	n=2	n=3		
0	0	0	0	0	0
0.5	18.60	18.24	18.57	18.47	0.20
1	23.42	24.36	24.70	24.53	0.67
2	55.84	75.82	59.87	63.85	10.57
4	97.93	102.93	100.99	100.62	2.52
8	103.27	102.34	101.10	102.24	1.09
MHA-CS NPs	%Release			mean	SD
Time (hours)	n=1	n=2	n=3		
0	0	0	0	0	0
0.5	17.48	17.44	17.39	17.44	0.04
1	29.79	33.14	28.90	30.61	2.24
2	74.18	70.16	75.00	73.11	2.59
4	99.11	100.30	102.01	100.48	1.46
8	102.10	101.34	101.49	101.64	0.40



APPENDIX D

Development of DOX-loaded NPs

1. Particle size and surface charge

Table 41 Particle size, size distribution, and surface charge of the DOX loaded NPs.

Ratio of NPs:DOX	NO.	Particle size (nm)		PDI			zeta potential (mV)			
			mean	SD		mean	SD		mean	SD
1:0.25	1	132.6	133.87	1.14	0.258	0.26	0.01	35.7	36.87	1.04
	2	134.8			0.262			37.7		
	3	134.2			0.27			37.2		
1:0.5	1	142.3	143.27	0.85	0.258	0.25	0.01	38.1	38.07	1.15
	2	143.6			0.256			36.9		
	3	143.9			0.241			39.2		
1:1	1	196.4	198.97	2.83	0.379	0.35	0.04	31.6	35.43	3.32
	2	198.5			0.302			37.4		
	3	202.0			0.36			37.3		

2. Drug loading

DOX standard curve for drug content

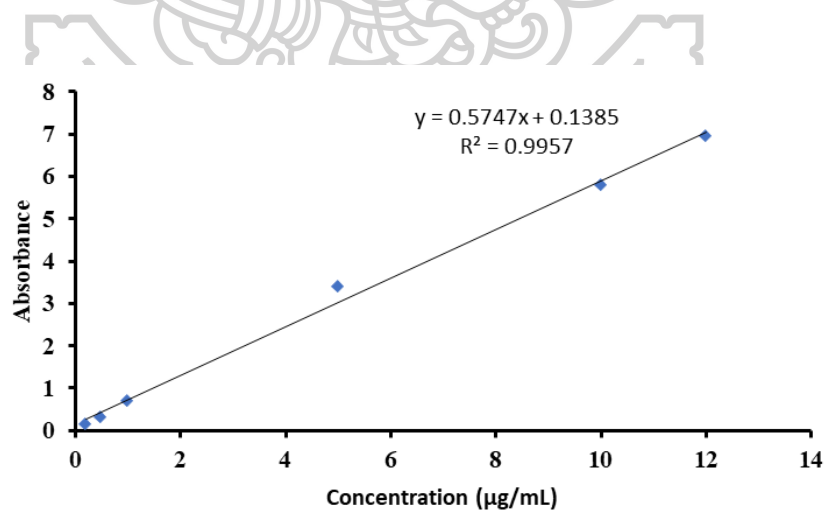


Figure 45 Standard curve for DOX content quantification.

Table 42 DOX content in the NHA-CS-Alg-Cat NPs.

NPs:DOX	No.	%Loading efficiency			Loading capacity ($\mu\text{g}/\text{mg}$)		
			mean	SD		mean	SD
1:0.25	1	41.01	40.9	0.36	57.41	57.27	0.50
	2	40.51			556.71		
	3	41.21			57.69		
1:0.5	1	74.41	74.7	0.3	248.02	249.03	0.97
	2	74.99			249.96		
	3	74.73			249.12		
1:1	1	53.65	53.94	0.50	241.43	242.71	2.24
	2	54.51			245.30		
	3	53.64			241.39		

3. Drug release

DOX standard curve for drug release

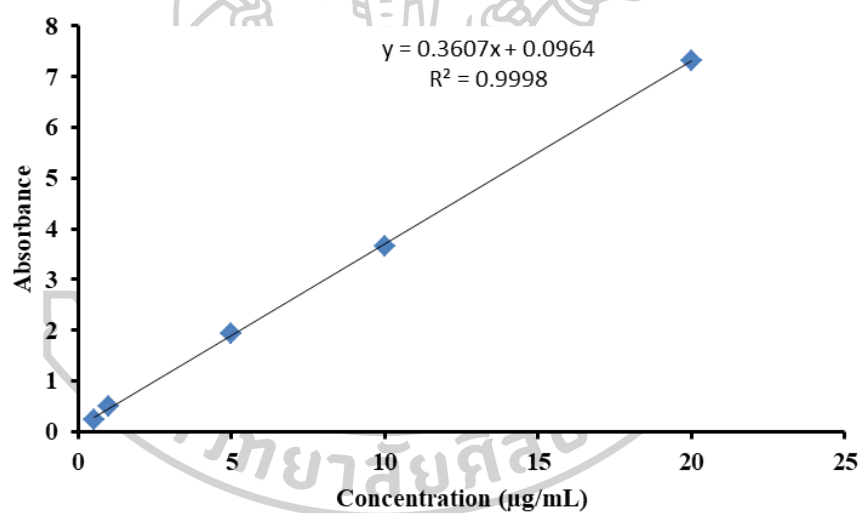
**Figure 46** Standard curve of DOX.

Table 43 DOX release from the MHA-CS-Alg-Cat NPs at different time point.

Free DOX	%Release			mean	SD
Time (min)	n=1	n=2	n=3		
0	0	0	0	0	0
5	28.87	30.29	29.64	29.26	0.55
10	38.62	38.85	38.72	38.73	0.11
15	46.16	45.91	47.84	46.64	1.05
30	61.15	60.49	61.47	61.03	0.50
60	75.10	77.06	77.14	76.43	1.15
120	95.40	96.22	98.50	96.71	1.61
240	110.04	117.41	120.51	115.99	5.38
480	108.18	58.27	109.77	92.07	29.28
720	110.66	60.74	112.50	94.63	29.37
1440	113.71	62.20	111.43	95.78	29.10
DOX-loaded NPs	%Release			mean	SD
Time (min)	n=1	n=2	n=3		
0	0	0	0	0	0
5	16.33	17.06	16.72	16.52	0.28
10	21.04	23.04	21.53	21.87	1.04
15	24.19	24.45	24.79	24.48	0.30
30	35.12	35.89	36.85	35.95	0.87
60	48.29	50.16	50.29	49.58	1.12
120	61.50	62.89	62.99	62.46	0.84
240	78.19	79.28	79.46	78.98	0.69
480	82.33	83.82	82.61	82.92	0.79
720	84.81	88.49	85.34	86.21	1.99
1440	87.86	91.27	84.28	87.80	3.50

VITA

NAME Miss Nitjawan Sahatsapan

DATE OF BIRTH 11 September 1993

PLACE OF BIRTH Uthai Thani, Thailand

INSTITUTIONS ATTENDED 2016 – 2022 Doctor of Philosophy, Ph.D. in Pharmaceutical Technology, Faculty of Pharmacy, Silpakorn University, Thailand.
2021 Fachbereich II: Labor Pharmazeutische Technologie and Chemical Engineering at the Berliner Hochschule für Technik, Berlin, Germany
2010 – 2015 Bachelor Degree, Science (Chemistry), Faculty of Liberal Arts and Science, Kasetsart University, Thailand

HOME ADDRESS Uthai Thani, Thailand

PUBLICATION International journal

1. Nitjawan Sahatsapana, Boonnada Pamornpathomkula, Theerasak Rojanarataa, Tanasait Ngawhirunpata, Raksawan Poonkhumb, Praneet Opanasopita, Prasopchai Patrojanasophon. Feasibility of mucoadhesive chitosan maleimide-coated liposomes for improved buccal delivery of a protein drug. *J Drug Deliv Sci Technol* 2022; 69: 103173.
2. Kwanputtha Arunprasert, Chaiyakarn Pornpitchanarong, Nitjawan Sahatsapan, Praneet Opanasopit, Prasopchai Patrojanasophon. Synthesis and evaluation of poly(Ethylene glycol) diacrylate-modified chitosan as a mucoadhesive polymer. *Thai J Pharm Sci*, 2021; 45(3):202–7.
3. Nitjawan Sahatsapan, Theerasak Rojanarata, Tanasait Ngawhirunpat, Praneet Opanasopit, Prasopchai Patrojanasophon. Doxorubicin-loaded chitosan-alginate nanoparticles with dual mucoadhesive functionalities for intravesical chemotherapy. *J Drug Deliv Sci Technol* 2021; 63: 102481.
4. Nitjawan Sahatsapan, Tanasait Ngawhirunpat, Theerasak Rojanarata, Praneet Opanasopit, Prasopchai Patrojanasophon. Catechol-functionalized alginate nanoparticles as mucoadhesive carriers for intravesical chemotherapy. *AAPS PharmSciTech* 2020; 21: 212.

5. Chaiyakarn Pornpitchanarong, Nitjawan Sahatsapan, Theerasak Rojanarata, Praneet Opanasopit, Tanasait Ngawhirunpat, Prasopchai Patrojanasophon. Curcumin-incorporated Thiolated Chitosan/alginate Nanocarriers: Physicochemical Properties and Release Mechanism. *Indian J Pharm Sci* 2020; 82(1): 97-103.
 6. Nitjawan Sahatsapan, Theerasak Rojanarata, Tanasait Ngawhirunpat, Praneet Opanasopit, Prasopchai Patrojanasophon. Catechol-Functionalized Succinyl Chitosan for Novel Mucoadhesive Drug Delivery. *Key Eng Mater.* 2019; 819: 21-26.
 7. Nitjawan Sahatsapan, Theerasak Rojanarata, Tanasait Ngawhirunpat, Praneet Opanasopit, Prasopchai Patrojanasophon. 6-Maleimidohexanoic acid-grafted chitosan: A new generation mucoadhesive polymer. *Carbohydr Polym.* 2018; 202: 258-264.
- AWARD RECEIVED** “Excellent Prize” – Oral Presentation. The 7th International Conference on Advanced Pharmaceutical Research (ICAPH 2020), Rangsit University, Bangkok, Thailand
- “Second Place” – Poster Presentation. The 6th International Conference on Advanced Pharmaceutical Research (ICAPH 2019), Rangsit University, Bangkok, Thailand

